NOAA TECHNICAL MEMORANDUM NWS CR-103

AN INVESTIGATION OF TWO MICROBURST PRODUCING STORMS USING A MICROBURST RECOGNITION ALGORITHM

David R. Eversole
National Weather Service Office
Kansas City, Missouri

January 1994

UNITED STATES
DEPARTMENT OF COMMERCE
Ronald H. Brown
Secretary

National Oceanic and
Atmospheric Administration
D. James Baker
Under Secretary

National Weather
Service
Elbert W. Friday, Jr.
Assistant Administrator

Table of Contents

An Investigation Of Two Microburst Producing Storms Using A Microburst Recognition Algorithm[1]

David Richard Eversole
National Weather Service Office
Kansas City, Missouri

ABSTRACT

A review of the history of the microburst, complete with current achievements, is given. Two microbursts are investigated and associated precursors were extracted with the use of a microburst recognition algorithm. The precursors were then used to determine the forcing mechanisms for the microbursts. The structure of the microbursts and the timing of the precursors were compared and contrasted with each other and also with a moderate reflectivity model, and differences are discussed. One microburst was initiated by a misocyclone which created vertical pressure gradients, while the other microburst was initiated by precipitation drag. All five precursors were detected in both events. It was discovered that several improvements could be made upon the microburst recognition algorithm. The algorithms main difficulty stemmed from the fact that it was tuned to high reflectivity events, and thus had difficulty with the two microbursts which were of a lower reflectivity class. It was pointed out that this could be solved by incorporating the moderate reflectivity model into the algorithm complete with a subroutine which enables the algorithm to determine the reflectivity class of microbursts.

A) INTRODUCTION

All throughout the history of aviation, pilots have had to be aware of dangerous wind shear which can occur as subtle turbulence or to an extreme such that it endangers the aircraft. Wind shear is defined as a sharp change in direction or speed. It is most dangerous to aircraft performance during takeoff and landing due to the aircrafts decreased airspeed and close proximity to the ground. Many aircraft accidents can be explained to a large degree by wind shear in the lowest few hundred meters (Fujita and Caracena, 1977 and others). In a study by Fujita and Byers (1977), four types of wind shear were defined: headwind shear in which the aircraft experiences an increase in airspeed, tailwind shear where airspeed decreases, crosswind shear which causes the aircraft to drift to the side, and downburst shear which causes the aircraft to sink due to vertical air currents. Strong wind shear which occurred near runways was discovered to play a part in several aircraft accidents during takeoff and landing.

The term wind shear comprises all events where wind speed or direction is changing over a short distance. This can be caused by many phenomena and is of course not limited to a layer near the surface. For the purpose of this thesis, a single type of wind shear event called a microburst will be studied. A microburst is a wind shear event which is caused by a highly con-

[1] This is a reprint of Mr. Eversole's Masters Thesis for the University of Kansas, 1992.

centrated, high speed column of air descending out of a thunderstorm which impacts the surface and spreads out horizontally. The purpose of this thesis is to investigate two microbursts and the in-storm features associated with their development. This will be accomplished using a computer algorithm designed to recognize low level wind shear events with the assistance of single- and dual-Doppler radar data and the synoptic situation. Certain key radar detectable phenomena will be discussed as will their application to the detection of wind shear events. In order to better understand the wind shear event, one must investigate the work that has gone into the study of the event in the past. The Literature Review section lists the past achievements aimed at understanding the microburst event.

1) LITERATURE REVIEW

1a) Beginning Work

In two studies by Fujita and Byers (1977) and Fujita and Caracena (1977), the source of the wind shear which caused several aircraft crashes was investigated. It was found that the cause of the wind shear was an intense, rapidly descending downdraft which was termed a "downburst." The downburst is characterized as having a horizontal size of at least 800 meters (so that it has an affect on the aircraft) and air descending at a rate 3.6 m/s or more at 91 meters above ground level (AGL), corresponding to the descent/ascent rate of an aircraft on the usual 3° glideslope. The downbursts create two hazards: first an intense descending air column which alone can push a plane into the ground and secondly horizontal wind shear as the downburst impacts the surface which causes the aircraft airspeed to decrease suddenly causing the aircraft to loose lift and fall (Figure I-1).

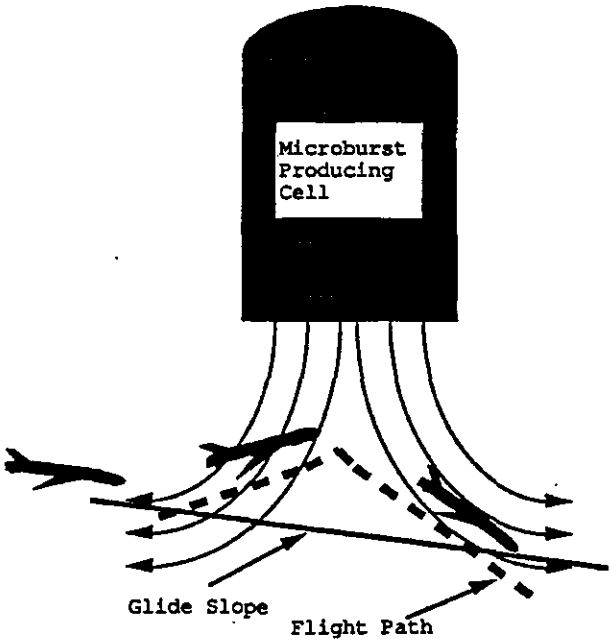

Figure I-1. Microburst Outflow and Aircraft Flight Path. (Redrawn from Campbell and Olson, 1986)

Strong outflows from storms have been recognized events for quite some time. In a study by Krumm (1954), one of the earliest attempts to model the cause of these strong outflows was made. Krumm, Wakimoto (1985) and others studied outflows from high-based (3 - 3.5 km AGL) cumulonimbi in the High Plains region and discovered that a strong outflow could occur if the subcloud layer contained a dry adiabatic mixed layer about 3 km deep. This lapse rate combined with low humidity conditions allows for sufficient evaporation of the precipitation causing the descending air to cool and become more negatively buoyant. Krumm observed that these strong outflows commonly had virga associated with them; the precipitation usually evaporated before it reached the ground. Therefore, Krumm pointed out that precipitation drag forces can essentially be ignored. This was some of the earliest work that recognized that strong outflows can be produced given specific subcloud conditions. The downbursts in the studies by Fujita and others differed from the strong outflows that Krumm observed in that heavy rain was associated with the strong winds. It was discovered several years later that there are in fact two types of downbursts: those with heavy rain and those with little or no rain. These two types will be discussed in more detail later.

The studies by Fujita and others were among the first to use radar in the investigation of the downbursts. They suggested that these downbursts originated from what was termed a "spearhead echo" which is an echo on a low resolution radar which takes the shape of a spearhead. The spearhead echo contains a strong updraft and several downdraft cells located on or near the southern edge which produce the downbursts. Fujita and Caracena (1977) suggested that cloud tops which are overshooting the tropopause collapse into the cloud, and incite large amounts of precipitation to descend rapidly through the cloud (entraining incloud air) and eventually reach the ground, producing a downburst. It was found that the upper-level wind speed alone could not account for the speed of the downburst; some other mechanism such as evaporation or entrainment was at work, and it was not clear that the downburst originated at the cloud top despite the descending cloud tops. Fujita (1981) suggested that a downdraft may be initiated by entrainment of dry air at midlevels within the cloud. This entrainment would subsequently erode the cloud by evaporating liquid water and create a notch which shows up as a bow shape on low resolution radars, called a "bow echo."

After the studies by Fujita and others, much interest was sparked into better understanding and characterizing the downburst event using radar data. The downburst definition was refined in Fujita (1981) to be both a misoscale and mesoscale event with a horizontal size of .4 km to about 20 km and defined a smaller and more concentrated downburst, the "microburst" which has a horizontal extent of .4 - 4 km with peak winds lasting 2 to 5 minutes. Wakimoto (1985) defined a larger and longer lasting outflow known as a "macroburst" which has an outflow size greater than 4 km with damaging winds lasting 5 to 20 minutes. Fujita (1981) defined two types of microbursts: the "traveling microburst" and the "stationary microburst." The traveling microburst has an asymmetric outflow with more damaging winds on the leading edge due to the fact that the descending air progresses at the leading edge leaving an area of cold air behind, whereas the stationary microburst impacts straight into the ground and produces a symmetrical outflow.

Fujita (1981) noted that downbursts can reach F3 intensity (70 - 92 m/s) and discovered "burst swaths" which are concentrated paths of high winds with an average size of 100 meters across. Fujita (1981) observed a horizontal vortex flow at the east and west edges of microburst outflows, and in a paper by Wolfson (1988), results from a 1984 paper by Fujita were discussed illustrating that as the microburst impacts the surface, the leading outflow is bent back into itself, creating a horizontal vortex roll called a rotor which was also noted by Kessinger et al (1988). The outflow continues expanding and the horizontal vortex spins up and eventually fragments creating runaway vortex rolls causing narrow areas of wind damage or burst swaths.

1b) Early Research Projects

Many authors who studied the microburst event came to the conclusion that some method of detection or warning should be developed. Several projects were consequently designed and developed to study microburst outflows, one of them the Northern Illinois Meteorological Research on Downbursts (NIMROD) which operated during 1978 near Chicago and made the first single-Doppler measurements of microburst outflows. Another was the Joint Airport Weather Studies Project (JAWS) which operated in the spring and summer of 1982 and was located near the Stapleton airport in Denver, Colorado (McCarthy, Wilson et al, 1982).

The JAWS project concentrated specifically on studying the three-dimensional structure of the microburst wind shear event to design a Doppler radar network for observing the microburst windfield. The JAWS project also provided insight into the frequency and characteristics of microburst events. The JAWS project did not suffer from the wide radar spacing of NIMROD in which only single-Doppler analyses were available as a result. Many microburst events were recorded in JAWS with single-Doppler and dual-Doppler radar data from three NCAR radars. Aircraft equipped with radar and 27 PAM (portable automated mesonet) stations were also used to study the phenomena.

Before JAWS, the hopes of quickly developing a warning system were dampened somewhat by the realization that the microburst event was complicated and that much data needed to be compiled before attempting a warning system. Collecting this badly needed data was the main purpose of the JAWS project, and as the data became available characterizing the microburst event and searching for similarities among events was the main task.

1c) Microburst Characteristics

Using JAWS data, Wilson et al (1984) characterized the microburst event by a minimum differential radial velocity of 10 m/s between the maximum receding and approaching velocities (across the divergence center) which are separated by about 3 km on average. Wilson et al (1984) found that the average height of the outflow is about 750 meters, and the maximum velocity in the microburst outflow typically occurred within 10 minutes after the initial outflow. Hjelmfelt (1988) found that the microburst typically has an average lifetime of 13 minutes. Wilson et al (1984) indicated that the maximum velocity had an average radial velocity difference of 22 m/s and was typically near the ground (50 - 100 meters) and was found to be uncorrelated with reflectivity in JAWS microbursts. Microbursts were observed to occur in mid-air

before impacting the surface, although this was not a common occurrence. These mid-air microbursts had been noted previously by Fujita (1981). Wilson et al (1984) also reported that the horizontal vortex flow (discovered by Fujita, 1981) was observed quite often.

Wakimoto (1985) and Wilson et al (1984) separated the micro-burst event into two classes: the "dry microburst", in which little or no rainfall is associated with the high winds, and the "wet microburst", which has heavy rain associated with the high winds. Wakimoto (1985) indicated that the dry microburst producing storm is typically a high based (3 - 4 km), shallow (2 - 3 km), low reflectivity cloud with weak convective elements. This is typical of a stratocumulus or altocumulus cloud with low reflectivities. Kessinger et al (1986) noted that dry microburst reflectivities ranged from 5 to 30 dBz at 500 meters AGL (while wet microbursts typically have >30 dBz at this height), and the dry microbursts in JAWS occurred mostly between 1400 and 1700 MDT. This is contrasted to the wet microburst producing storm which has stronger vertical currents, is larger and has high reflectivity values (> 40 dBz). The wet microburst typically descends from either cumulus congestus or cumulonimbus clouds (Wolfson, 1988).

Wilson et al (1984) noted during JAWS that both wet and dry microbursts can occur in families, therefore the occurrence of a microburst indicates the likelihood that others may follow. Wolfson (1988) noted microburst families were also common in Huntsville, Alabama. Microbursts themselves do not have to occur as individual outflows, several may combine to become one large outflow. These large outflows or "microburst lines" which are created when two or more individual microburst outflows combine to create a longer lasting, larger outflow were also noted in JAWS data (Hjelmfelt, 1987,1988).

In the early eighties, the microburst event was beginning to come into focus and some common aspects of dry microbursts indicated that some form of forecasting was possible. Wilson et al (1984) found that general area-wide alerts for dry microbursts can be made based upon upper air soundings. Wakimoto (1985) also noted that dry microburst activity corresponds to a particular sounding type with a dry adiabatic layer 3 - 4 km deep and dry air at the surface (dewpoint depression > 30 °C) which reaches saturation at the cloud base. A study by Caplan et al (1990) found that for the Denver area, the 700 - 500 mb lapse rate provided a way to forecast microburst activity. They found that 67% of dry microburst activity occurred with a morning (1200 UT) lapse rate of at least 8 °C/km and that 89% occurred with an evening (2200 UT) lapse rate of the same value. So, the microburst activity was better correlated with an evening lapse rate of at least 8 °C/km.

1d) Microburst Forcing Mechanisms

One of the first "forcing mechanisms" applied to the forecasting of microburst activity was based upon the fact that a specific subcloud environment favored microburst development. A forcing mechanism is a mechanism that is associated with microburst initiation and development. Different forcing mechanisms are associated with dry and wet microbursts. It was later found that the forcing mechanisms also vary geographically in type and strength, creating the need for continuing research in different areas of the country. The following describes the forcing mechanisms responsible for three types of microburst producing storms.

Roberts and Wilson (1984) divided the microburst producing storms into three classes (each assumes a dry adiabatic subcloud environment) and identified probable forcing mechanisms for each. The first class is for high-based shallow convective clouds that tend to produce dry microbursts with virga located below the cloud base; the forcing mechanisms were most likely evaporation and/or melting of particles below the cloud base.

The second class is for storms which contain a precipitation core which is descending out of a dissipating cell, producing wet microbursts. This class generally has strong convergence and rotation associated with the descending precipitation shaft, with the forcing mechanisms being subcloud and incloud evaporation and/ or melting and precipitation drag to a lesser degree. Rotation within clouds can cause a non-hydrostatic pressure situation (to be discussed later) which can act as a forcing mechanism also. The third class is for storms which contain large hail and also produces wet microburst events. In this case the forcing mechanisms are subcloud and incloud precipitation melting, evaporation and drag.

The significance of subcloud evaporation is exemplified in a study by Srivastava (1985) who found that by evaporation, the weight of water is replaced by a negative buoyancy 10 times as large. This study also contained the results of a 1-dimensional model of the dry microburst event which showed that dry microbursts will occur with almost any rainwater mixing ratio given that the subcloud environment has a nearly dry adiabatic lapse rate and that more intense cooling will occur with small drops in dry air. Krumm (1954) and Wakimoto (1985) also noted the significance of a nearly dry adiabatic lapse rate. Roberts and Wilson (1984) noted that evaporation contributed twice as much to the negative buoyancy of the downdraft than melting or precipitation loading. Srivastava's model also indicated that entrainment into the downdraft is minimal as long as the downdraft diameter is at least 1 km, and JAWS data indicates that downdrafts (> 5 m/s) are typically larger than this at about 1 - 1.5 km AGL (Hjelmfelt, 1987).

Roberts and Wilson (1987) summarized the downdraft forcing mechanisms to be evaporative cooling (subcloud and incloud), melting cooling, precipitation drag and vertical pressure gradients (mentioned earlier). Vertical pressure gradients are set up by rotation which can centrifuge out water mass and create an area of relatively less dense air. This creates a non-hydrostatic situation with more dense air above less dense air which incites a downdraft. Fujita and Byers (1977) also identified overshooting tops as a possible forcing mechanism.

1e) Microburst Precursors

Roberts and Wilson (1984) also investigated "precursors" to microburst events using JAWS data. Precursors are defined as radar detectable features within storms which precede or accompany the surface divergence (Isaminger, 1987). A descending reflectivity core was identified as a precursor since a downdraft is initiated by the descent of the high reflectivity core from mid-levels (Roberts and Wilson, 1984,1986). Kessinger et al (1986) also noted convergence located near the cloud base of dry microburst events from the JAWS data set. Rotation was found to be associated with some JAWS dry microburst events although this was not the cause of the event, evaporation was the primary forcing mechanism since Srivastavas model closely predicted the speed of the outflows. The rotation may spin up as the downdraft stretches, due to the conserva-

tion of angular momentum, and entrainment into the downdraft may be limited as a result of the rotation. Robert and Wilson (1986) identified the following microburst precursors for the Denver area: 1) a descending reflectivity core, 2) organized convergence above or near the cloud base, 3) a reflectivity notch, and 4) rotation.

It is important to remember that factors other than evaporation or centrifuge in a vortex can cause a reflectivity notch or a bounded weak echo region. A reflectivity notch can also be caused by changes in precipitation type, size, and fall speed (Roberts and Wilson, 1987). Also, small drops play a stronger role in evaporation (Srivastava, 1985) since they evaporate easily (more surface area per unit mass), and these small drops do not have a large affect on reflectivity, which is proportional to the 6th power of the diameter of the hydrometeor and the number of drops.

Isaminger (1987) listed the microburst precursors which are acknowledged to be rotation, convergence, descending reflectivity core, reflectivity notching and introduced a new microburst precursor, upper-level divergence. Another possible microburst precursor is negative velocities in a "flare echo" (Wilson and Reum, 1988) which appears as an appendage on the far side of the core. The flare is created by the radar beam being deflected off hailstones in the core to the ground, bouncing back off the ground to the hailstones and back to the radar. The extra distance traveled causes a false echo on the back of the core. Positive Doppler velocities indicate that the hydrometeors that caused the deflection were rising, and negative velocities indicate they were descending. Isaminger (1987) discussed a Huntsville, Alabama microburst producing storm that had a flare echo.

It was found that microburst precursor signatures vary geographically. In Huntsville, Alabama, the most common features were a descending core (95%) and divergent tops (93% of storms scanned to storm top) while rotation was detected to a lesser degree (59%) (Isaminger, 1987). However, in Norman, Oklahoma, descending cores (100%) and convergence (100%) are the most common features of six microburst producing cells on the same day (Eilts, 1987). In Denver, Colorado, convergence (Roberts and Wilson, 1984) and rotation are common features (Roberts and Wilson, 1986), however mid-level convergence was typically stronger in Huntsville events (Biron and Isaminger, 1989). Lower level divergence was detected before 75% of the microburst outflows in Denver, but only 2% of those at Huntsville (Biron and Isaminger, 1989). Kansas City, Kansas micro-bursts were almost always associated with a descending core and to a slightly lesser degree rotation, convergence and upper-level divergence (Campbell and Isaminger, 1990).

The subcloud environment also varies geographically. Eilts (1987) noted that the Norman, Oklahoma environment has a shallow moist boundary layer. The Denver, Colorado environment is typically dry adiabatic (Wakimoto, 1985 and others) with a very dry layer near the surface and increasing moisture with height (Kessinger et al, 1986). Kansas City, Kansas tends to have a somewhat drier environment (authors observations).

1f) Microburst Recognition

The development of a warning system requires an understanding of the microburst event, as mentioned earlier. The development of that warning system was based to a degree on the work of Roberts and Wilson (1986), who created three different models for micro-burst events based upon the storm reflectivity structure: the "low reflectivity model" with reflectivities less than 35 dBz, the "moderate reflectivity model" with reflectivities 40 - 55 dBz, and the "high reflectivity model" with reflectivities of 55 dBz or greater. Convergence aloft was detected 5 - 6 minutes before the surface microburst outflow in all three models. The moderate and high reflectivity models are characterized by a reflectivity core which begins descending 5 - 6 minutes before the first signs of the outflow at the surface. All three models show that the reflectivity/precipitation core is initially collocated at the surface with the developing microburst.

These three models allowed for the detection and recognition of microburst events based upon the precursors in the model. The next task was deciding what the best equipment and method to use for detection was. Wilson et al (1984) studied the ability to nowcast (0 to 30 minutes) the microburst using one or two radars and various microwave wavelengths. Another study by Roberts and Wilson (1984) suggested that nowcasting microbursts is possible using a single-Doppler radar.

Along with the microburst models they created, Roberts and Wilson (1984, 1986) proposed a method of nowcasting microbursts by using computer generated time-height profiles of the reflectivity structure of storms. The method was a forecaster-computer interactive environment in which the forecaster analyzes the time-height profiles for indications of a descending reflectivity core suggesting an impending microburst. Based upon evidence that a microburst typically occurs about 5 minutes after the detection of a descending reflectivity core and reaches peak intensity 5 minutes after that (Roberts and Wilson, 1986), there should be enough time for the forecaster to warn pilots and air traffic controllers. The forecaster-computer nowcasting concept was developed further in Roberts and Wilson (1987) in which the forecaster watched radar displays and time/ height profiles for downdraft forcing mechanisms which can be quickly identified from radar signatures. The forecaster directs the computer to perform various tasks such as time/height profiles of reflectivity and velocity in the vicinity of interest.

The growing understanding in microburst processes and radar signatures lead to the idea of developing a completely automated wind shear recognition system which would operate on single-Doppler radar data and not require the forecaster as needed in the models by Roberts and Wilson (1986,1987). The first microburst recognition algorithm was developed at M.I.T. Lincoln Laboratory by Merritt (1987). This algorithm was based solely on the surface radial velocity divergence feature of the microburst event. This algorithm was tested at the FL-2 site in Huntsville, Alabama and successfully detected 98% of the outflows of wet microbursts with radial velocity differences of 20 - 24 m/s and slightly lower for other velocities. The disadvantage of this system is that the warning time depends on the amount of time between the initial divergence and the maximum radial velocity difference of the outflow which can occur simultaneously (Wilson et al, 1984).

Campbell and Olson (1986) developed a rule-based expert system to detect wind shear from Doppler radar data and named this system WX1. An expert system is one which attempts to model the structure of the process of deduction and the knowledge of the forecaster. The WX1 system has the capability of predicting microburst outflows in a more timely manner than the surface outflow algorithm by considering features other than just surface divergence, such as features at middle- and upper-levels. The WX1 system recognizes surface (below 1 km AGL) divergence, middle-level (1 to 2.5 km AGL) rotation, upper-level (above 2.5 km AGL) convergence and high reflectivity areas or reflectivity cores (Campbell 1986, 1989). Reflectivity cores are determined by a minimum and maximum reflec-tivity. That is, the reflectivity core is the area within the cloud which contains at least a minimum reflectivity (such as 45 dBz) and also at least a maximum reflectivity value (such as 54 dBz). Combinations of these features such as convergence aloft combined with a descending reflectivity core are recognized to be microburst precursors. These additional features increase the time between microburst precursor detection and microburst occurrence to 5 to 10 minutes (Roberts and Wilson, 1986).

The WX1 system performs successive stages of abstraction of the radar data in the interpretation of wind shear events. First, a feature extraction algorithm is executed, and then the extracted features are compared to several wind shear models (microburst, gust front, bad data) and also to previous features which may have been detected on previous volume scans. Confidence factors were used in order to rank features as to the certainty that they represent meteorological phenomena. For example, if a surface divergence feature was detected on a given volume scan and on a previous volume scan it was associated with mid- or upper-level microburst precursors, it would have a very high confidence factor whereas a surface divergence feature alone would have a low confidence
factor.

The microburst recognition system was developed further in Campbell (1988), in which the new system was called WX2. The WX2 system which is the successor to the WX1 system is a combination of Merritts algorithm and features aloft (microburst precursors). The WX2 system is based upon the microburst models put forth in Roberts and Wilson (1989). The WX2 system contains more microburst precursors which include upper-level (above 7 km AGL) divergence, middle-level convergence (1.5 to 7 km AGL), middle-level rotation (1 to 5 km AGL), lower divergence (0.3 to 1 km AGL), surface divergence (below 0.3 km AGL), storm cells (30 dBz contour) and storm cores (50 dBz contour). In addition to these, descending reflectivity cores are recognized to be when the lower limit of the core descends below 2.5 km AGL. All of these parameters are site adjustable and vary geographically. The use of these microburst precursors allows the system to make a microburst declaration while the outflow is still less than 10 m/s, thus increasing the warning time. Also, since the strength of the features aloft is somewhat related to the strength of the outflow in some areas (Biron and Isaminger, 1989), the strength of features aloft adds clues to the changing strength of the surface outflow (Isaminger, 1987). An example was given showing that by using microburst precursors, a microburst hazard was recognized 1.3 minutes earlier than would have been possible and a middle-level microburst precursor was recognized 7.5 minutes prior to the event.

The WX2 system structure is similar to WX1 and is broken into two parts: feature extraction and symbolic reasoning. The feature extraction step is when two-dimensional features are extracted from the radar data such as rotation or reflectivity cores. The symbolic reasoning step is when the two-dimensional features are combined into three-dimensional features. There are two stages in the symbolic reasoning: vertically correlate features of the same type to produce velocity and reflectivity structures and second to create complex structures which contain features of different types.

The WX2 system was used to develop the prototype TDWR microburst recognition algorithm. The prototype algorithm has three sections: feature extraction, vertical integration and microburst recognition (Campbell, 1989). The feature extraction section is the same as the WX2 system and the vertical integration is essentially the symbolic reasoning step in WX2. The microburst recognition step is made up of two algorithms: the surface outflow algorithm which evaluates the spatial and temporal aspects of the surface outflow and the microburst precursor algorithm which evaluates structures aloft to determine if a microburst is expected. The microburst recognition algorithm can declare a microburst if there is a weak surface outflow that is less than the threshold of 10 m/s and one of the following three microburst precursor signatures: 1) a descending reflectivity core and convergence aloft, rotation aloft, divergence aloft or lower divergence, or 2) a reflectivity core and convergence aloft or rotation aloft which extend below 3.5 km AGL or 3) descending convergence or rotation aloft. The descending reflectivity core was changed from the WX2 system value in Campbell (1988) to occur when the lower limit of the reflectivity core descends below 2 km AGL (Campbell, 1989) and is based on Isaminger (1987). Based upon results from 26 microbursts in Denver, Colorado in 1988, the use of features aloft increase the probability of detection of microbursts from 85.5% to 90%, and in 1989 at Kansas City, Kansas the prototype microburst recognition algorithm successfully predicted 89% of the microburst outflows of at least 10 m/s (Campbell and Isaminger, 1990).

A problem associated with all of the microburst recognition algorithms which are based on single-Doppler radar data is when the microburst outflow is asymmetrical. Wilson et al (1984) found that microburst asymmetry increased with increasing diameter and that on average, the maximum shear axis is twice that of the minimum shear axis. Microburst asymmetry makes recognition much more difficult due to a possible under or over estimation of the microburst outflow speed (Hjelmfelt, 1988, Wilson et al, 1984). An example would be if an asymmetrical microburst outflow was oriented with respect to the radar such that the radial velocity difference was less than the threshold value of 7.5 m/s (assuming a precursor was detected), but the maximum shear axis had a radial velocity difference of 30 m/s or more. The microburst outflow would be underestimated by the radar and a potentially hazardous situation could exist to aircraft. Asymmetry may be caused by several things such as storm motion, an asymmetrical reflectivity core or contamination from other outflows. Eilts (1987) reported that microburst asymmetry is apparently common in Oklahoma, and Hjelmfelt (1987) reported that asymmetry is also common in Denver.

Some of the parameters in the microburst recognition algorithm are site adjustable and vary with geographical location, and this variation is related to the fact that the microburst precursor signatures vary geographically. In Denver, Colorado the reflectivity core had to

develop at a height of at least 5 km AGL and descend below 2.5 km and have a maximum reflectivity of at least 50 dBz (Campbell, 1988), whereas in Kansas City, Kansas the reflectivity core must have a minimum height of 4.5 km and a maximum reflectivity of at least 54 dBz (Campbell and Isaminger, 1990). These minimum height and maximum reflectivity criteria were based on a previous study by Isaminger (1987). The Kansas City, Kansas area was found to have several microburst events which did not develop the minimum height of the reflectivity core and were subsequently missed. It was found that by lowering the maximum reflectivity threshold to 51 dBz would increase the amount of microbursts detected without a significant increase in the false alarm rate (Campbell and Isaminger, 1990). Table I-1 summarizes the microburst detection algorithms.

It became apparent that the next generation radar system (NEXRAD) would generally not be located near enough to all of the airport locations in the United States to observe microburst outflow characteristics. Also, the NEXRAD system is not designed to provide surface measurements often enough (5 - 6 minutes whereas the TDWR updates volume scans every 2 - 3 minutes). In response to these problems, the Terminal Doppler Weather Program was developed (TDWR) (Turnbull et al, 1989). The TDWR project is being developed by Lincoln Laboratory (M.I.T.) under sponsorship of the FAA and is being tested by using the FAA/Lincoln Laboratory FL-2 radar (Evans and Johnson, 1984).

Table I-1. Algorithm Comparison.

	Recognized Features	Method	Warning Time
Merritts	-Surface Divergence		About 0-5 min.
WX1	-Surface Divergence -Mid-Level Rotation -Upper-Level Conv. -Reflectivity Cores -Descending Cores	2 Stage: 1) Feature Extraction 2) Model Comparison	About 5-10 min.
WX2	-Surface Divergence -Lower Divergence -Mid-Level Rotation -Mid-Level Conv. -Upper-Level Div. -Storm Cells -Reflectivity Cores -Descending Cores	2 Stage: 1) Feature Extraction 2) Symbolic Reasoning	About 5-10 min.
TDWR Microburst Algorithm	-Surface Divergence -Lower Divergence -Mid-Level Rotation -Mid-Level Conv. -Upper-Level Div. -Storm Cells -Reflectivity Cores -Descending Cores	3 Stage: 1) Feature Extraction 2) Vertical Integration 3) Microburst Recognition	About 5-15 min.

The FL-2 testbed radar is testing and developing several algorithms associated with predicting and detecting wind shear. The FL-2 radar is a portable pulsed S-band Doppler radar which was in Memphis, Tennessee in 1985, Huntsville, Alabama in 1986, Denver, Colorado in 1987 and 1988, Kansas City, Kansas in 1989 and is currently operating in Orlando, Florida. The goal of the TDWR program is to locate a single-Doppler radar in the vicinity of an airport. Computer algorithms, which create geographic situation displays placed in the airport control towers so that air traffic controllers can advise pilots of hazardous wind shear, have been developed as of today.

2) MICROBURST MODEL

The microburst recognition algorithm employed at the TDWR testbed site is used in this thesis in the interpretation and location of microburst precursors. This algorithm is not infallible, and this is especially true in the case of multi-cellular storms such as August 28, 1989. The algorithm data was edited for the August 28, 1989 storm in order to improve the accuracy of the interpretation of the microburst event.

The microburst recognition algorithm is based upon the high reflectivity microburst model (Roberts and Wilson, 1989). The two microbursts that will be studied in this thesis are of a lesser reflectivity class and actually fit the criteria for the moderate reflectivity microburst model (Roberts and Wilson, 1989). Consequently, the timing of the precursors associated with the two microburst events will be compared to the moderate reflectivity model. Despite the fact that the microburst recognition algorithm is based upon the high reflectivity event, the criteria for recognizing the precursors differ only in the minimum reflectivity threshold for the maximum reflectivity core (54 dBz). Since both storm types fail to attain this reflectivity, the algorithm has difficulty recognizing cores and descending cores.

Table I-2 compares the timing of the two microburst models. The main differences between the two are that a descending reflectivity core is more common in the moderate reflectivity event, and that the storm continues to grow after the microburst event in the high reflectivity model, while it quickly dissipates during the microburst event in the moderate reflectivity model.

Table I-3 lists the precursors that will be used to infer the forcing mechanisms of the two microbursts. A brief description of the importance of each precursor with respect to the two microburst events is summarized in the right hand column. It must be stressed that not all possible precursor functions are listed, only those relevant to the investigation of the microburst events in this thesis. Figure I-2 illustrates the structure of a microburst and the process of development.

Table I-2. Microburst Model Event Sequence.
(Based upon Roberts and Wilson, 1989)

Event Time	Moderate Reflectivity Event (40 - 55 dBz)	High Reflectivity Event (> 55 dBz)
T-10	-Some convergence is present incloud betweem 3 and 8 km	-Storm grows rapidly. -Convergence is increasing at 6 km.
T-5	-Reflectivity core is descending. -Incloud convergence increasing . -Rotation below 3 km and a reflectivity notch above 4 km may be evident.	-Storm continues rapid growth. -Convergence at 6 km continues to increase. -Rotation just prior to the surface divergence is likely in the lowest 3 km. -Reflectivity core might be descending.
T=0	-Convergence has increased further. -Rotation is likely. -A reflectivity notchn is becoming more apparent between 3 and 6 km. -The reflectivity core has descended from 6km and is now collocated with the surface divergence.	-Storm attains 60-65 dBz. -Widespread convergence exists throughout the storm. -The reflectivity core has most likely reached the surface.
T+5	-Convergence at 6 km has decreased. -Convergence at 3 km has increased. -Rotation is more obvious. -The storm typically dissipates rapidly after the microburst attains its maximum strength.	-Rotation and convergence are apparent at 3 km. -The reflectivity core is at the surface. -The storm continues to grow. -The diverging outflow can evolve into a macroburst.

Table I-3. Precursors Used in Thesis for Microburst Recognition.

Precursor	Functions or Indications
Descending Reflectivity Core	-Indicates imminent microburst development. -Triggered by precipitation loading, evaporation, vertical pressure gradients, etc.
Mid-Level Convergence	-Supplies dry air which results in evaporation. -Response to descending reflectivity core.
Mid-Level Rotation	-Vorticity stretching in response to descending reflectivity core. -Creates vertical pressure gradients which instigat the descent of the reflectivity core.
Upper-Level Divergence	-Associated with strengthening outflow velocities. -Indicates the top of an updraft.

3) THESIS TOPIC

As stated earlier, the purpose of this thesis is to study two microbursts which originated from two thunderstorms in the Kansas City area. The first microburst producing thunderstorm occurred on May 14, 1989 and the second on August 28, 1989. Both of these thunderstorms produced multiple microbursts, but for this thesis only one from each will be investigated. The format will be to determine which precursors played roles in the development of the microbursts and from this, the forcing mechanisms for the microbursts will be determined.

The precursors and forcing mechanisms of these two microbursts will be compared and contrasted with each other and with the typical microburst event (Figure I-2) which is based upon the microburst model of Roberts and Wilson (1989). In addition, the environmental situation for each storm will be discussed in order to substantiate the hypothetical forcing mechanisms and to give clues as to the factors associated with the storm development. In the course of the investigation, certain weaknesses in the microburst recognition algorithm were detected. Suggestions for improving certain aspects of precursor detection will be given.

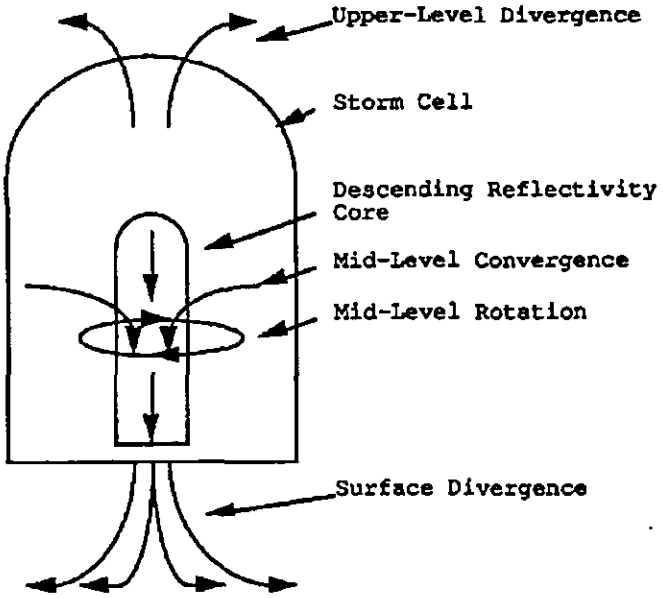

Figure I-2. Typical Microburst Event. (Redrawn from Campbell and Isaminger, 1990.)

B) DATA

The radar and computer algorithm data used in this thesis were provided by the mobile FL-2 site of the Lincoln Laboratory of the Massachusetts Institute of Technology under sponsorship of the Federal Aviation Administration. Other forms of data were provided by the author excepting the satellite map and sounding for May 14, 1989 which were also provided by Lincoln Laboratory.

1) FL-2 AND UND RADAR DATA INFORMATION

The FL-2 Doppler radar is an S-band radar and was located about 10 km SSW of the KCI airport and cooperated with the University of North Dakotas (UND) C-band Doppler radar which was located about 20 km to the east. These two Doppler radars enabled the development of three dimensional dual-Doppler analyses of wind shear events. Table II-1 shows the attributes of the two radars. The FL-2 radar is a more powerful (peak power of 1100 kW vs. 250 kW), more accurate (resolution of 120 m vs. 250 m) and more sensitive radar than the UND radar. Also, the FL-2 S-band radar does not suffer from attenuation due to scattering by water as is possible with the UND C-band radar. Consequently, FL-2 single-Doppler radar data was used in the analysis of the two storms due to its superior qualities.

Table II-1. Characteristics of the FL-2 and UND Radars.

Characteristic	FL-2	UND
Beamwidth	1°	1°
Wavelength (cm)	10.6	5.4
Peak Power (kw)	1100	250
Sensitivity At Nominal Range of 50 km (dBz)	-5.5	-3.1
Clutter Suppression (dB)	50	20
Maximum Range (km)	456	226
Range Gate Spacing (m)	120	250
Scan Strategy	PPI/RHI	PPI/RHI
Maximum Scan Rate (deg/sec)	10	16

(Table taken from Isaminger, 1989)

Two storms were studied; one which occurred on August 28, 1989 and another which occurred on May 14, 1989. One microburst from each storm will be studied. Figure II-1 shows the location of the two microbursts to the two radars and the KCI airport.

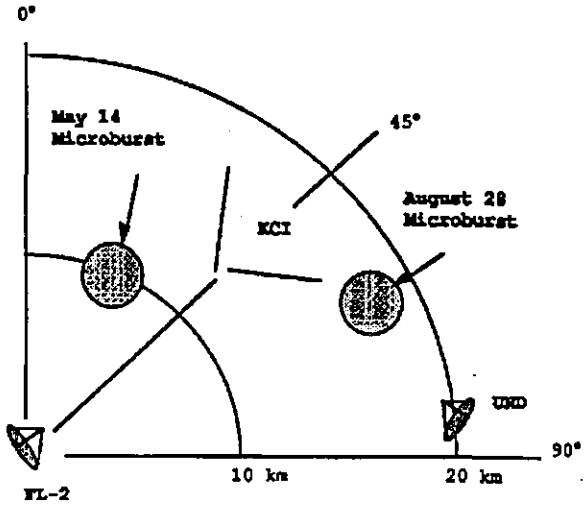

Figure II-1. Radar and Microburst Locations.

2) DUAL-DOPPLER RADAR DATA LIMITATIONS

For the investigation of these two storms, single-Doppler and dual-Doppler analyses were performed. Unfortunately, only surface dual-Doppler analyses are available due to the fact that both storms were too close to the FL-2 Doppler radar and the UND Doppler radar. The problem is a result of the manner in which the dual-Doppler data is produced. In order to produce a dual-Doppler image, one must construct a layer (which looks like a box) with a specified thickness and horizontal dimensions at the point of interest.

The first step in this procedure is to fill the layer with radar data using scans which increase consecutively in elevation angle. This is done for every available radar, (a minimum of two radars is required) so that layers are obtained for each radar, with all layers having the same size and location. The last step is to run a processing program which produces the dual-Doppler analyses.

The problems associated with this process are that the closer the layer is to the radar, the higher the elevation angle which is required to fill the layer; a layer which is farther away from the radar will not require as many consecutive scans. Another disadvantage to having a storm that is too close to the radar which requires several scans to fill with data (at close distances, the scan volume is smaller, thus requiring more scans to fill the volume of the layer), is that time elapses between the first and the last scans required for the layer. Consequently, if more scans are required to fill the layer, then the storm may have evolved during the time required to scan the storm, making the layer data inaccurate. The storms in this study were too close to the two radars for upper air dual-Doppler analyses. Therefore, only surface dual-Doppler analyses were available.

3) MAY 14, 1989 DATA

3a) Single-Doppler Radar Data

The following two tables are the single-Doppler data for the first storm which occurred on May 14, 1989. Table II-2 lists the PPI (Plan Position Indicator) data which will be used to recognize upper air precursors such as convergence, rotation, divergence and reflectivity core location. Only scans of the portion of the cloud above the lowest kilometer are used since the precursors are generally mid- and upper-level phenomena excepting the surface divergence feature of the surface outflow which will be displayed using dual-Doppler analyses.

Table II-2. FL-2 PPI Plots for May 14, 1989.

Time (U.T.)	Elevation Angle	Reflectivity Plot	Velocity Plot
19:23:01	18.6°		Figure III-17
19:28:22	13.1°	Figure III-9	
19:31:31	13.1°		Figure III-16

Table II-3 lists the RHI (Range Height Indicator) data used for the study of the May 14, 1989 microburst. The RHI data will be used to interpret precursor signatures such as reflectivity cores, convergence and divergence. No RHIs are available earlier than 19:30:15 from either radar since the radars were not scanning RHIs in the area of the microburst.

Table II-3. FL-2 RHI Plots for May 14, 1989.

Time (U.T.)	Azimuth Angle	Reflectivity Plot	Velocity Plot
19:30:15	14.0°	Figure III-6	Figure III-11
19:33:16	14.0°	Figure III-7	Figure III-12
19:39:32	20.0°	Figure III-8	Figure III-13

3b) Dual-Doppler Radar Data

Table II-4 shows the dual-Doppler surface plots to be used to interpret surface precursor signatures such as a surface divergence and reflectivity associated with the outflow. The smoothed windsplots have had the average environmental wind component removed from the observed wind field to enhance the microburst outflow. The resolution of the plots is 250 meters which is because this cannot be better than the radar with the poorest resolution (the UND radar). Plot times correspond (in order) to the following events: initial outflow, peak radial velocity and radial shear, and the dissipating outflow.

Table II-4. Dual-Doppler Surface Plots for May 14, 1989.

Time (U.T.)	UV Wind Component Removed (m/s)	Winds	Event
19:26:23	-4.7/-0.8	Figure III-1	Initial Outflow
19:38:42	-5.1/-0.2	Figure III-2	Peak Velocity
19:56:40	-5.5/+1.0	Figure III-3	Dissipation

3c) Microburst Recognition Algorithm Output

The computer algorithm used in this thesis is the microburst recognition algorithm discussed in the Introduction. As discussed earlier, this program searches for and evaluates precursors such as a descending reflectivity core, surface divergence, upper-level divergence, mid-level cyclonic and anticyclonic rotation, and mid-level convergence. The algorithm is subject to certain limitations such as a difficulty discerning individual reflectivity cores and/or attributing features to the wrong microburst in multi-cellular storms. These limitations are of particular importance when considering the August 28, 1989 storm due to its multi-cellular structure with multiple outflows, but not in the case of the May 14, 1989 storm due to its essentially single cellular structure and relatively few outflows. The algorithm correctly detected the features of the May 14, 1989 microburst and no substitutions or alterations of the data were necessary. The confidence in the algorithm output is enhanced by the fact that no other microbursts were operating in the immediate vicinity of the May 14, 1989 microburst, thus ensuring that the recognized precursors are solely associated with the one microburst.

Table II-5 is a summary of the microburst event. The microburst started at 19:26:23 and lasted for about 30 minutes with a radial velocity difference of at least 10 m/s. Compared to the average microburst lifetime of 13 minutes (Hjelmfelt, 1988) this is an unusually long lived event. The diameter of the microburst never exceeded 4 km, the upper limit on the size of a microburst (Fujita, 1981). The maximum radial shear was 23 m/s and is close to the average maximum value of 22 m/s (Wilson et al, 1984). Radial shear, the radial velocity with respect to radial distance, can be used as a measure of the intensity of a microburst. A minimum value would be 10 m/s of outflow speed over the maximum diameter of a microburst (4 km), yielding 2.5 m/s/km. An average value can be inferred from the average radial velocity and distance of 22 m/s and 3.1 km (Wilson et al, 1984) which yields an average radial shear of 7.10 m/s/km. The May 14, 1989 microburst had an average radial shear of 7.07 m/s/km, which compared to the average value, makes this a microburst of average intensity. Based upon the maximum radial velocity of this microburst, this would be classified a "strong" (20 - 24 m/s) microburst based upon the categories set up by Biron and Isaminger (1989).

Table II-5. Microburst Characteristics for May 14, 1989.

Start Time (U.T.)	19:26:23
End Time (U.T.)	19:56:40
Average Range Center	9.80 km
Average Range Center Difference	2.67 km
Average Azimuth Center	22.29°
Average Radial Velocity Difference	16.52 m/s
Average Radial Shear	7.07 m/s/km
Maximum Radial Shear	11.5 m/s/km
Maximum Radial Velocity Difference	23 m/s

Table II-6 is a list of the surface outflow features of the microburst. The centers of the outflow are calculated by the algorithm, and since this determination is based upon single-Doppler data, the apparent location of the center of the outflow may differ from the actual location due to asymmetry of the outflow. This may account for some erratic locations during the lifetime of the microburst since the outflow was in fact asymmetrical, which will be discussed later. The erratic locations show up primarily in the azimuth values which show a sharp change from 19:27:27 to 19:28:31 and significant changes from 19:51:57 to 19:56:40. These erratic values will not impair the investigation of the microburst for three reasons: 1) the variation is on a relatively small scale, 2) the general track of the storm is easily identified, and 3) since no other microburst outflows were in the immediate area, the variation was not due to distortions of the outflow caused by intersecting outflows.

Table II-7 is a list of the microburst reflectivity core attributes. Only reflectivities of 45 dBz or greater are included since the algorithm does not recognize reflectivity cores with a lower reflectivity than this value. This fact will prove to be a shortcoming of the algorithm in this case since this storm contains reflectivities which are frequently less than this minimum value and always less than the maximum reflectivity threshold of 54 dBz. Campbell and Isaminger (1990) noted that the maximum reflectivity criteria may be too restrictive for Kansas City microbursts and that more microbursts can be correctly detected by lowering the maximum value to 51 dBz.

The maximum reflectivities in this microburst never exceed even 51 dBz, indicating that the reflectivity core was not a leading precursor in the recognition of this microburst by the algorithm.

The core locations also display variability, and this is probably due to the fact that the algorithm searches for relative maximums in the reflectivity field and then attributes these maximums to a neighboring microburst. The reflectivity maximum associated with the microburst may be obscured by a neighboring higher reflectivity area and go undetected. This is usually not significant except in the case of multi-cellular storms, in which a neighboring higher reflectivity core may overshadow the actual lower reflectivity core of another microburst.

Table II-6. Surface Outflow Characteristics for May 14, 1989.

Time (U.T.)	RAC	Radial Velocity Difference (m/s)	Radial Distance (km)	Radial Shear (m/s/km)
19:26:23	10.2/09.3°	11	1.6	6.87
19:27:27	10.2/09.3°	13	1.6	8.12
19:28:31	9.7/14.0°	13	1.3	10.00
19:29:32	9.8/13.1°	15	1.6	9.37
19:30:32	9.7/12.9°	15	2.0	7.50
19:31:40	9.6/14.5°	15	1.6	9.37
19:32:34	9.5/15.4°	16	1.6	10.00
19:33:34	9.2/12.5°	17	1.7	10.00
19:34:39	9.5/14.6°	18	2.1	8.57
19:35:39	9.5/12.8°	20	2.7	7.41
19:36:40	9.3/15.7°	20	1.8	11.10
19:37:47	9.4/17.2°	23	2.0	11.50
19:38:42	9.4/17.2°	23	2.0	11.50
19:39:42	9.3/17.7°	23	2.0	11.50
19:40:46	9.4/19.7°	23	2.0	11.50
19:41:47	9.7/22.3°	22	2.4	9.17
19:42:47	9.8/23.7°	22	2.6	8.46
19:43:55	10.0/26.1°	21	4.0	5.25
19:44:50	10.0/26.1°	19	4.0	4.75
19:45:50	10.0/26.1°	18	4.0	4.50
19:46:53	10.2/27.3°	16	3.5	4.57
19:47:53	10.2/27.3°	14	3.5	4.00
19:48:53	10.2/25.3°	16	3.4	4.71
19:50:02	9.9/25.9°	15	3.2	4.69
19:50:56	9.9/25.9°	13	3.2	4.06
19:51:57	9.9/25.9°	13	3.2	4.06
19:53:00	9.9/32.3°	13	3.4	3.82
19:54:00	10.1/40.2°	12	3.7	3.24
19:54:37	10.1/40.2°	12	3.6	3.33
19:55:40	10.1/40.2°	11	3.6	3.06
19:56:40	10.1/40.2°	10	3.8	3.25

Table II-7. Microburst Reflectivity Core Locations for May 14, 1989.

Time (U.T.)	RAC	Height (km)	Core dBz
19:18:55	10.8/11.2°	1.3	45
19:19:01	10.8/11.2°	1.7	47
19:21:39	10.4/12.1°	0.4	47
19:21:46	10.4/12.1°	0.8	45
19:21:52	10.4/12.1°	1.2	48
19:21:59	10.1/07.7°	1.6	46
19:22:30	10.5/11.2°	0.2	47
19:23:22	10.3/09.7°	0.1	46
19:24:22	10.2/09.1°	0.1	46
19:24:30	10.2/09.1°	0.2	47
19:24:39	11.4/09.1°	0.4	46
19:24:54	10.3/12.5°	0.8	47
19:25:01	10.3/12.5°	1.2	49
19:25:08	10.3/12.5°	1.6	45
19:25:14	10.0/12.8°	1.9	45
19:25:21	10.0/12.8°	2.3	45
19:25:29	10.1/09.9°	0.1	49
19:26:23	10.1/09.9°	0.1	45
19:27:27	10.1/09.9°	0.1	45
19:27:55	10.3/10.9°	0.8	48
19:28:02	10.6/11.6°	1.2	48
19:28:09	10.3/12.4°	1.6	47
19:28:16	10.3/12.4°	2.0	45
19:31:04	10.2/12.9°	0.8	47
19:31:18	10.2/12.9°	1.5	45
19:34:02	9.7/15.2°	0.8	45
19:34:09	9.7/15.2°	1.1	45
19:34:23	9.7/15.2°	1.9	45
19:35:39	9.7/15.2°	0.1	45
19:36:40	9.7/15.2°	0.1	45
19:36:57	10.3/10.4°	0.4	45
19:37:12	9.5/16.2°	0.8	46
19:37:19	9.5/16.2°	1.1	45
19:37:25	9.5/16.2°	1.4	46
19:38:42	9.5/16.2°	0.1	45

Table II-8 shows the cyclonic rotation recognized by the algorithm. Some variability in the location is apparent but is probably due to the easterly storm movement during the nine minute gap between detection of the rotation. Table II-9 shows the anticyclonic rotation recognized by the algorithm. No large variability in locations is noted except for the time between 19:40:23 and 19:43:27, which could be due to storm motion during the three minute gap.

Table II-8. Mid-Level Cyclonic Rotation for May 14, 1989.

Time (U.T.)	RAC	Height (km)	Radial Velocity Difference (m/s)
19:23:01	11.9/16.9	3.8	10
19:23:07	11.9/16.9	4.5	9
19:23:14	11.9/16.9	5.2	12
19:32:05	9.3/19.4	2.5	11
19:32:12	9.3/19.4	3.0	10

TableII-9. Mid-Level Anticyclonic Rotation for May 14, 1989.

Time (U.T.)	RAC	Height (km)	Radial Velocity Difference (m/s)
19:28:22	10.2/12.6°	2.3	11
19:31:18	9.7/11.2°	1.5	11
19:31:31	9.8/13.6°	2.2	12
19:34:16	9.7/11.2°	1.5	10
19:34:23	10.1/11.9°	1.9	10
19:34:29	10.1/11.9°	2.3	10
19:37:19	9.4/12.2°	1.1	10
19:37:25	9.4/11.7°	1.4	13
19:40:23	10.0/12.7°	1.5	11
19:43:27	9.6/25.6°	1.1	10
19:43:43	9.6/25.6°	1.5	10
19:43:40	9.6/25.6°	1.8	10

Table II-10 shows the upper-level divergence recognized by the algorithm. The locations exhibit considerable variability and this is associated with the azimuth values. This is probably due to the fact the the upper portion of the storm had a wide area of divergence aloft (to be illustrated later) and the algorithm was again searching for relative maximum values which can move around. These erratic locations are acceptable since there was only one microburst operating in the area. Table II-11 shows the mid-level convergence recognized by the algorithm. In this case, the locations show only a minor variation.

Table II-10. Upper-Level Divergence for May 14, 1989.

Time (U.T.)	RAC	Height (km)	Radial Velocity Difference (m/s)
19:23:40	12.0/09.8°	6.6	14
19:23:46	10.8/17.2°	6.9	13
19:26:41	10.7/29.8°	6.1	14
19:26:47	10.7/29.8°	6.9	18
19:29:50	12.0/18.8°	6.8	15
19:29:57	12.0/18.8°	7.7	10
19:32:58	10.2/31.2°	6.6	15
19:35:58	11.0/37.4°	6.3	12
19:39:05	10.2/33.1°	6.6	13

Table II-11. Mid-Level Convergence for May 14, 1989.

Time (U.T.)	RAC	Height (km)	Radial Velocity Difference (m/s)
19:21:59	10.1/07.7¯	1.6	11
19:22:06	10.1/07.7¯	1.9	10
19:22:13	10.4/12.3¯	2.4	10
19:22:54	10.8/14.4¯	2.9	10
19:25:14	9.8/09.3¯	1.9	11
19:25:21	9.8/09.3¯	2.3	10
19:25:55	10.1/16.0¯	2.7	10
19:28:16	10.1/11.6¯	2.0	12
19:28:22	10.2/12.6¯	2.3	10
19:29:03	9.8/15.6¯	2.6	10
19:31:24	9.8/11.2¯	1.9	10
19:34:23	9.8/13.3¯	1.9	14
19:40:30	10.3/08.3¯	2.0	10

3d) Synoptic Situation

By examining the surface map for 18:00 U.T. on May 14, 1989 (Figure II-2), a converging band is visible in the Midwest. The converging flow in the Midwest is the result of the circulation pattern created by the high pressure area in the Great Lakes region and the low pressure area in the desert southwest. The satellite map near the time of the microburst (Figure II-3) shows the development along the band of convergent flow. The storm under study is located near Kansas City, Kansas. The sounding for 12:00 U.T. at Topeka, Kansas (Figure II-4), indicates a somewhat dry environment except for a moist area near 4 km. The vertical coordinate is given in height in order to ease the comparison of the vertical structure of the storm to the environment.

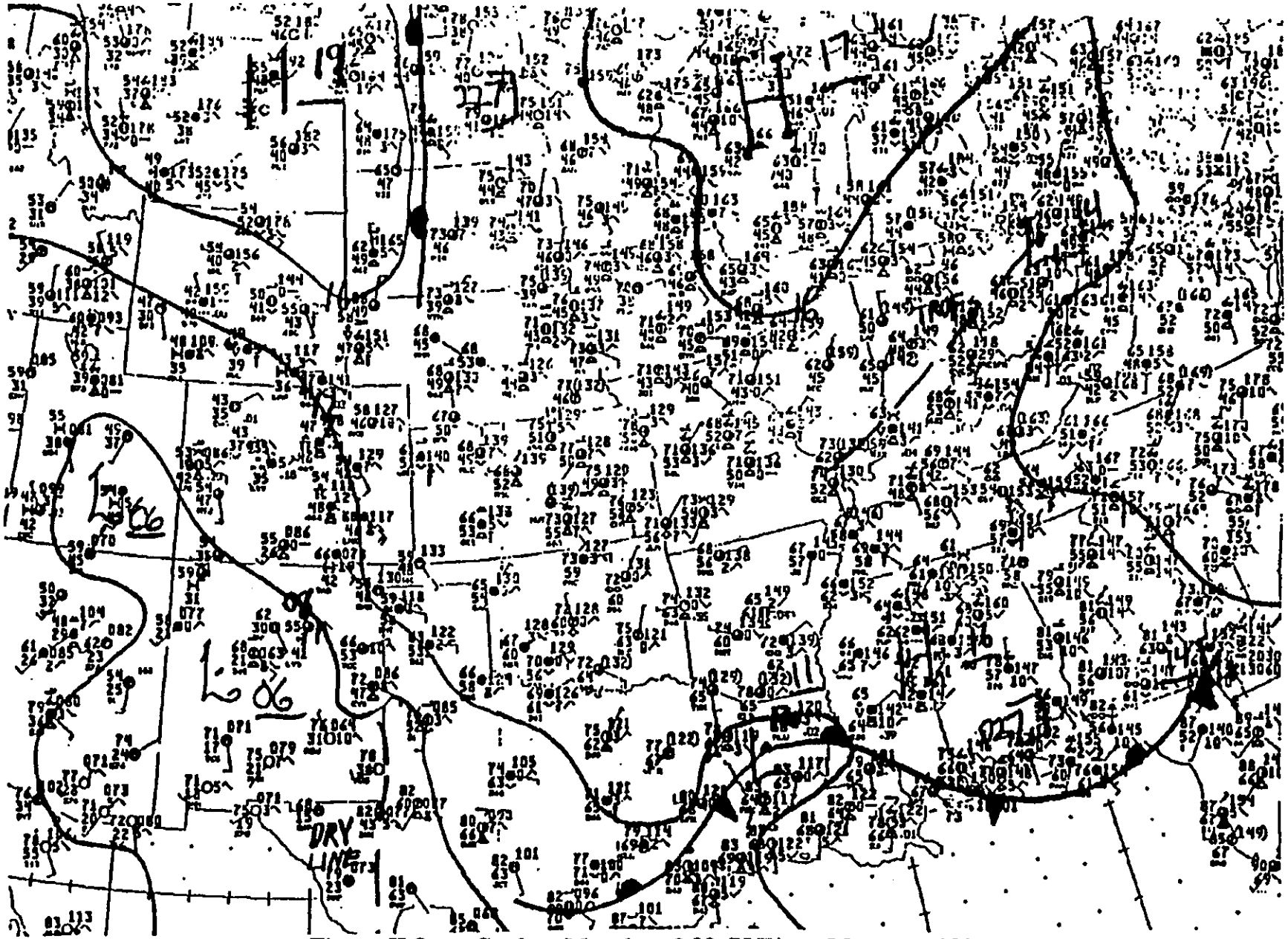

Figure II-2. Surface Map for 18:00 (U.T.) on May 14, 1989.

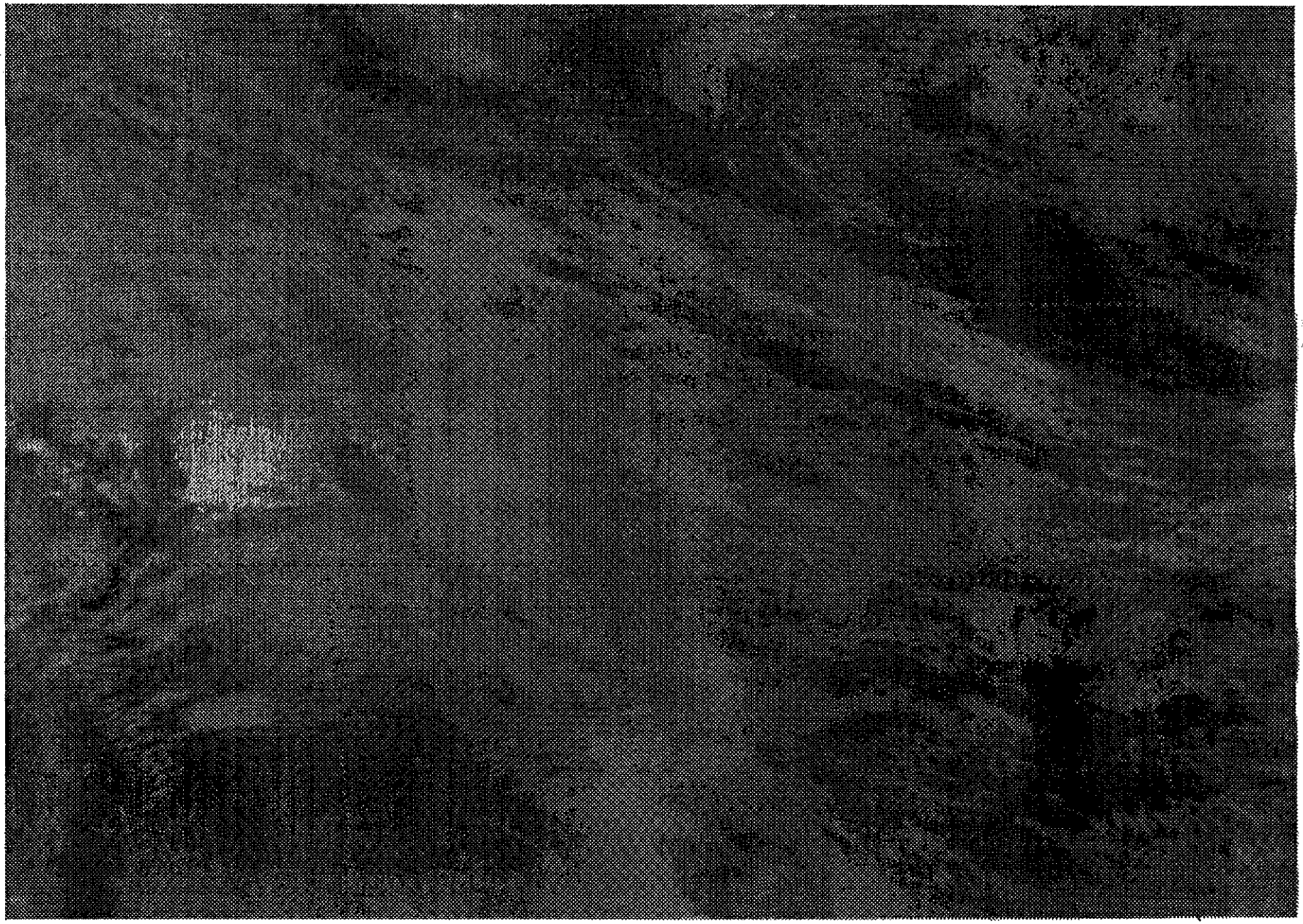

Figure II-3. Satellite Map for 19:31 (U.T.) on May 14, 1989.

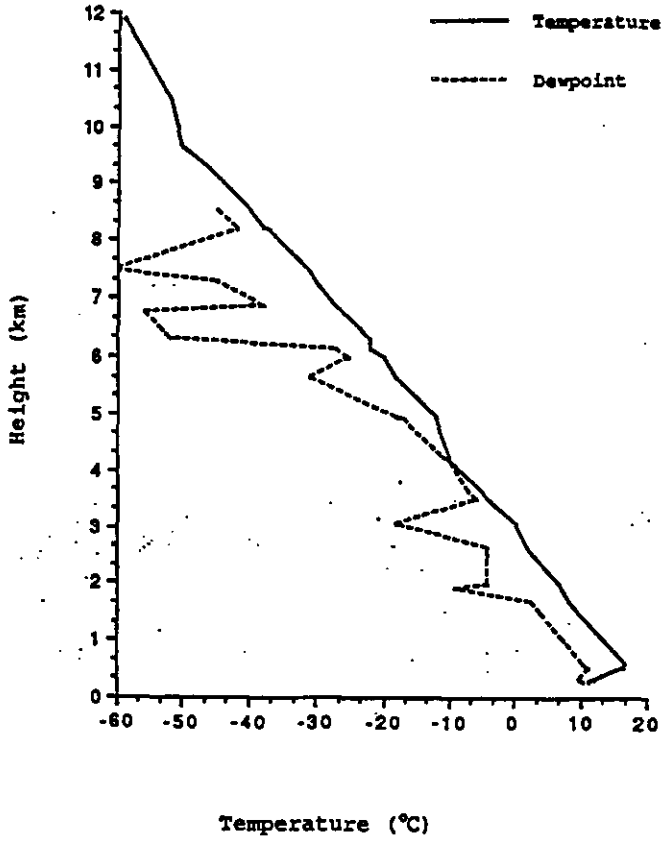

Figure II-4 Topeka, Kansas Upper Air Sounding.

At the time of the sounding, the air mass is relatively stable with a lifted index of 2.2 °C. However, at 19:00 U.T., near the time of the storm development, the surface temperature had increased to 23.3 °C with the same dewpoint temperature as before, creating a drier, more unstable environment with a lifted index of -1.4 °C and a near dry lapse rate of 8.75 °C/km in the lowest 1.5 km. As Srivastava (1985) pointed out, microburst activity can be accelerated in the subcloud region by evaporation for any rainwater mixing ratio, given a near dry lapse rate below cloud base. Since this lapse rate differs slightly from a dry lapse rate, slightly more water would be required to drive the downdraft than for a dry lapse rate.

4) AUGUST 28, 1989 DATA

4a) Single-Doppler Radar Data

The following two tables are the single-Doppler data for the second storm which occurred on August 28, 1989. Table II-12 lists the PPI plots to be used in identifying the same precursors as outlined earlier. Only data from the FL-2 site are included for the same reasons as for the May 14, 1989 storm.

Table II-12. FL-2 PPI Plots for August 28, 1989.

Time (U.T.)	Elevation Angle	Reflectivity Plot	Velocity Plot
21:39:45	13.1°		Figure III-35
21:40:21	15.6°	Figure III-27	Figure III-36
21:40:29	18.6°	Figure III-26	
21:40:35	21.8°		Figure III-32
21:42:29	6.7°		Figure III-31
21:43:27	15.6°	Figure III-28	
21:45:33	8.8°	Figure III-30	
21:46:25	15.6°	Figure III-29	

Table II-13 lists the RHI data used for the study of the August 28, 1989 microburst. This data will be used to recognize the same precursor signatures outlined in the May 14, 1989 microburst discussion. No RHIs are available earlier than 21:41:27 due to the fact that the radar was not scanning RHIs in the area. The two RHIs are not aimed exactly at the core locations but are the closest available.

Table II-13. FL-2 RHI Plots for August 28, 1989.

Time (U.T.)	Azimuth Angle	Reflectivity/Velocity Plot
21:41:33	68.0°	Figure III-24
21:47:30	66.0°	Figure III-25

4b) Dual-Doppler Radar Data

Table II-14 shows the dual-Doppler surface plots to be used in the interpretation of the surface precursor signatures. As in the May 14, 1989 storm, the smoothed wind plots have had the average environmental wind component removed from the observed wind field. More plots are included in the study of this storm due to the complex structure of the outflow. The complexity of the outflow is a result of many concurrent microbursts in the area creating colliding outflows. The resolution of the plots is 120 meters since the UND radar was using a pulse-paired processing technique which essentially doubled the resolution of that radar and consequently the resolution of the dual-Doppler analyses. Plots times correspond (in order) to the following events: initial outflow, peak radial velocity, peak radial shear, algorithm coast, and the dissipating outflow. A coast is performed every time a microburst drops below 10 m/s, in which most of the time, the microburst is dissipating. However, as in this case, the microburst may reattain the 10 m/s winds and continue. The coast occurred at 21:54:09 and accounts for that missing time period in Table II-16.

Table II-14. Dual-Doppler Surface Plots for August 28, 1989.

Time (U.T.)	Uv Wind Component Removed (m/s)	Winds	Event
21:46:55	-2.1/+5.9	Figure III-18	Initial Outflow
21:48:56	-1.2/+5.6	Figure III-19	Peak Velocity
21:50:52	-1.2/+5.0	Figure III-20	Peak Shear
21:54:09	-1.5/+3.6	Figure III-21	Coast
21:55:14	-1.4/+3.2	Figure III-22	Dissipation

4c) Microburst Recognition Algorithm Output

The following tables are the output from the microburst recognition algorithm. As mentioned earlier, the algorithm can attribute features to the wrong microburst when the individual microbursts are located close to each other. At instances where this occurs, substitutions or deletions in the algorithm data will be noted.

Table II-15 is a summary of the microburst event. This microburst started at 21:46:55 (U.T.) and lasted for only about 8 minutes. Compared to the average microburst lifetime of 13 minutes (Hjelmfelt, 1988), this is a relatively short lived event. The diameter of the microburst never exceeded 2.2 km, making this microburst a rather small microburst compared to the average size of 3.1 km (Wilson et al, 1984). The maximum radial velocity was 17 m/s, less than the average value of 22 m/s (Wilson et al, 1984). As a result of the small diameter, the average radial shear was 7.45 m/s/km which is somewhat larger than the average value of 7.10 m/s/km indicating that this was a somewhat intense microburst despite the below average radial velocities. This would be classified a moderate (15 - 19 m/s) microburst based upon the categories set up by Biron and Isaminger (1989).

Table II-15. Microburst Characteristics for August 28, 1989.

Start Time (U.T.)	21:46:55
End Time (U.T.)	21:55:14
Average Range Center	16.95 km
Average Range Center Difference	1.85 km
Average Azimuth Center	67.90 ^{0}
Average Radial Velocity Difference	13.13 m/s
Average Radial Shear	7.45 m/s/km
Maximum Radial Shear	11.54 m/s/km
Maximum Radial Velocity Difference	17.0 m/s

Table II-16 is a list of the surface outflow features of the microburst. As in the May 14, 1989 microburst, there is some variability in the location of the center of the outflow. This could be due to asymmetry but could also be caused by the fact that this storm produced many microbursts, several of which were occurring simultaneously. In fact, three other microburst outflows were located within three kilometers of the outflow and it is highly likely that the outflows were interacting, thus distorting the center of the outflow under consideration.

Table II-16. Surface Outflow Characteristics for August 28, 1989.

Time (U.T.)	RAC	Radial Velocity Difference (m/s)	Radial Distance (km)	Radial Shear (m/s/km)
21:46:55	16.9/63.2°	11	2.2	5.00
21:47:53	16.8/66.4°	12	1.9	6.32
21:48:56	16.9/64.5°	17	2.2	7.73
21:50:01	17.1/69.1°	15	1.6	9.37
21:50:52	16.9/69.8°	15	1.3	11.54
21:51:58	17.0/71.0°	14	1.5	9.33
21:53:03	17.0/70.1°	10	2.2	4.54
21:55:14	17.0/69.1°	11	1.9	5.79

During the lifetime of this microburst, the data contains a gap between 21:53:03 and 21:55:14 where the minimum velocity of 10 m/s was not detected at 21:54:09. This is the aforementioned algorithm coast. In this case, the outflow had not dissipated yet and produced 11 m/s one minute later and then dissipated. The outflow structure at the time of the coast is quite apparent on dual-Doppler plots and will be discussed further in the Analysis ofData section. Three minutes after the end of this microburst, another microburst reached full strength just 3 km away. This creates the illusion that the microburst under study had simply moved eastward when in fact it had dissipated.

Table II-17 is a list of the microburst reflectivity core attributes. The core locations suffer from the same type of erratic behavior as in the May 14, 1989 microburst but to a greater degree. This is most likely caused by: 1) the movement of the reflectivity maxima in the reflectivity field as mentioned earlier, and 2) the evaporation of the core associated with the microburst, causing the algorithm to attribute neighboring reflectivity maxima to this microburst. This is an example of when this works to a great disadvantage since the actual core associated with the microburst probably remained collocated with the outflow but had a lesser reflectivity, thus being ignored by the algorithm. A suggestion for the algorithm programming would be to consider evaporation processes and look more closely for the reflectivity maxima or minima in the case of extreme evaporation.

The plain text data are those considered to be truly associated with and correctly attributed by the algorithm to the microburst. The bold-faced data was attributed by the algorithm to this microburst but is most likely not associated with this microburst for two reasons: 1) the reflectivity cores were much closer to other microburst events, or 2) the higher reflectivity areas were not associated with any microburst events and were located in an area of the storm not involved in microburst production. The algorithm only attributed other reflectivity core areas to this microburst and not the other way around: no other core areas associated with this microburst were incorrectly attributed to other microbursts.

Table II-17. Microburst Reflectivity Core Locations for August 28, 1989.

Time (U.T.)	RAC	Height (km)	Core dBz
21:42:43	14.8/59.1°	2.9	54
21:45:13	16.4/56.2°	0.6	49
21:45:20	17.1/59.3°	1.3	51
21:45:33	16.5/62.0°	2.6	53
21:45:56	15.5/64.7°	0.1	48
21:46:39	12.1/57.1°	4.8	46
21:47:05	9.7/61.9°	5.6	51
21:48:46	20.5/68.0°	4.0	52
21:48:56	17.5/70.5°	0.1	48
21:49:06	20.7/68.8°	4.8	48
21:49:31	14.8/62.6°	4.1	50
21:49:38	13.2/66.3°	4.4	53
21:49:45	12.8/58.8°	5.1	56
21:50:01	18.0/70.9°	0.1	48
21:50:52	17.8/70.2°	0.1	48
21:50:58	21.9/70.9°	0.4	48
21:51:03	16.6/61.9°	0.6	53
21:51:09	17.0/63.4°	0.9	53
21:51:19	18.2/65.9°	1.6	48
21:51:25	22.2/63.3°	2.3	49
21:51:30	16.1/64.7°	2.0	52
21:51:58	18.5/76.2°	0.1	47
21:52:03	18.3/74.9°	0.3	48
21:52:09	17.8/72.9°	0.6	48
21:52:14	18.3/72.4°	1.0	49
21:52:19	16.9/66.2°	1.2	52
21:52:25	16.6/65.5°	1.5	53
21:52:30	17.2/66.4°	1.8	53
21:53:14	17.2/66.5°	0.6	51
21:53:20	17.4/66.5°	0.9	48
21:53:25	17.3/65.3°	1.2	54
21:53:30	17.5/63.9°	1.5	52
21:53:36	18.5/66.6°	1.9	46
21:54:20	17.9/65.7°	0.6	53
21:54:25	18.3/65.4°	1.0	53
21:54:30	17.7/64.9°	1.2	53
21:54:36	17.4/66.5°	1.5	48
21:54:41	17.5/67.0°	1.8	55
21:54:46	17.9/66.6°	2.2	53
21:55:14	18.2/63.9°	0.1	49
21:55:19	18.1/64.3°	0.3	51
21:55:25	19.1/66.3°	0.7	49
21:55:30	18.8/63.8°	1.0	49
21:55:35	18.7/66.2°	1.3	51
21:55:41	18.3/66.5°	1.6	53

Table II-18 shows the cyclonic rotation recognized by the algorithm. This rotation is interesting since it existed for only one volume scan and then dissipated. Table II-19 lists the anticyclonic rotation detected by the algorithm. Bold type is data incorrectly attributed to another microburst, where the rotation was much closer to this microburst event. Italic type is data wrongly attributed to this microburst, where the data was much closer to another microburst event.

Table II-18. Mid-Level Cyclonic Rotation for August 28, 1989.

Time (U.T.)	RAC	Height (km)	Radial Velocity Difference (m/s)
21:48:32	17.0/71.3°	2.0	11
21:48:39	17.0/72.8°	2.7	14
21:48:56	16.8/74.8°	3.3	11
21:49:06	16.8/74.7°	3.9	14
21:49:31	18.4/78.1°	5.2	22
21:49:38	18.0/78.7°	6.1	26
21:49:45	18.0/75.2°	7.2	19
21:49:52	16.6/77.2°	8.2	23

Table II-19. Mid-Level Anticyclonic Rotation for August 28, 1989

Time (U.T.)	RAC	Height (km)	Radial Velocity Difference (m/s)
21:39:45	12.9/57.6°	3.0	30
21:40:21	14.6/62.8°	4.1	29
21:40:35	14.2/60.7°	5.6	14
21:42:36	15.2/58.6°	2.4	19
21:42:43	15.7/60.3°	3.0	28
21:43:02	15.5/63.1°	3.6	23
21:43:27	15.9/69.6°	4.5	26
21:45:33	16.1/63.1°	2.5	16
21:45:40	18.2/64.6°	3.5	19
21:45:47	16.8/66.1°	4.0	15
21:46:25	16.7/68.8°	4.7	20
21:48:32	17.4/66.3°	2.0	14
21:48:39	16.9/68.0°	2.6	19
21:48:46	17.1/69.0°	3.3	18
21:49:06	16.6/71.8°	3.9	19
21:49:31	17.6/72.5°	4.9	21
21:49:38	18.0/73.1°	6.2	25
21:49:45	16.3/70.8°	6.6	22
21:49:52	17.1/67.7°	8.3	24
21:51:30	17.4/69.9°	2.2	10
21:52:35	17.7/69.9°	2.2	13
21:53:36	18.1/70.2°	1.9	13
21:53:41	17.5/70.5°	2.2	14
21:54:41	18.2/70.7°	1.9	13
21:54:46	17.7/70.0°	2.2	11

Table II-20 shows the upper-level divergence recognized by the algorithm. Only one instance was correctly attributed (plain text) by the algorithm to this microburst while the bold faced data was incorrectly attributed to another, more distant microburst. The two RHI plots show that upper-level divergence did in fact exist during periods other than those recognized by the algorithm. The RHIs indicate divergence at 16/68° on 21:41:33 and at 18.5/66° on 21:47:30. Upper-level divergence could not be determined past 21:50:25 because the scan strategy of the FL-2 radar did not scan high enough to determine features at that height. Table II-21 is the convergence as detected by the algorithm. The data in bold face was incorrectly attributed to a distant microburst while the plain text data was incorrectly attributed to this microburst despite the fact it was much closer to another microburst.

Table II-20. Upper-Level Divergence for August 28, 1989.

Time (U.T.)	RAC	Height (km)	Radial Velocity Difference (m/s)
21:44:14	16.9/66.5°	11.6	14
21:44:21	13.8/62.2°	11.8	13
21:50:19	17.5/73.1°	12.5	20

Table II-21. Mid-Level Convergence for August 28, 1989.

Time (U.T.)	RAC	Height (km)	Radial Velocity Difference (m/s)
21:42:29	15.2/59.5°	1.7	11
21:49:06	14.7/76.7°	3.4	13

4d) Synoptic Situation

By viewing the surface map for for 21:00 U.T. (Figure II-5), a weak cold front can be seen extending from the Dakotas to the desert southwest. A trough axis extends from near the Great Lakes region to near southern Kansas City, Missouri. Mild convergence exists near Kansas City as a result of the trough axis. Although the surface map does not show this entirely, I believe the convergence zone created by the trough axis actually extended further west than depicted, to western Kansas City, Kansas. This is supported by the east winds at Kansas City compared to the surrounding flow pattern. This convergence set off the storm which is visible near Kansas City on the satellite map of 21:31 U.T. (Figure II-6).

The sounding for Topeka, Kansas (Figure II-7) at 12:00 U.T. on August 28, 1989 indicates a fair amount of moisture aloft with a somewhat drier layer from the surface up to 2 km. Near the time the storm developed, the temperature and dew point had risen to 30.6°C and 24.4°C, respectively. The lifted index at the time of the sounding was a stable 2.5°C but destabilized significantly to -6.3°C at the time of storm development. The lapse rate in the lowest 2 km at the time of storm development was only 6.6°C/km. Based upon this lapse rate, a significantly greater amount of moisture would be required than for a dry lapse rate (based upon Srivastava, 1985), but microburst activity can certainly still be forced by evaporation processes in this environment.

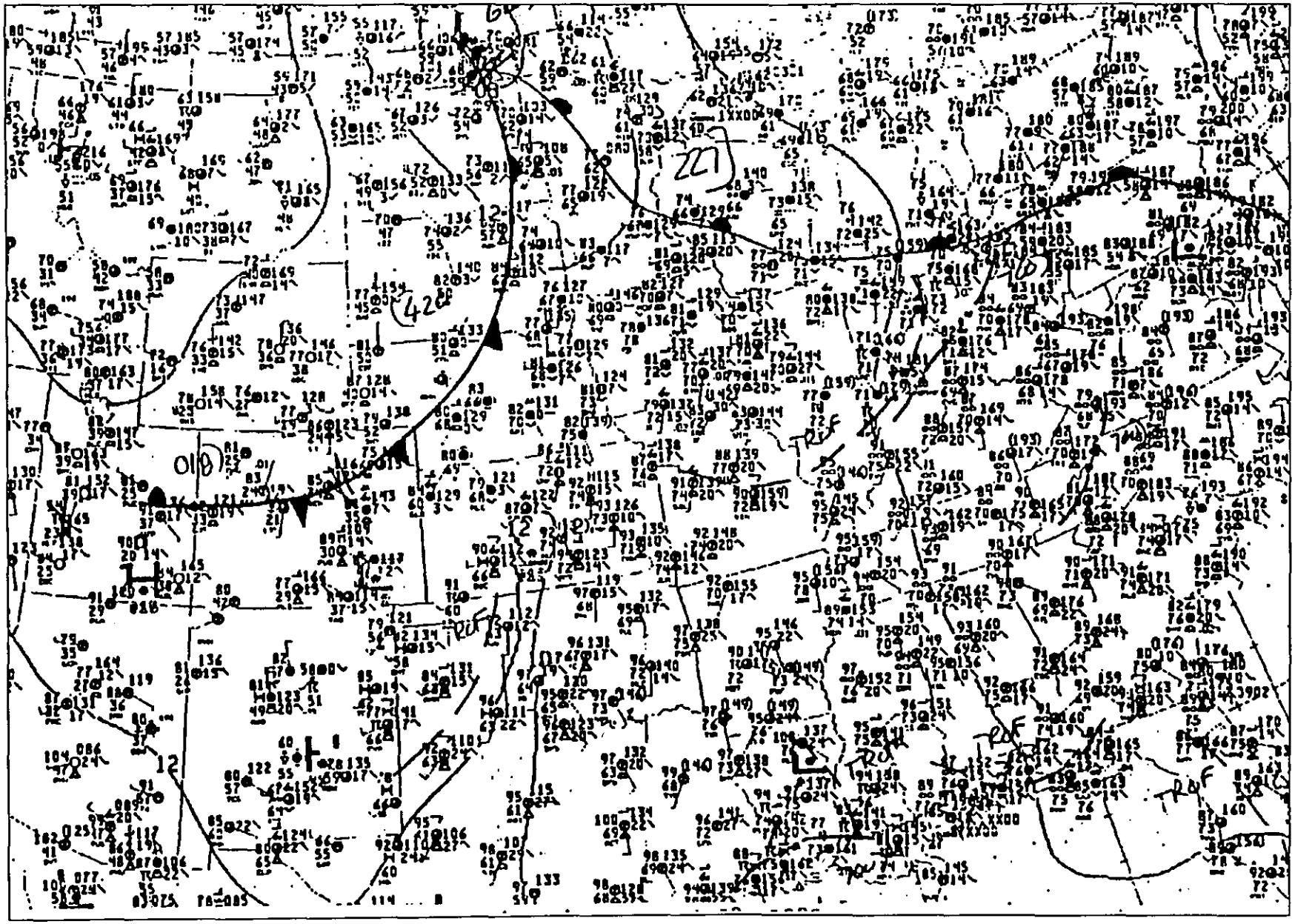

Figure II-5. Surface Map 21:00 (U.T.) on August 28, 1989.

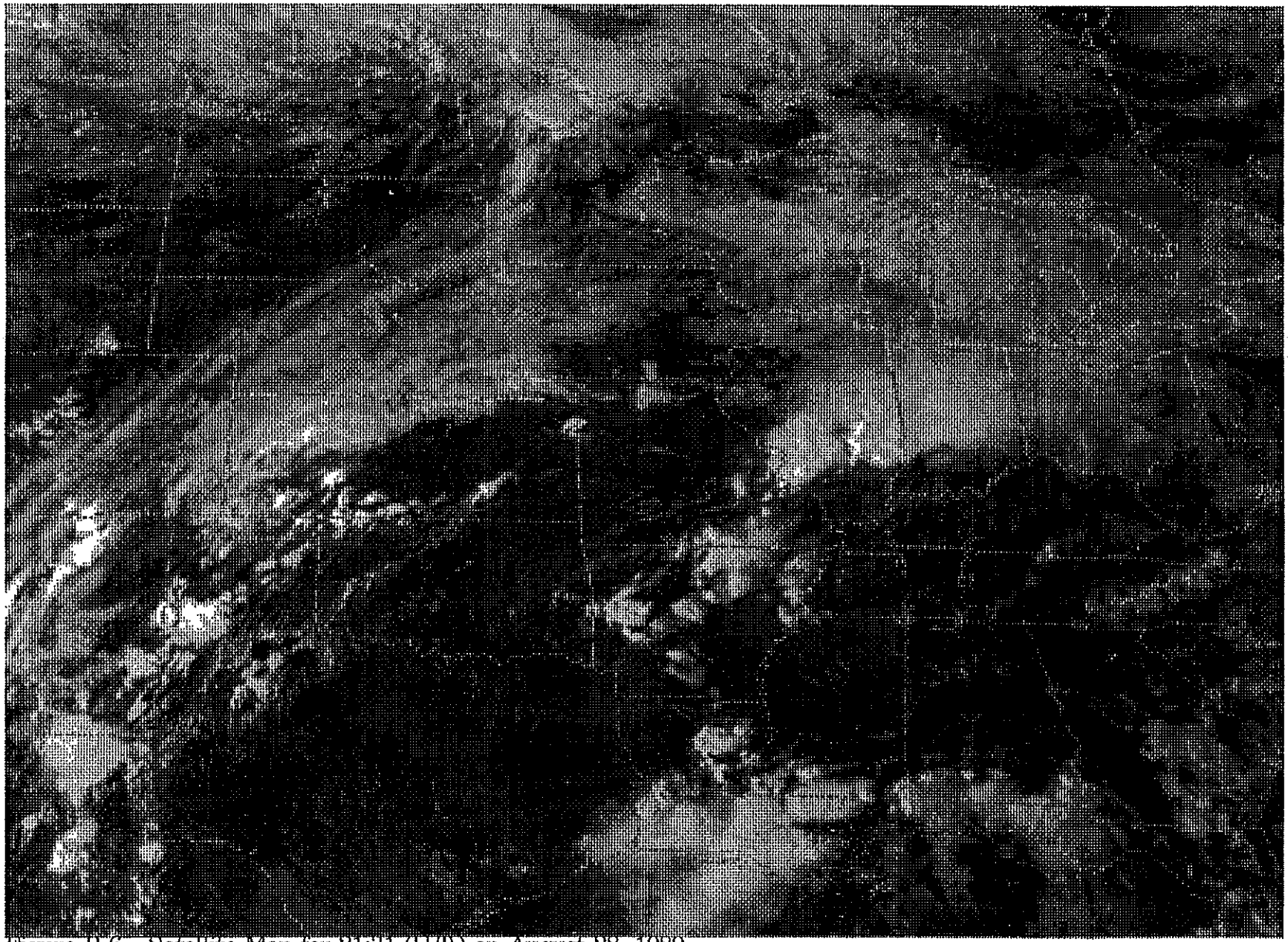

Figure II-6. Satellite Map for 21:31 (U.T.) on August 28, 1989.

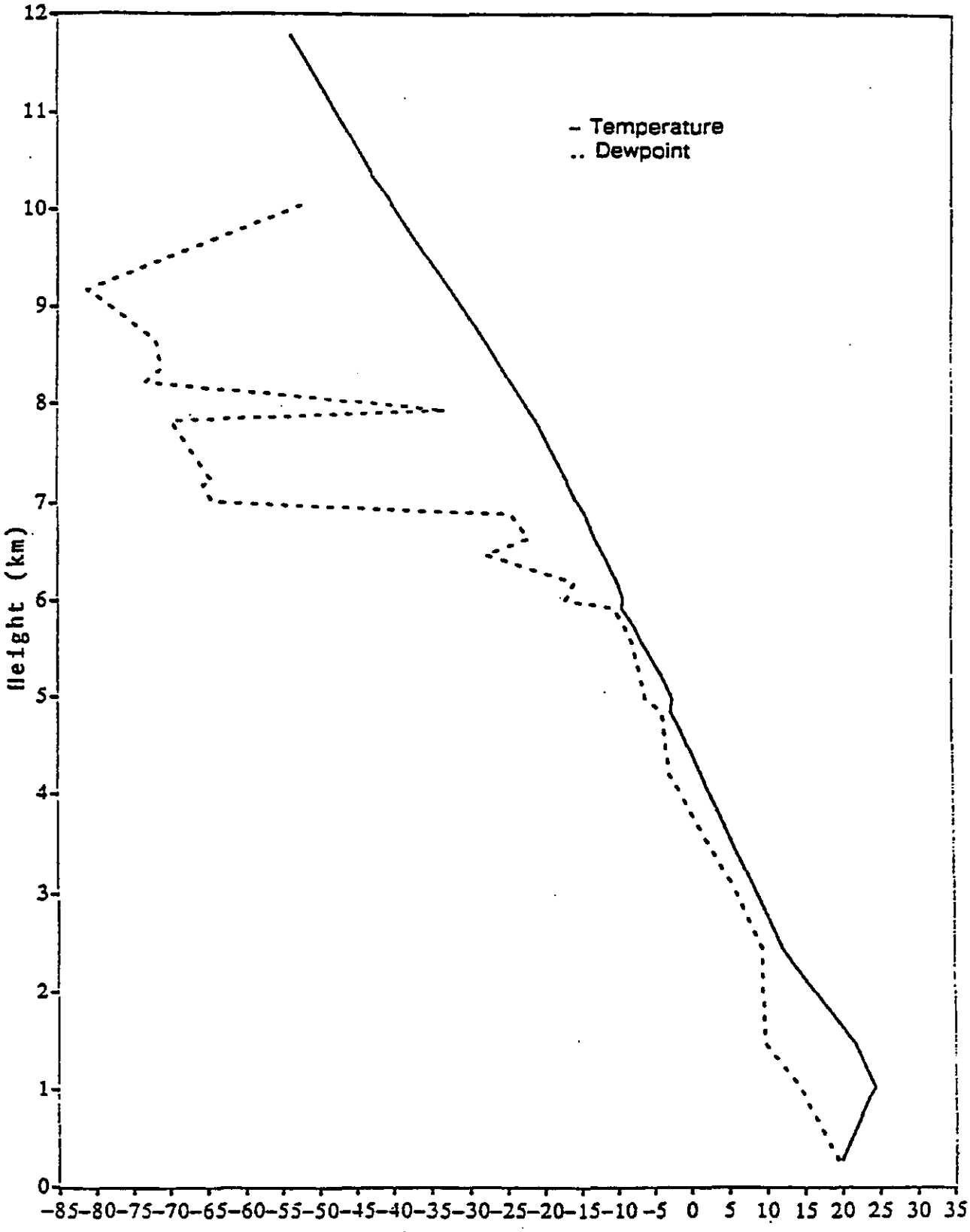

Figure II-7. Topeka, Kansas Upper Air Sounding.

5) SUMMARY

Both of these storms developed in relatively stable and somewhat dry environments. In both instances, surface convergence due to a trough axis or shear line played a key role in storm development. The atmosphere itself contained dry layers aloft.

The microburst recognition algorithm detected all of the precursors associated with the May 14, 1989 storm, but had a difficult time with the August 28, 1989 storm. These mislabeled data were a result of features being attributed to more distant microbursts rather than the microburst with which it was in close proximity. In addition, in the case of the August 28, 1989 storm, it was found that additional information could be added by including features recognized from RHIs. In instances where either substitution or deletion was made, the data was highlighted to indicate what data was to be used.

C) ANALYSIS OF DATA

For each storm, the microburst precursors recognized by the microburst recognition algorithm will be studied in conjunction with the radar data in order to determine the forcing mechanisms of the 5/14/89 and the 8/28/89 microbursts. Later, the microburst events will be compared and contrasted.

1) MAY 14 FORCING MECHANISMS AND PRECURSORS

For each storm, the first step in the analysis will be to show the surface divergence feature and then compare the important temporal features of the microburst outflow with the upper-air precursors. The last step will be to summarize the precursors involved in the microburst and state a hypothesis as to the forcing mechanisms of the microburst, as well as discuss the performance of the microburst recognition algorithm. During the study of the timing of the precursors, comparisons will be made to previous works and the moderate reflectivity model.

1a) Surface Divergence

The set of three dual-Doppler smoothed winds plots show the outflow throughout its lifetime: initial outflow (Figure III-1), peak (Figure III-2) and dissipating (Figure III-3). The smoothed winds have had the mean wind removed in order to show the direction of the actual winds associated with the microburst outflow. Figure III-1 is the winds analysis for 19:26:23, the first time the outflow reached 10 m/s. The outflow is located in the left central portion of the plot at xy grid point (19,43). An interesting phenomena associated with this microburst is the asymmetrical shape of the outflow. The asymmetry is quite apparent since the outflow is confined mainly to flowing north, south and somewhat east.

Figure III-2 is the winds analysis for 19:38:42, the time of the peak radial velocity and also the peak radial shear. The center of the outflow is at xy grid point (31,27). The asymmetrical shape of the outflow is even more apparent and is confined to flowing northeast, east and south.

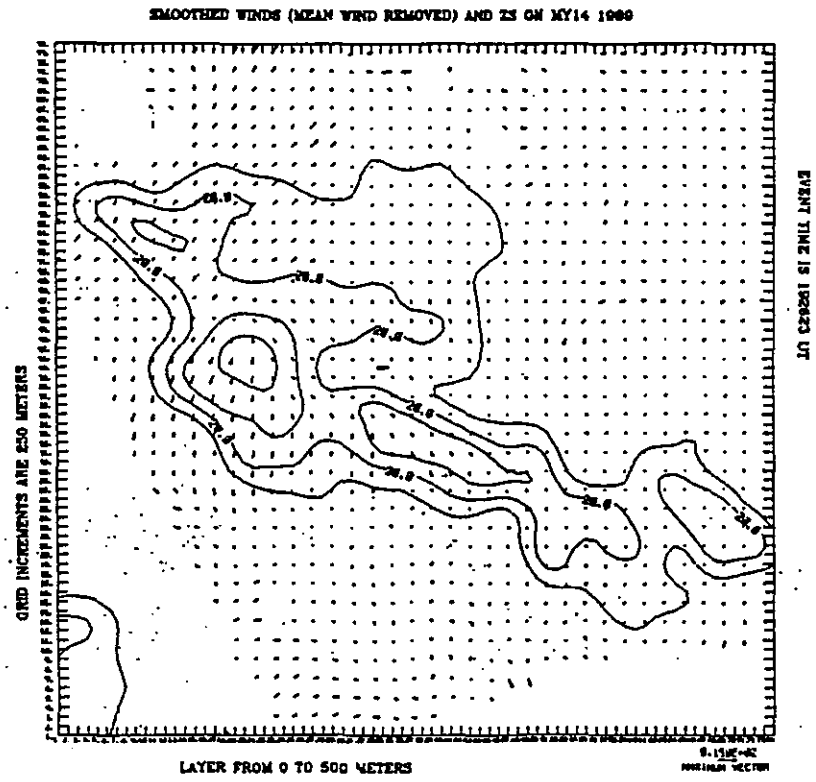

Figure III-1. 19:26:23 Dual-Doppler Winds and dBz Plot.

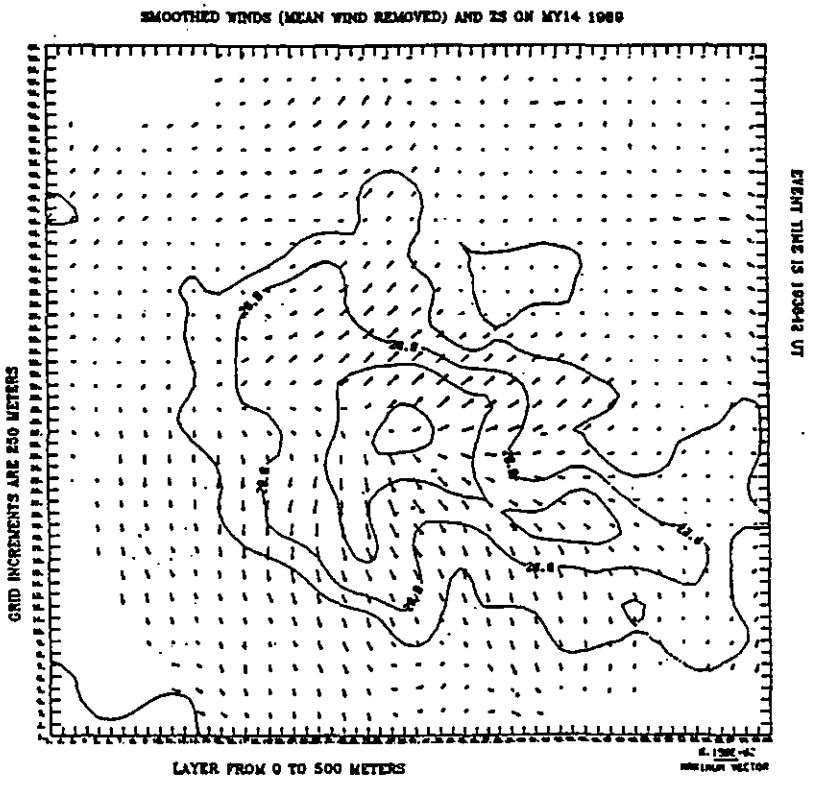

Figure III-2. 19:38:42 Dual-Doppler Winds and dBz Plot.

Figure III-3 is the winds analysis for 19:56:40, the last time the algorithm detected a radial shear of 10 m/s. The center of the outflow is positioned at (31,35). The asymmetry is still quite apparent and is confined to mostly north and south directions.

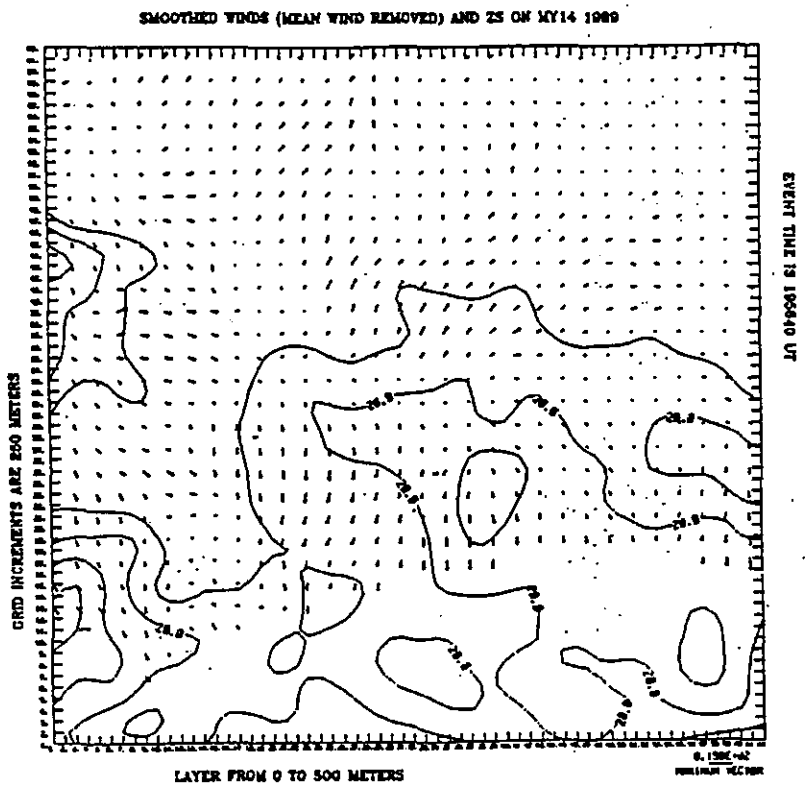

Figure III-3. 19:56:40 Dual-Doppler Winds and dBz Plot.

Microburst asymmetry is of particular concern to aviation since an asymmetrical microburst can have its stronger winds oriented perpendicular to a Doppler radar such that the radial velocity never appears to exceed 10 m/s. This outflow has significant asymmetry and this is easily seen in Figure III-4: a plot of the FL-2 observed velocity compared to the velocity observed by UND. In this case, the UND radar had difficulty observing the winds due to its orientation to the microburst and would not have issued a microburst alert in an operational mode despite the high winds that were actually present. Microburst asymmetry has been noted previously in microbursts in various parts of the country by Isaminger (1989), Eilts (1987) and others, with typical ratios on the order of 2 to 3:1. This microburst had an asymmetry ratio of about 3:1.

Microburst asymmetry is a relatively common occurrence and this is one of the arguments for developing a dual radar system to detect microbursts. The comparison of the observed velocities of both radars is only valid for single-cell storms with few concurrent surface outflows. This is because the combining of two or more microburst outflows may cause the outflows to appear asymmetrical due to contamination by other outflows. For this reason, microburst asymmetry will not be addressed in the multi-cellular August 28, 1989 storm.

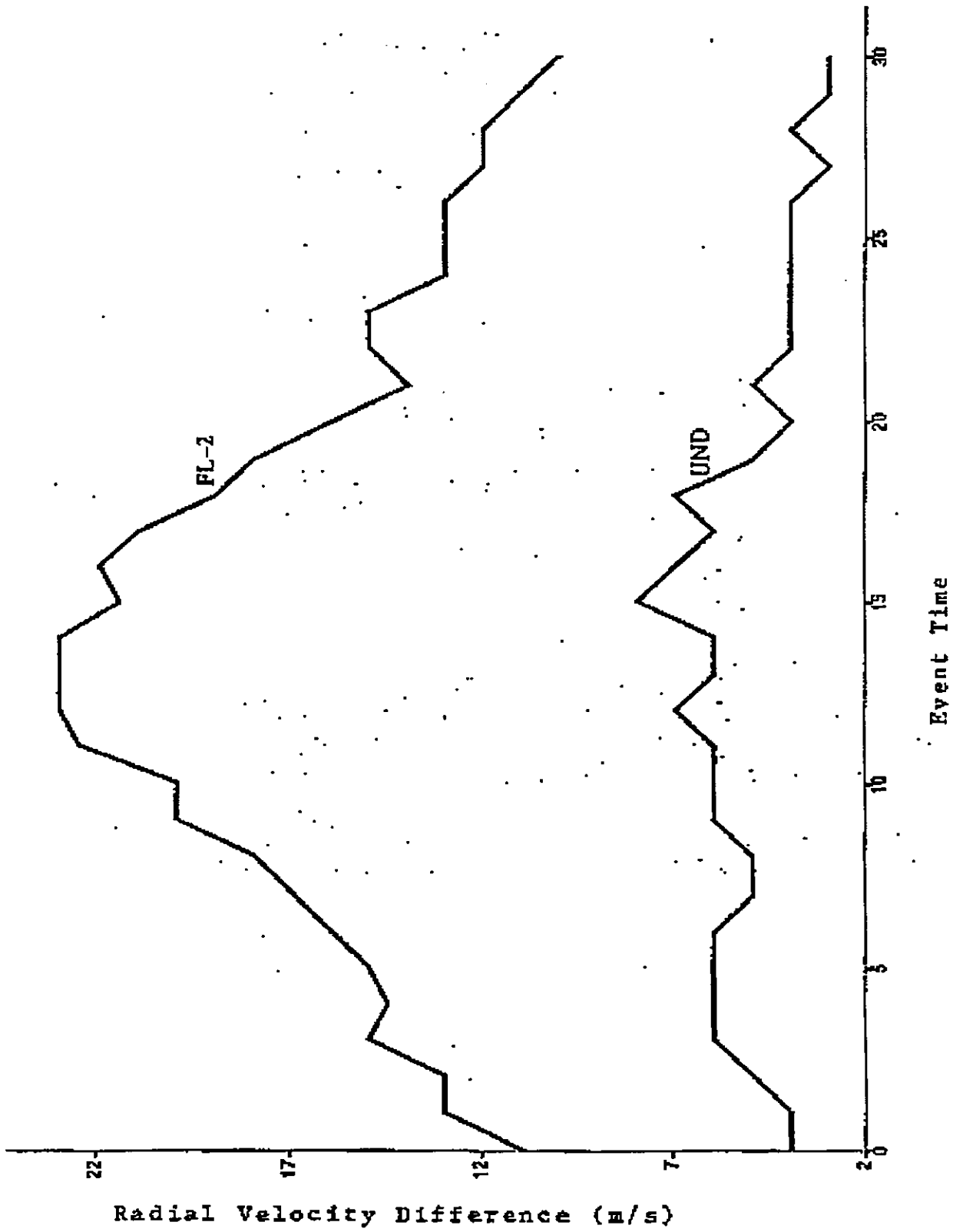

Figure III-4. FL-2 and UND Observed Outlow Velocities.

1b) Descending Reflectivity Core

Figure III-5 is a plot of the highest and lowest points the algorithm detected the reflectivity core for each volume scan. Based upon this plot, the reflectivity core begins descending between T-7 and T-5. Based upon the moderate reflectivity model (Table I-2), this is the typical time of descent for the core. The reflectivity core reaches the surface at T-3 and by T=0 is collocated with the microburst outflow, which is in accordance with the moderate reflectivity model. A series of RHI plots does the best job of illustrating the descent of a high reflectivity area. Unfortunately, neither the FL-2 radar nor the UND radar were scanning RHIs in the vicinity of the microburst until near 19:30:00, thus limiting the depiction of the descent of the core to RHIs after this time. A series of three RHIs will be used to display the descent: Figure III-6 (19:30:15), Figure III-7 (19:33:16) and Figure III-8 (19:39:32). Figures III-6 and 7 are at azimuth 14° and dont initially show where the 45 dBz area reached the ground since it reached the surface first at azimuth 10°, some seven minutes earlier. However, by viewing the three RHI plots, the descent of the core can be seen to continue over the nine minute period.

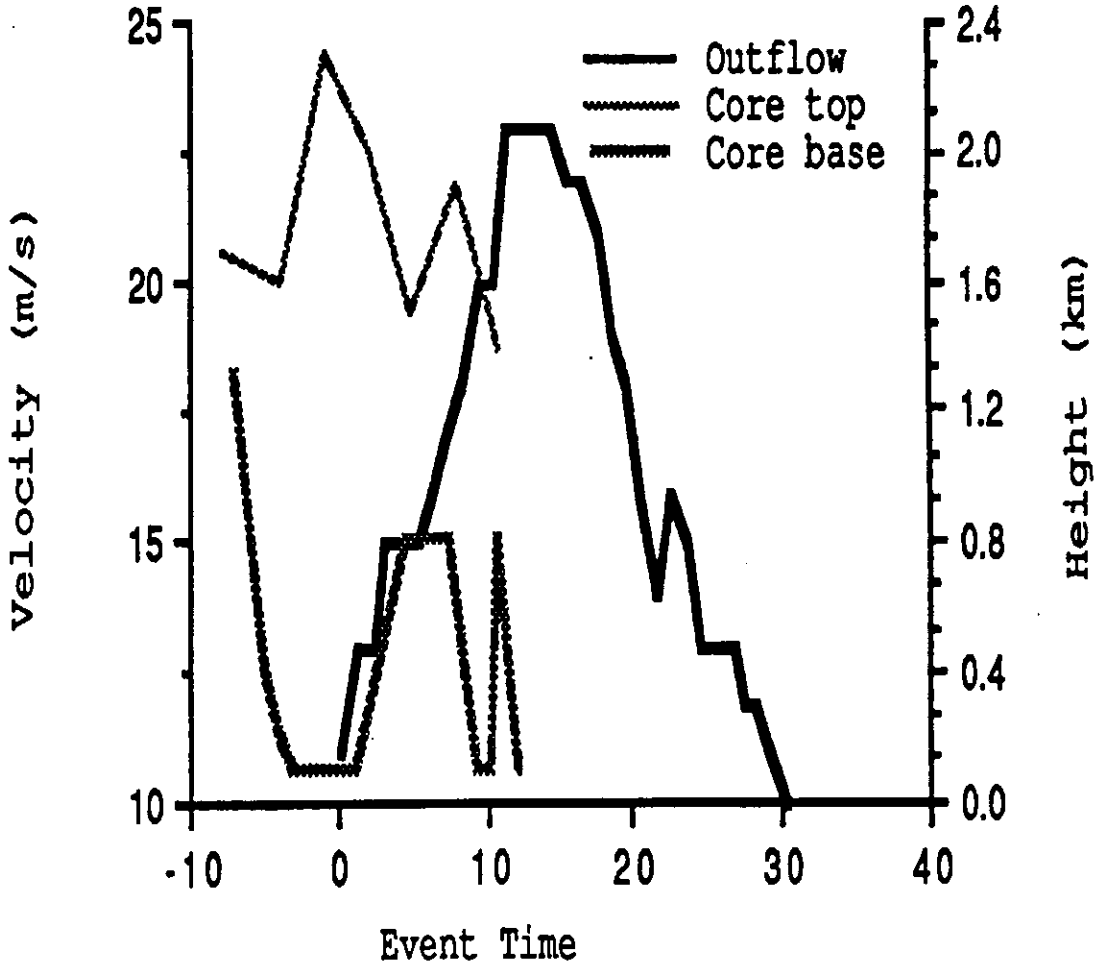

Figure III-5. Core Structure and Outflow Characteristics for May 14, 1989.

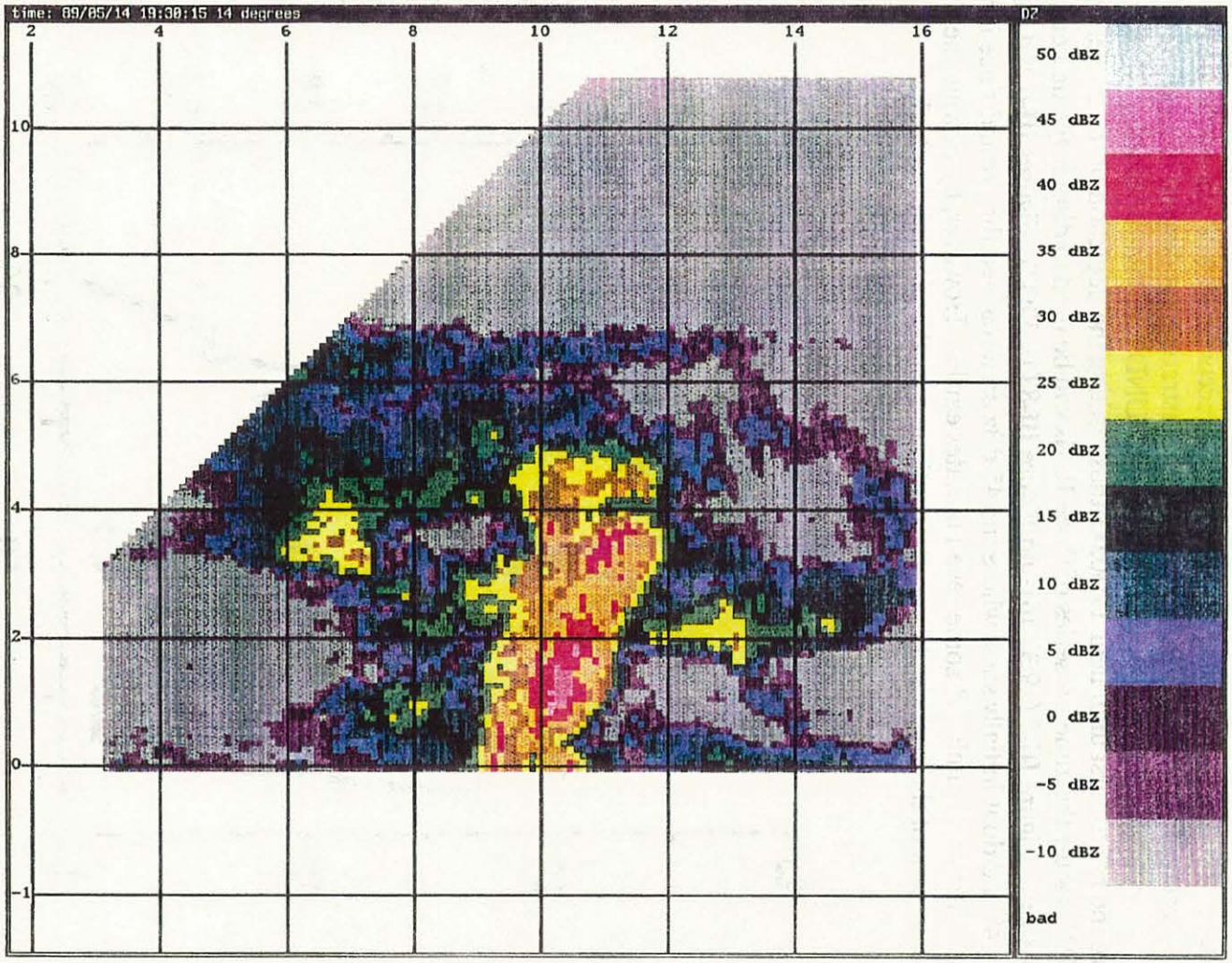

Figure III-6. 19:30:15 RHI Reflectivity Plot - Az. 14.

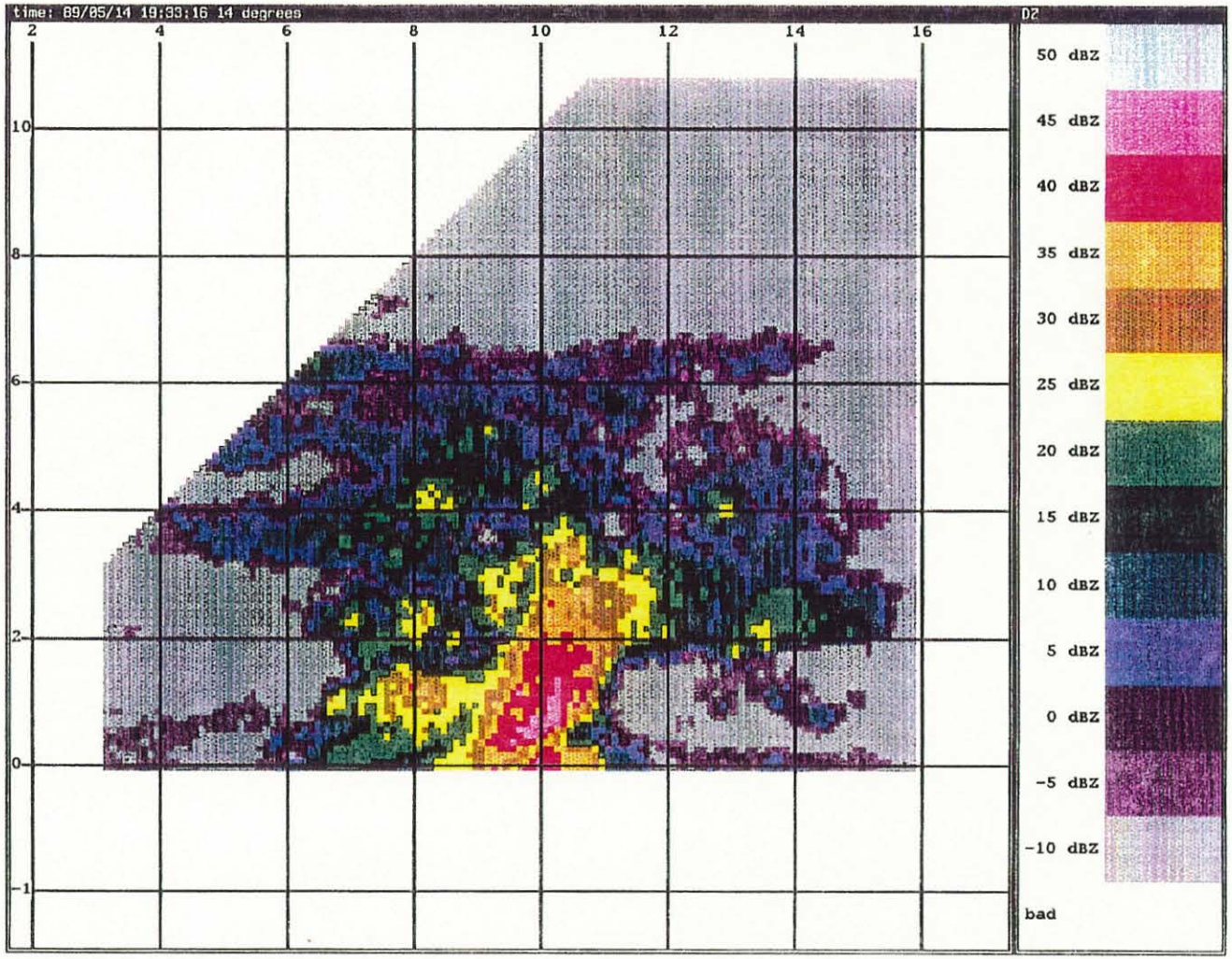

Figure III-7. 19:33:16 RHI Reflectivity Plot - Az/ 14.

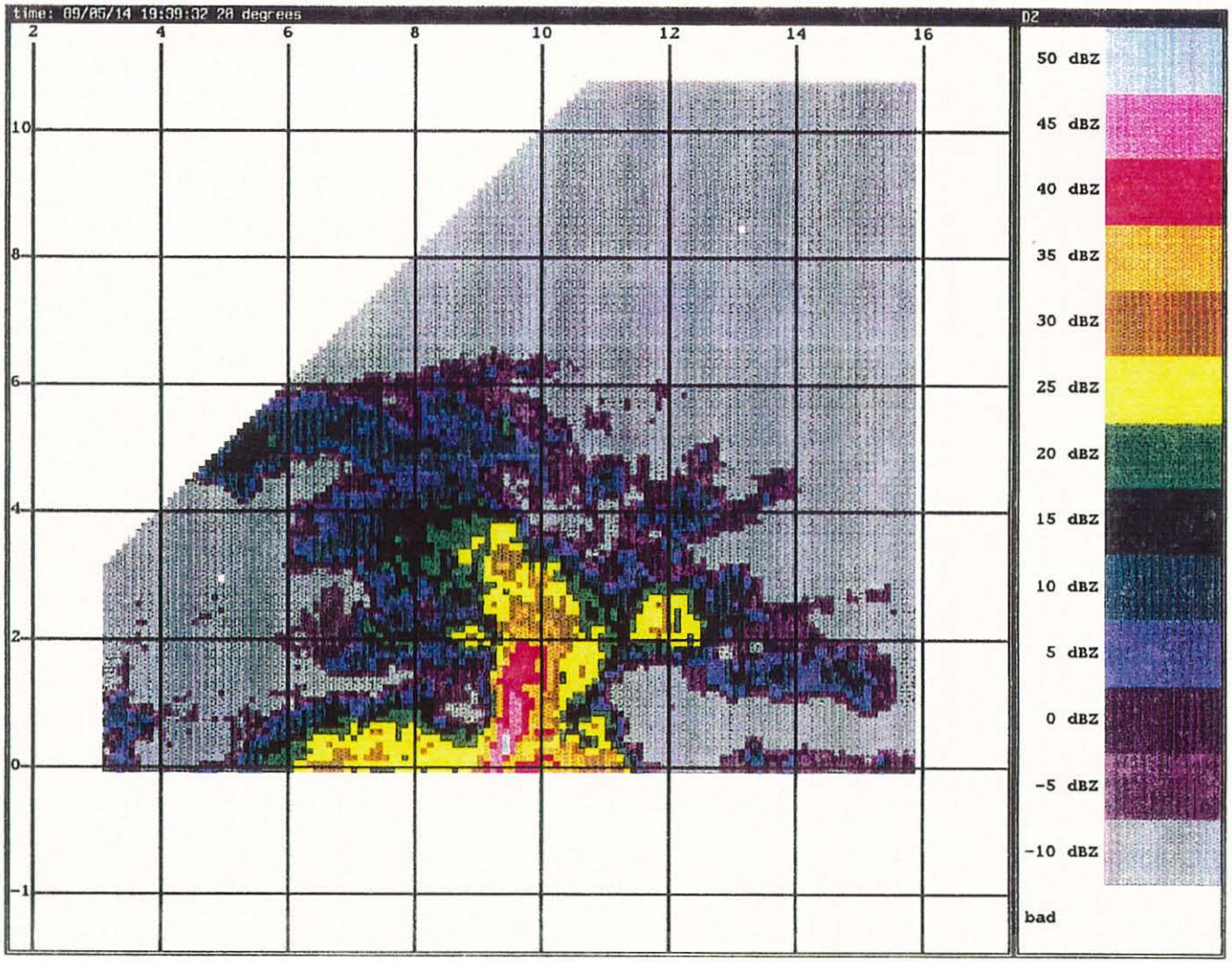

Figure III-8. 19:39:32 RHI Reflectivity Plot - Az. 20

The asymmetry mentioned earlier may be a result of either the easterly storm motion or the shape of the reflectivity core throughout the storm. In the case of the reflectivity core, by comparing the reflectivity plot of 19:28:22 (Figure III-9) and the reflectivity contours on the surface winds plot (Figure III-1), it can be seen that both display the same asymmetrical shape. The asymmetry of the core could be due to the fact that the storm developed along the shear axis illustrated in the surface and satellite illustrations.

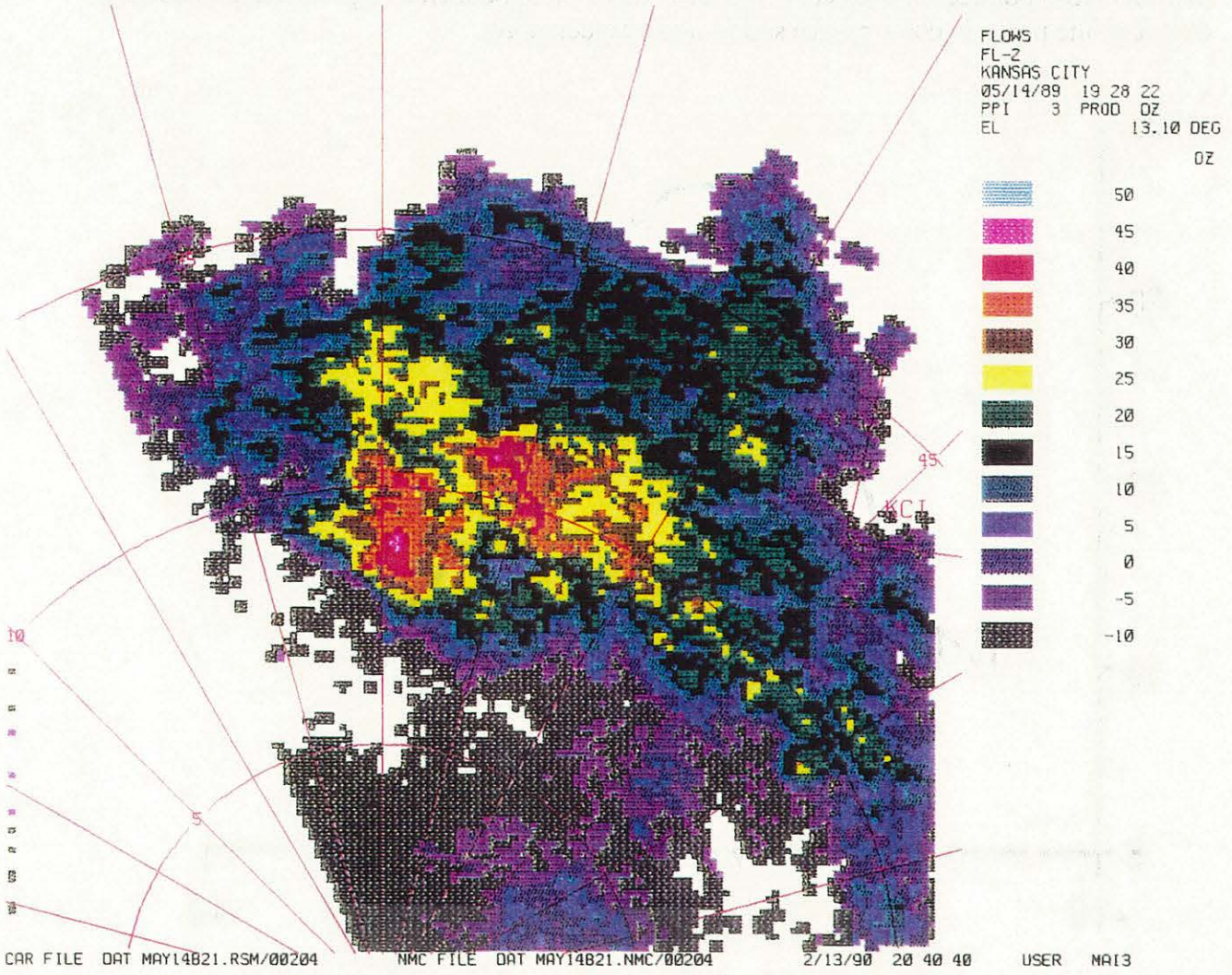

Figure III-9. 19:28:22 PPI Reflectivity Plot - Elevation 13.1

1c) Mid-Level Convergence

Convergence into the storm was first detected by the algorithm at T-4.4 and continued steadily until T+14 and is apparent in Figure III-10. The series of three RHI velocity plots for 19:30:15 (Figure III-11), 19:33:16 (Figure III-12) and 19:39:32 (Figure III-13) illustrate the convergence into the storm. Over time, the convergence dissipates somewhat in areal extent and strength. The convergence peaks slightly about four minutes prior to the peak in the microburst winds and displays some even more subtle peaks as the outflow intensifies. The timing of the convergence differs from the values suggested by the moderate reflectivity model (Table I-2) in which convergence should have been present by T-10, increased by T-5 and continued increasing until T=0. The convergence can be considered increasing near T-4.4 since this is when it attained 10 m/s of velocity difference. However, after this point the convergence continues rather steadily but does peak several times during the intensification of the outflow. Roberts and Wilson (1989) pointed out that convergence is expected to be increasing with the descending core, and the peaks in convergence satisfy these expectations.

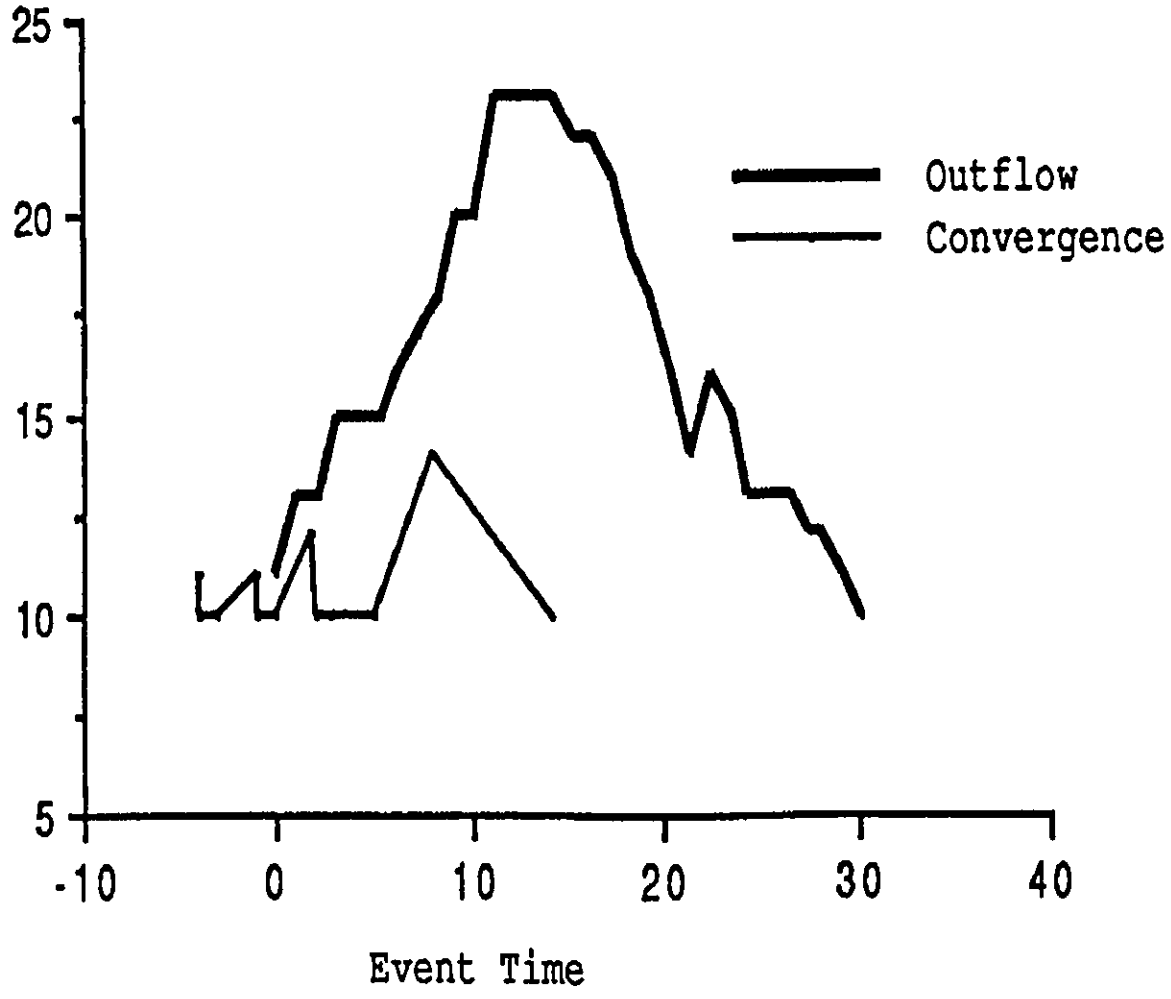

Figure III-10. Convergence and Outflow Velocities for May 14, 1989.

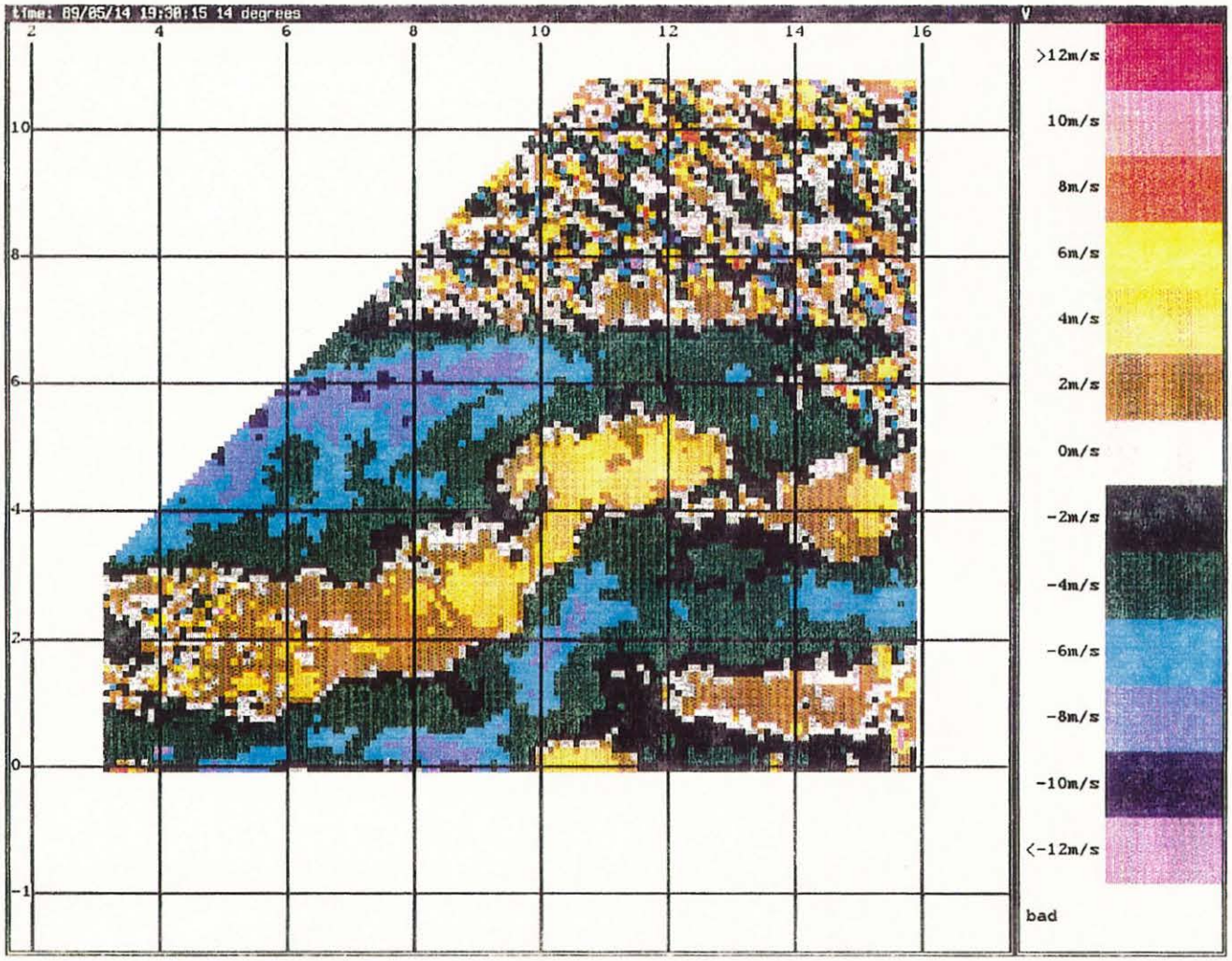

Figure III-11. 19:30:15 RHI Velocity Plot - Az. 14.

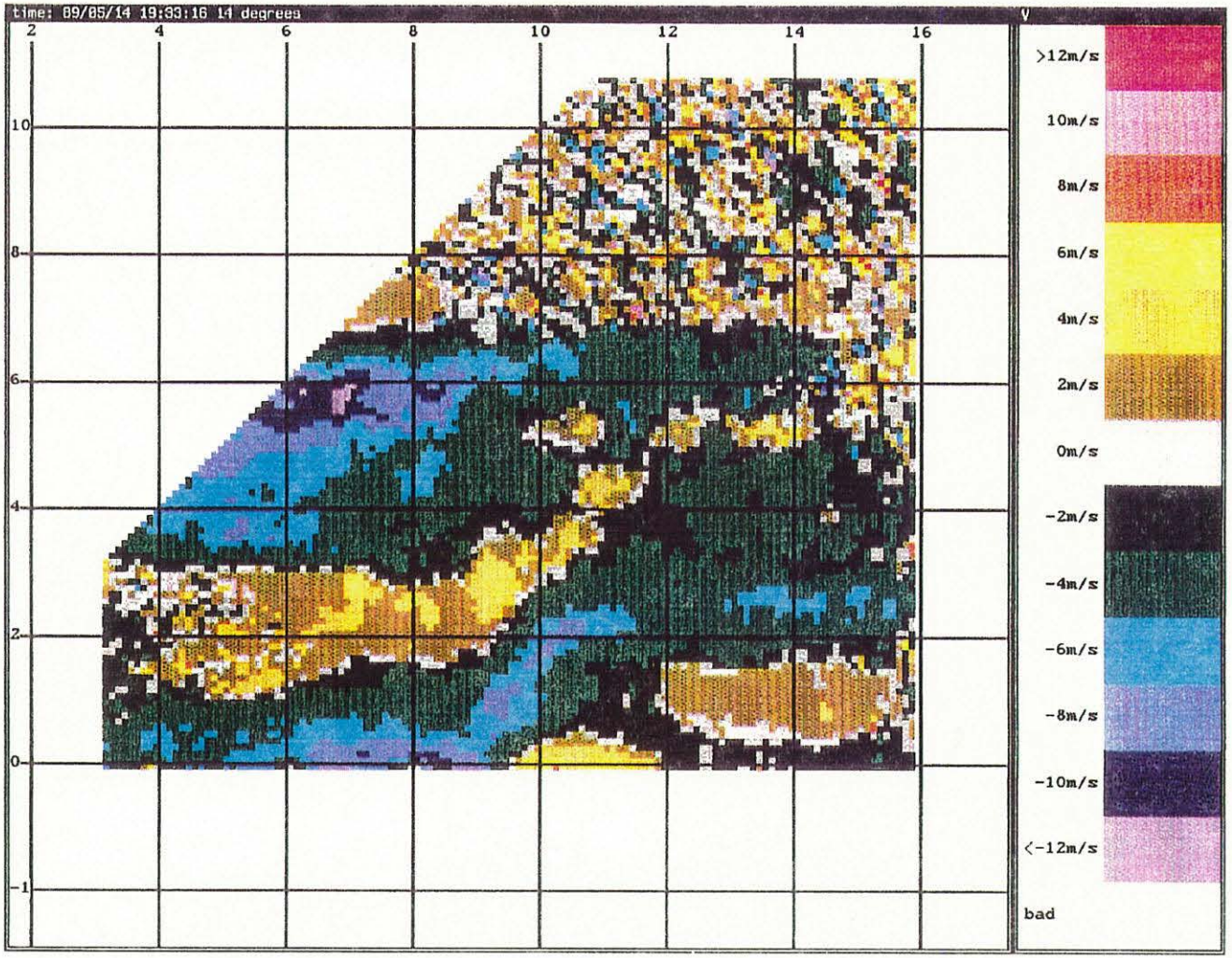

Figure III-12. 19:33:16 RHI Doppler Velocity Plot - Az. 14.

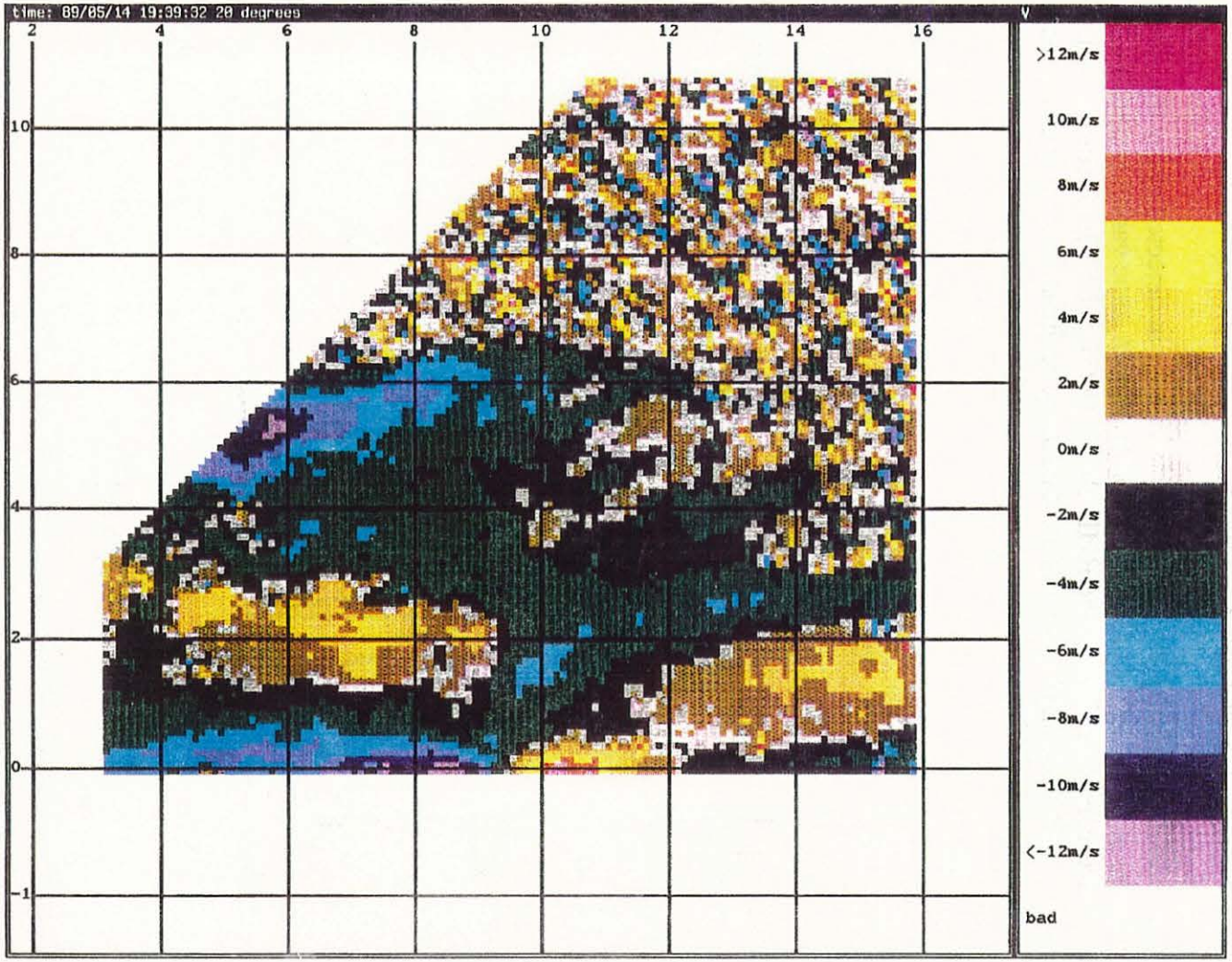

Figure III-13. 19:39:32 RHI Doppler Velocity Plot - Az. 20.

The convergence into the storm is most likely a result of the shear axis shown to exist near the area on the surface maps. Despite the fact that the shear line is not entirely evident on the surface maps, this is probably due to the fact that the convergence is elevated to a height of about 2 to 3 km as is apparent in the RHIs.

1d) Upper-Level Divergency

Figure III-14 is a plot of the upper-level divergence as detected by the algorithm. Upper-level divergence is first detected at T-2.7 and continues with some variation until T+12.7. The upper-level divergence is visible on the RHI velocity plots of 19:30:15 (Figure III-11), 19:33:16 (Figure III-12), and 19:39:32 (Figure III-13). The upper-level divergence peaks at the time that the outflow first reaches microburst strength.

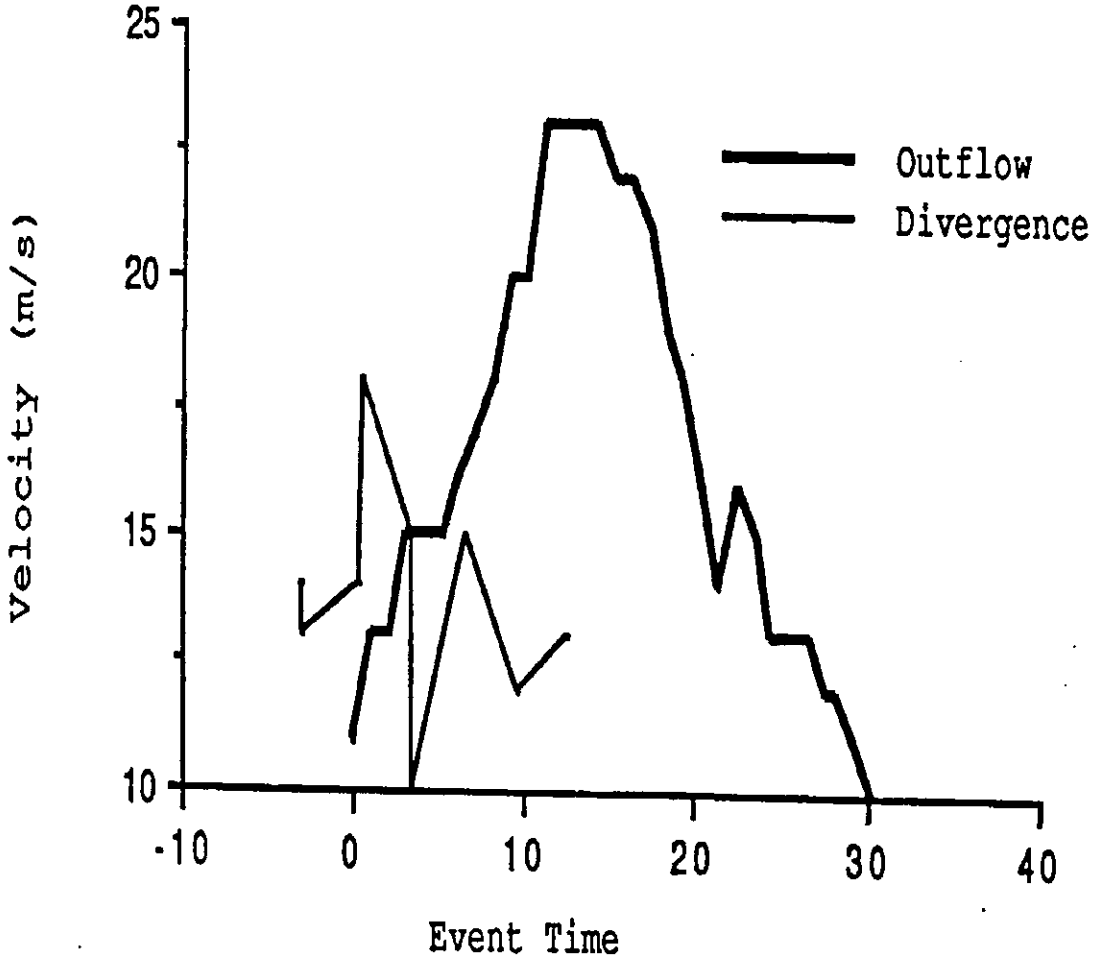

Figure III-14. Upper-Level Divergence and Outflow Velocities for May 14, 1989.

It is apparent that over time the upper-level divergence is increasing in areal extent, indicating that it is not caused entirely by an updraft. It also could be the result of synoptic scale flow such as the shear axis upon which this storm formed, in which flow over the converging air mass could appear as divergence aloft.

1e) Mid-Level Rotation

Of the two types of rotation, anticyclonic rotation was the most prevalent during the lifetime of the microburst. Figure III-15 shows the anticyclonic rotation as detected by the algorithm compared to the strength of the outflow. The anticyclonic rotation was first detected at T+2 and continued fairly steadily until T+17. An example of the anticyclonic rotation is shown in Figure III-16, the PPI velocity plot of 19:31:31. The anticyclonic rotation shows a subtle peak at the time that the peak winds of the microburst are attained. Biron et al (1990), noted that anticyclonic rotation peaked slightly after the peak winds in a Kansas City microburst.

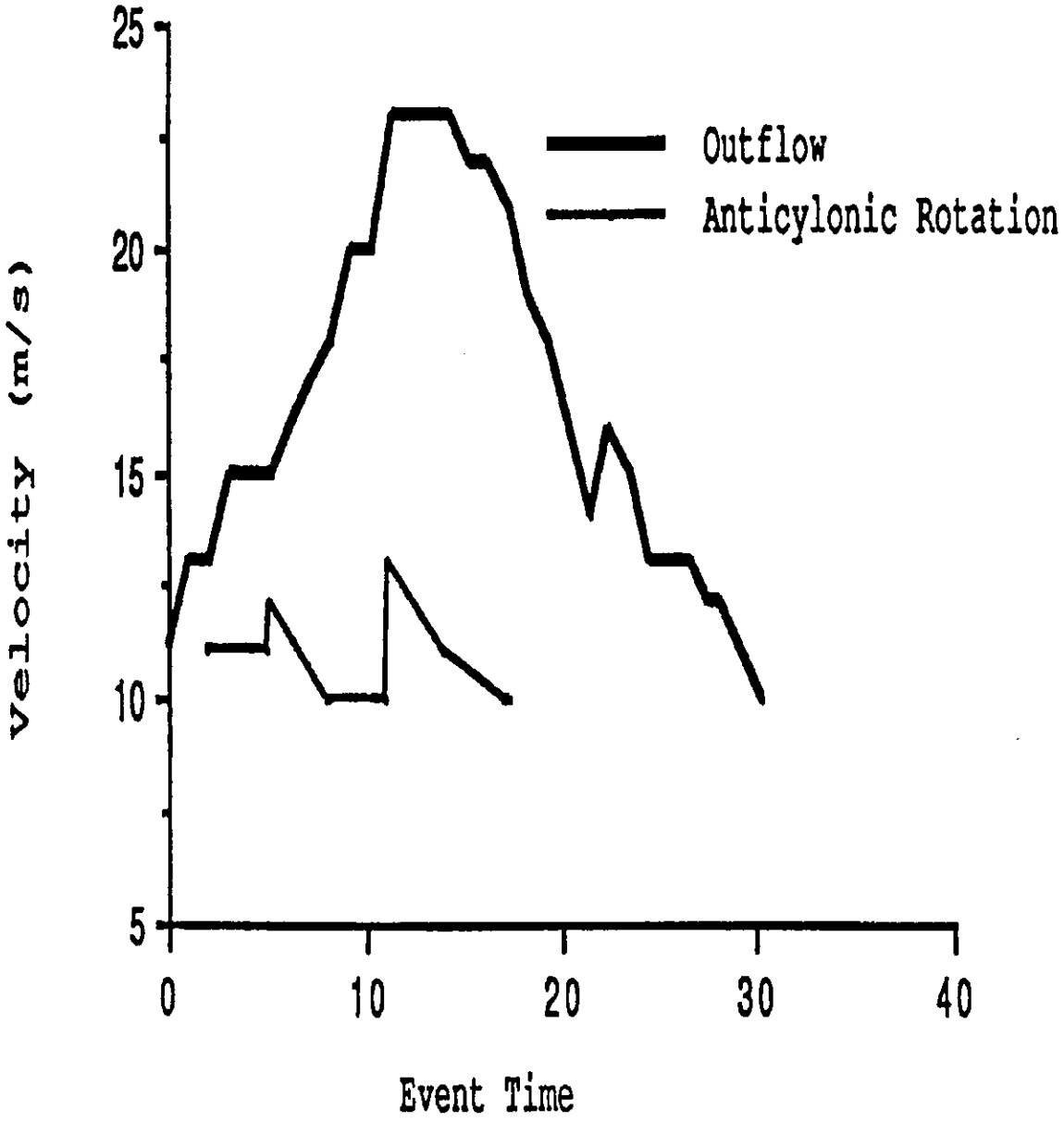

Figure III-15. Anticyclonic Rotation and Outflow Velocities for May 14, 1989.

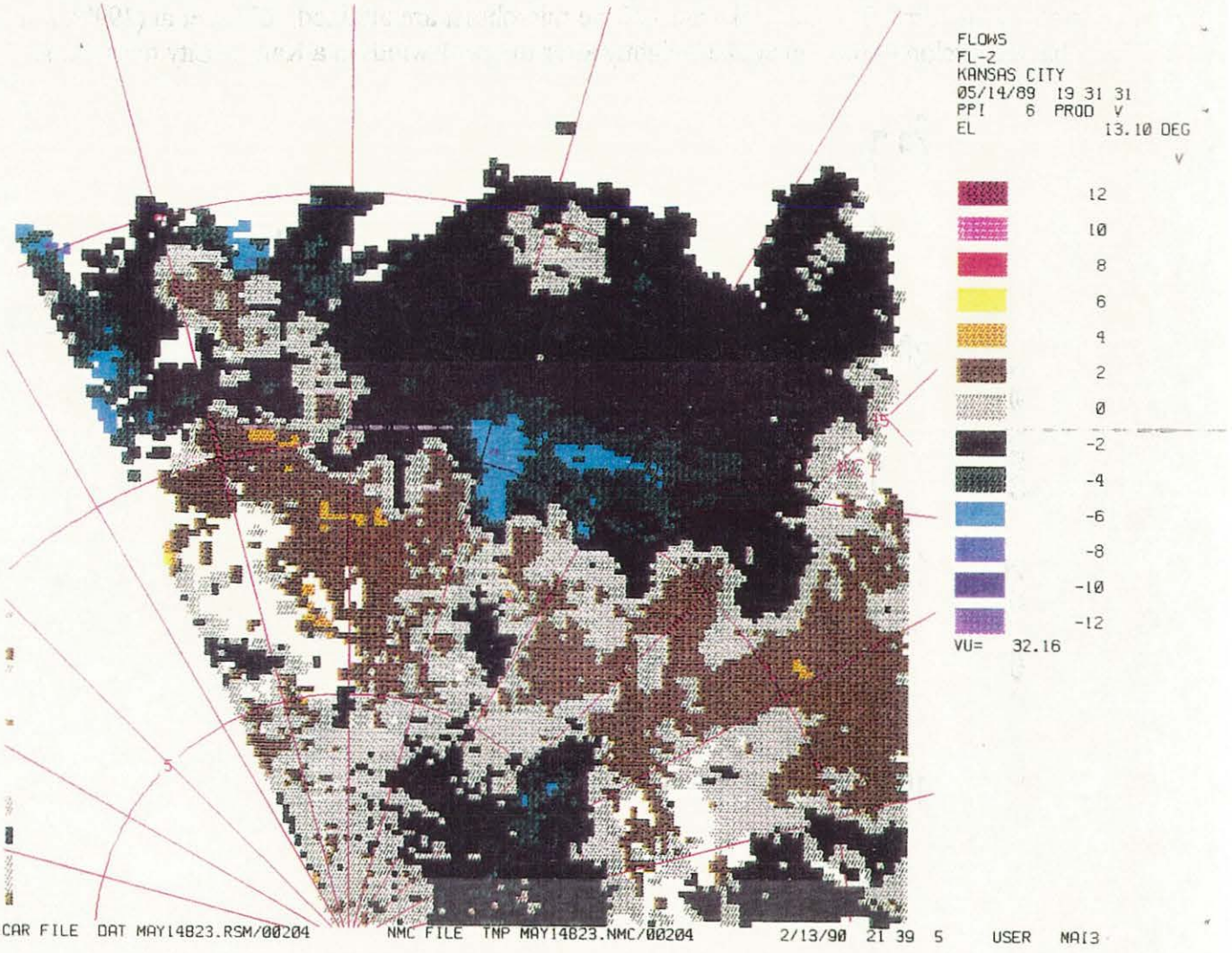

Figure III-16. 19:31:31 PPI Doppler Velocity Plot - Elevation 13.1.

Cyclonic rotation existed for brief moments at two time periods: at T-3 and at T+6. The cyclonic rotation was not included on the figure since it would have only constituted two points. The PPI velocity plot of 19:23:01 (Figure III-17) illustrates the rotation. In the moderate reflectivity model (Table I-2), rotation may be evident by T-5 and more obvious by T+5. This is true in this case since cyclonic rotation appeared at T-3 and anticyclonic rotation continued until T+17.

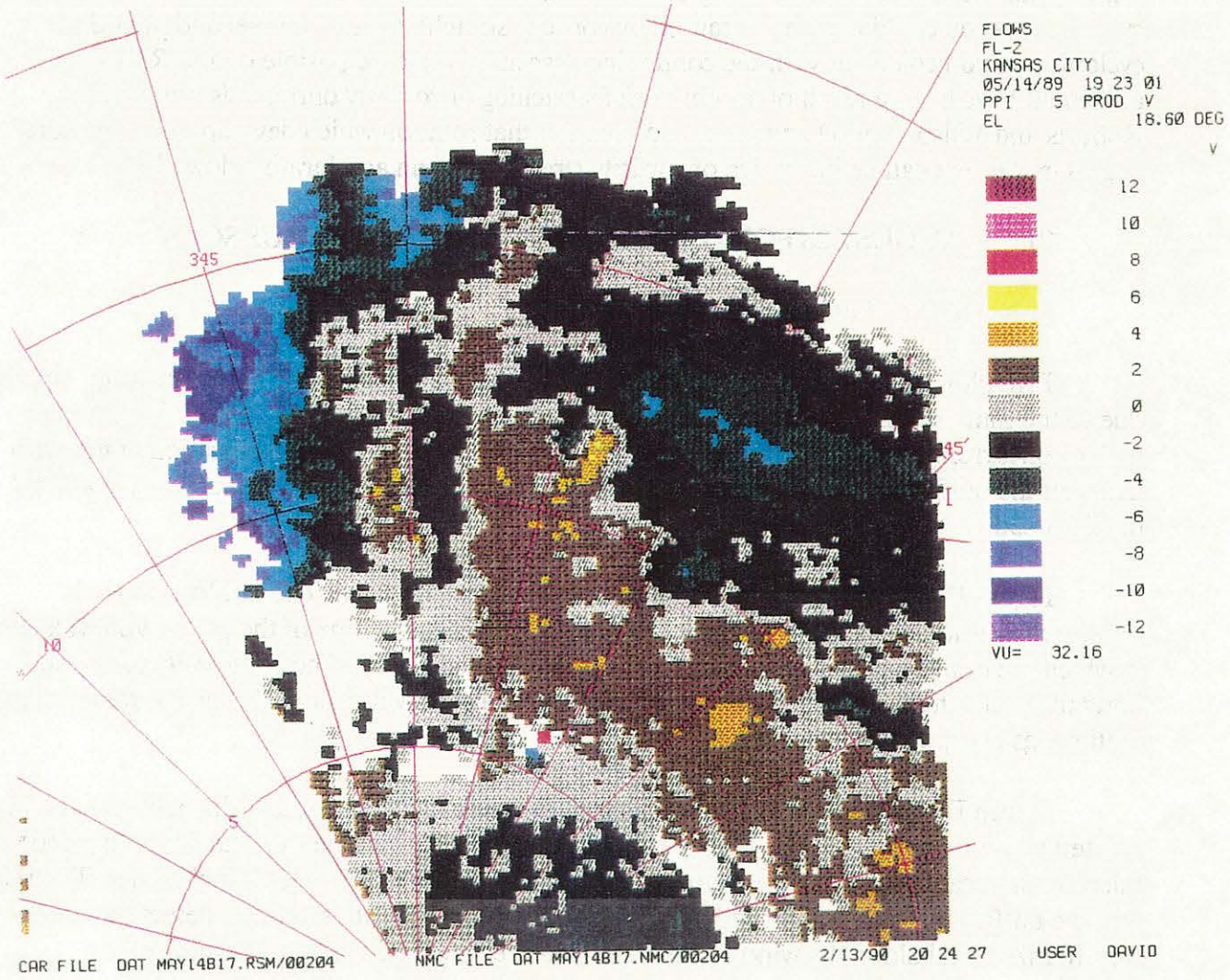

Figure III-17. 19:23:01 PPI Doppler Velocity Plot - Elevation 18.6.

1f) Hypothetical Forcing Mechanisms

This microburst was probably caused by precipitation drag and subcloud evaporation and/or incloud evaporation. This is supported by the rapid loss of reflectivity over time and the constant convergence into the storm, supplying dry air which instigated evaporation. This is supported by Roberts and Wilson (1989) who noted that convergence is often in association with a descending core, which suggests that a downdraft is initiated within the cloud by precipitation drag forces and is accelerated by evaporational cooling as dry environmental air converges into the downdraft. Roberts and Wilson (1987) had noted previously that evaporative cooling is evidenced by convergence and a descending reflectivity core.

Anticyclonic rotation developed after the initial onset of high winds and indicates that this rotation was caused by stretching of existing vorticity in the cloud. The brief initial period of cyclonic rotation could have been caused by vorticity stretching also. The second period of cyclonic rotation coincides with the continuing descent of the core (visible on the RHI series) and could have been a result of another brief stretching of vorticity during this time period. Roberts and Wilson (1987) and others pointed out that rotation which develops after the core begins its descent can be indicative of vorticity stretching by an accelerating downdraft.

2) AUGUST 28 FORCING MECHANISMS AND PRECURSORS

2a) Surface Divergence

Five plots are required to sufficiently display the microburst outflow under study. This is due to the multi-cellular structure of the storm and also the fact that several microbursts were acting concurrently nearby with the microburst of interest. Since the interpretation of the symmetry of the outflow is meaningless due to the closeness of the neighboring outflows, it will not be discussed.

Figure III-18 (21:46:55), is for the time of the initial outflow. The outflow center is located at xy grid point (38,30). Figure III-19 is for 21:48:56, the time of the peak radial velocity, in which the outflow center is now located at xy grid point (41,24). The complexity of the outflows from this storm are readily apparent, and this complexity increases during the microbursts lifetime, as is apparent in later plots.

Figure III-20 (21:50:52) is for the time of the peak radial shear, and the outflow center is located at xy grid point (41,29). Figure III-21 is for 21:54:09, the time the algorithm "coasted" the microburst because the apparent velocity was less than 10 m/s. This plot is included to illustrate that the outflow pattern was indeed apparent, however the algorithm did not detect the necessary 10 m/s threshold in the winds. The outflow center is located at xy grid point (42,23).

Figure III-22 (21:55:14) is for the time the outflow dissipated below the 10 m/s threshold. The outflow center is located at xy grid point (41,25). This dissipation of this microburst is not

readily apparent from the plots themselves, but this is due to the fact that a new microburst is developing immediately east of the microburst and will be at xy grid point (58,27). The outflow of this new microburst obscures the dissipating one and gives the appearance that the same microburst is continuing.

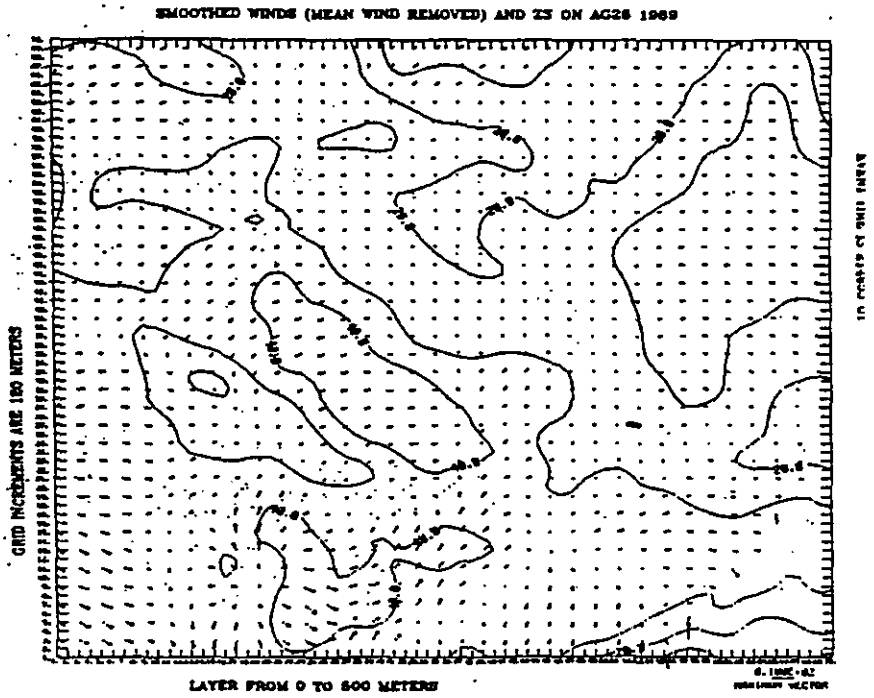

Figure III-18. 21:46:55 Dual-Doppler Winds and dBz Plot.

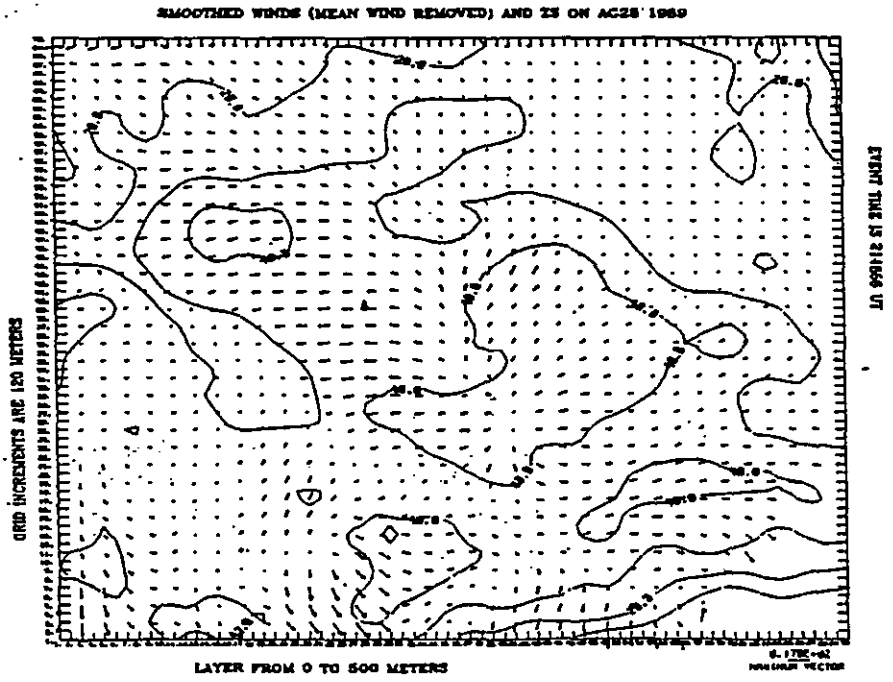

Figure III-19. 21:48:56 Dual-Doppler Winds and dBz Plot.

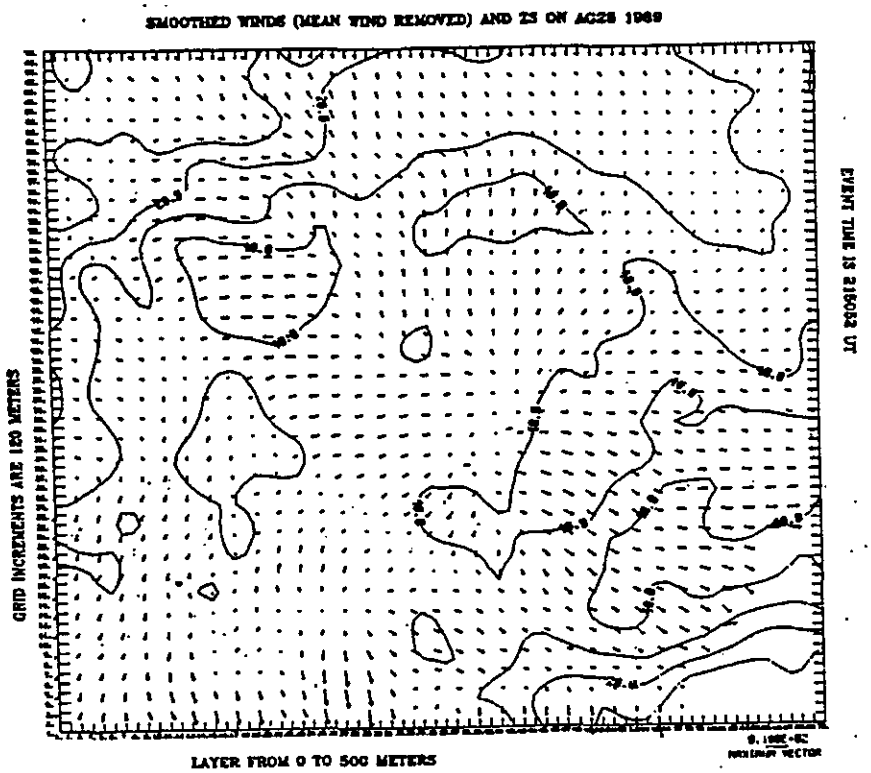

Figure III-20. 21:50:52 Dual-Doppler Winds and dBz Plot.

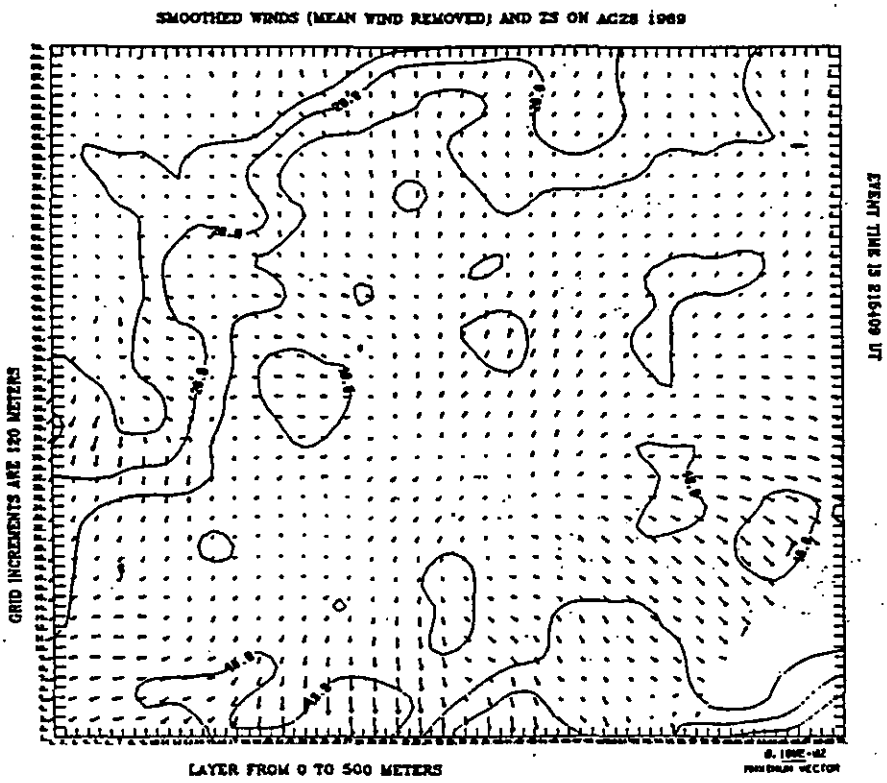

Figure III-21. 21:54:09 Dual-Doppler Winds and dBz Plot.

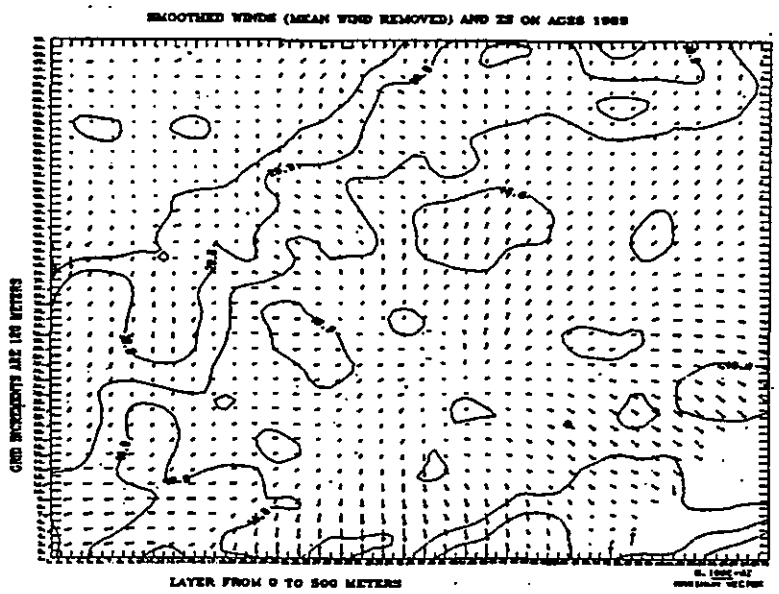

Figure III-22. 21:55:14 Dual-Doppler Winds and dBz Plot.

2b) Descending Reflectivity Core

Due to the scarcity of correct reflectivity core locations as recognized by the algorithm, Figure III-23, which is based upon the algorithm data, does not adequately display when the reflectivity core started its descent other than starting at T-2. However, the use of the actual radar data is helpful in inferring when the descent began. The two RHIs of 21:41:33 (Figure III-24) and 21:47:30 (Figure III-25) illustrate the dramatic loss of reflectivity (at a range of 14-16 km) during this six minute period and suggest that the core began its descent between T-5.3 and T+0.6. The PPI reflectivity plot of 21:40:29 (Figure III-26) and the PPI reflectivity plot of 21:40:21 (Figure III-27) show the large area of reflectivity which existed aloft near 14 km/62°.

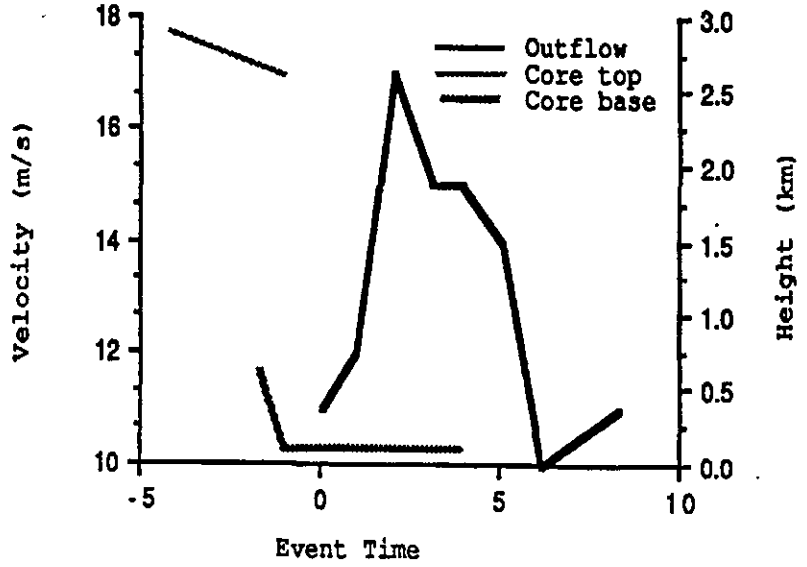

Figure III-23. Core Structure and Outflow Characteristics for August 28, 1989.

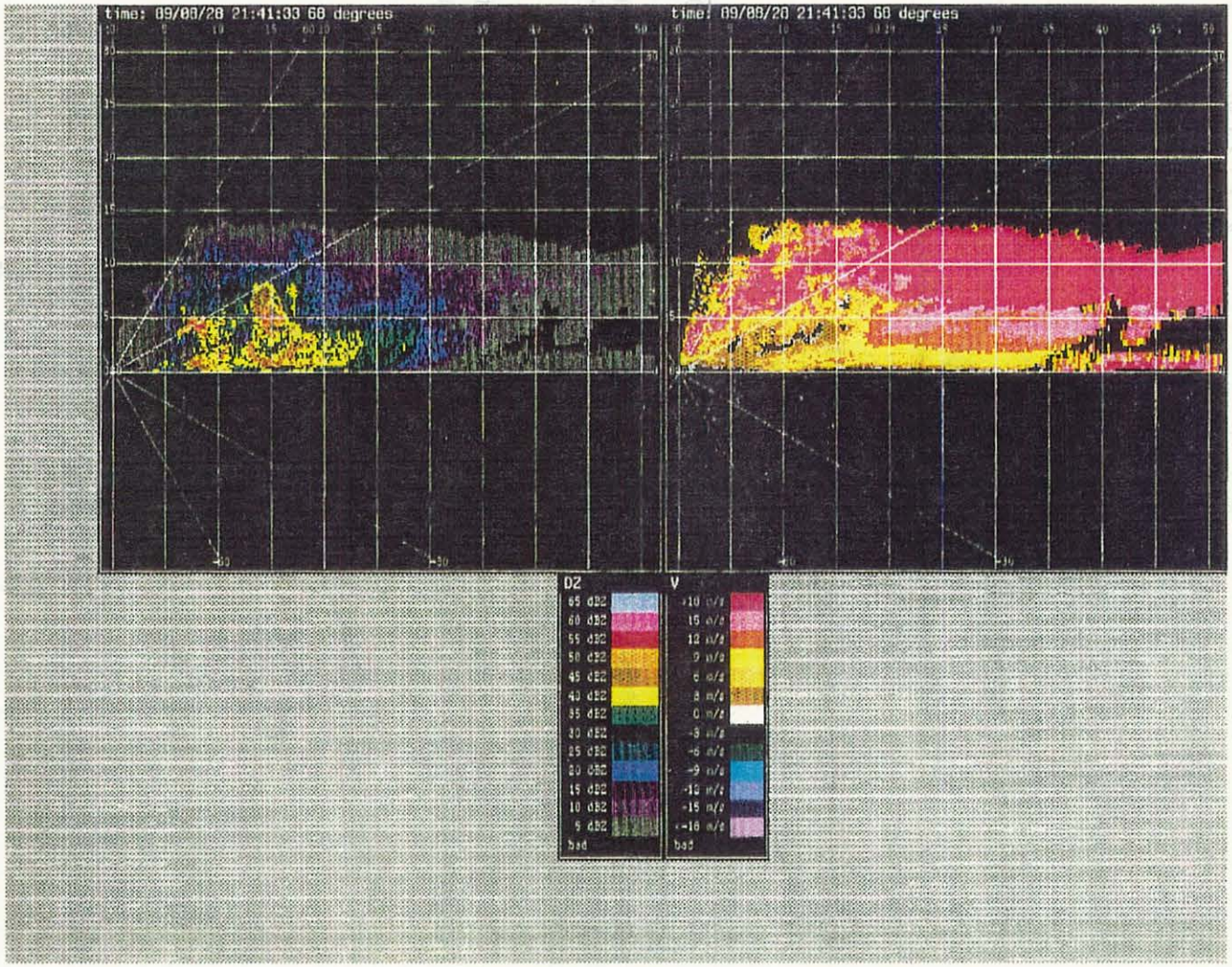

Figure III-24. 21:41:33 RHI Reflectivity and Doppler Velocity Plot.

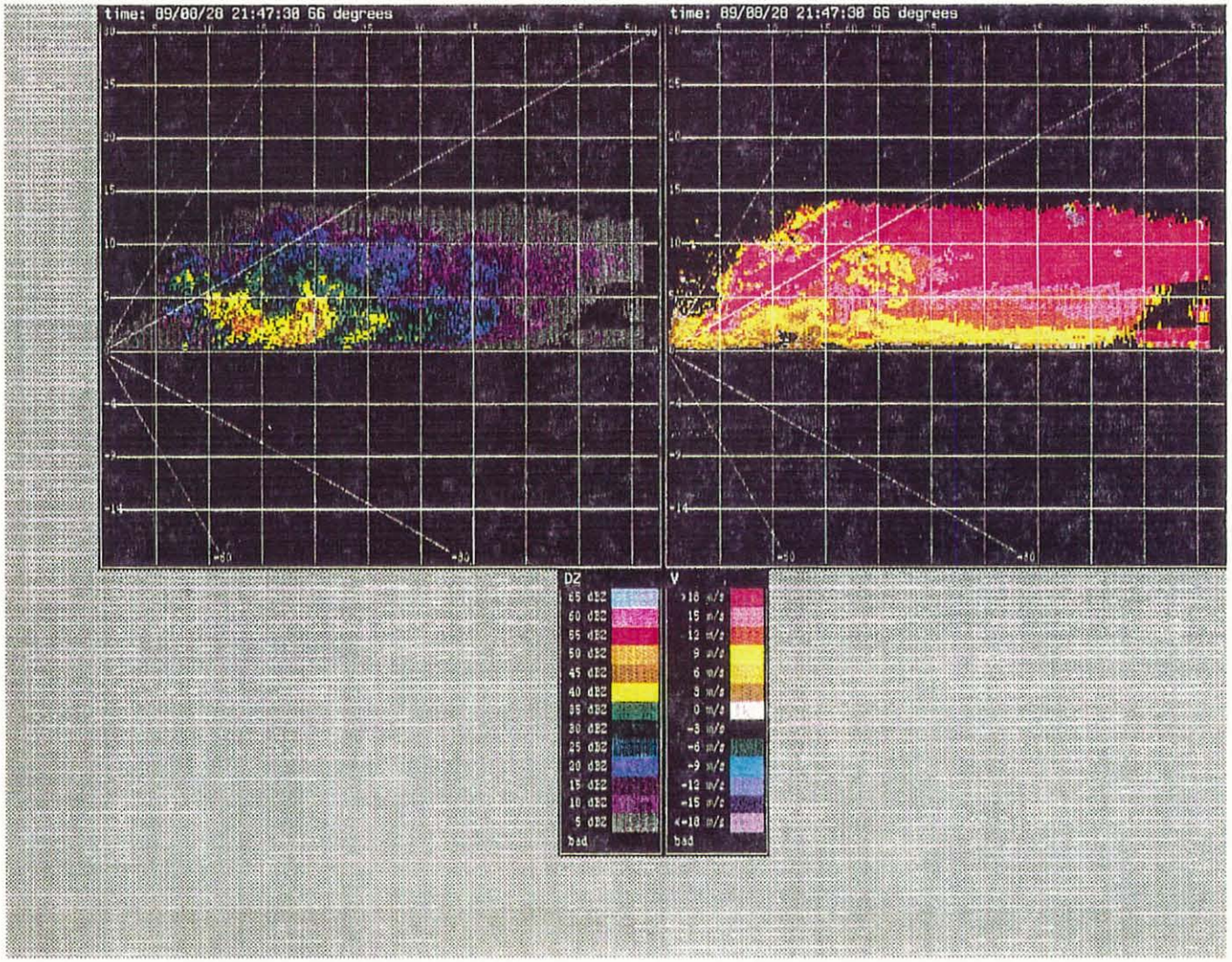

Figure III-25. 21:47:30 RHI Relectivity and Doppler Velocity Plot.

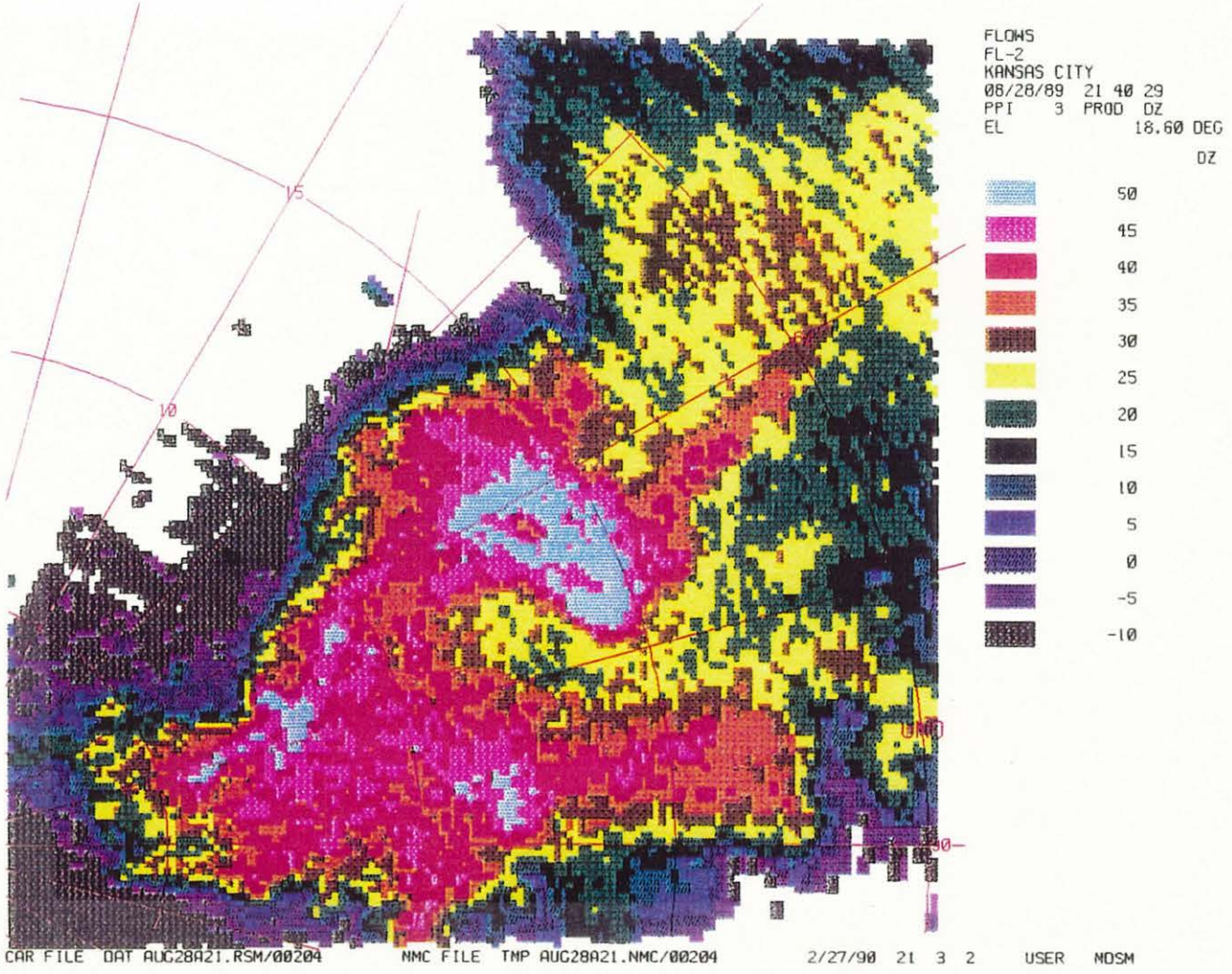

Figure III-26. 21:40:29 PPI Reflectivity Plot - Elevation 18.6.

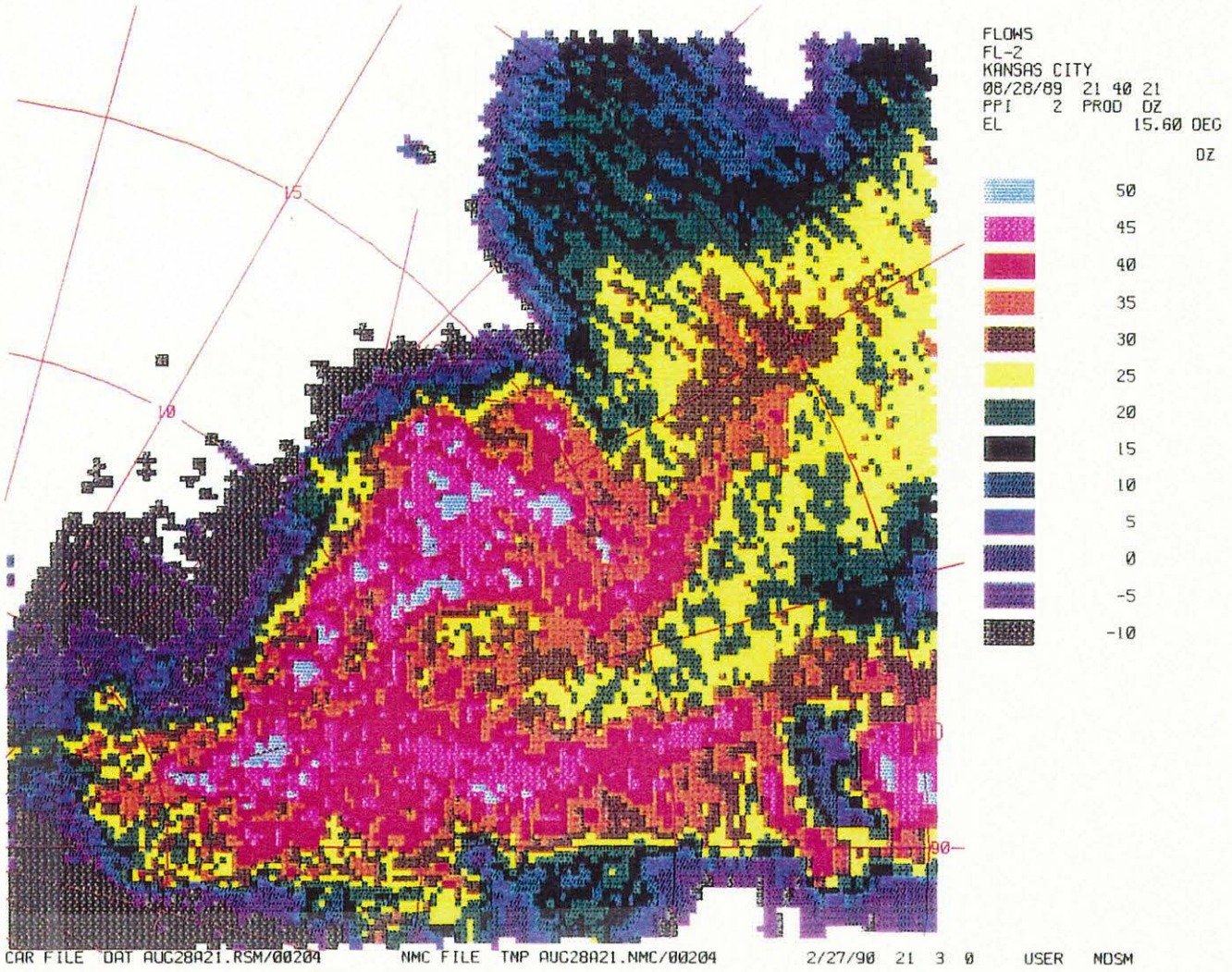

Figure III-27. 21:40:21 PPI Reflectivity Plot - Elevation 15.6.

By the PPI reflectivity plot of 21:43:27 (Figure III-28), the core area has now descended to this height where it did not exist previously and has decreased in intensity aloft (not shown). Based upon this series, the time when the core began its descent can be refined more than from the RHI estimate to have began its descent between T-6.4 and T-3.5, which corresponds to the timing of the moderate reflectivity event (Table I-2). The continuing descent of the core is evident in the reflectivity plots of 21:46:25 (Figure III-29), in which the core area has now descended past this height, and in 21:45:33 (Figure III-30) which shows the highest point that the core exists at this time in the area of the microburst. The fact that a downdraft now exists is supported by Roberts and Wilson (1987), who state that the observation of a descending core with the dissipation of the reflectivity echo aloft is indicative of the presence of a downdraft.

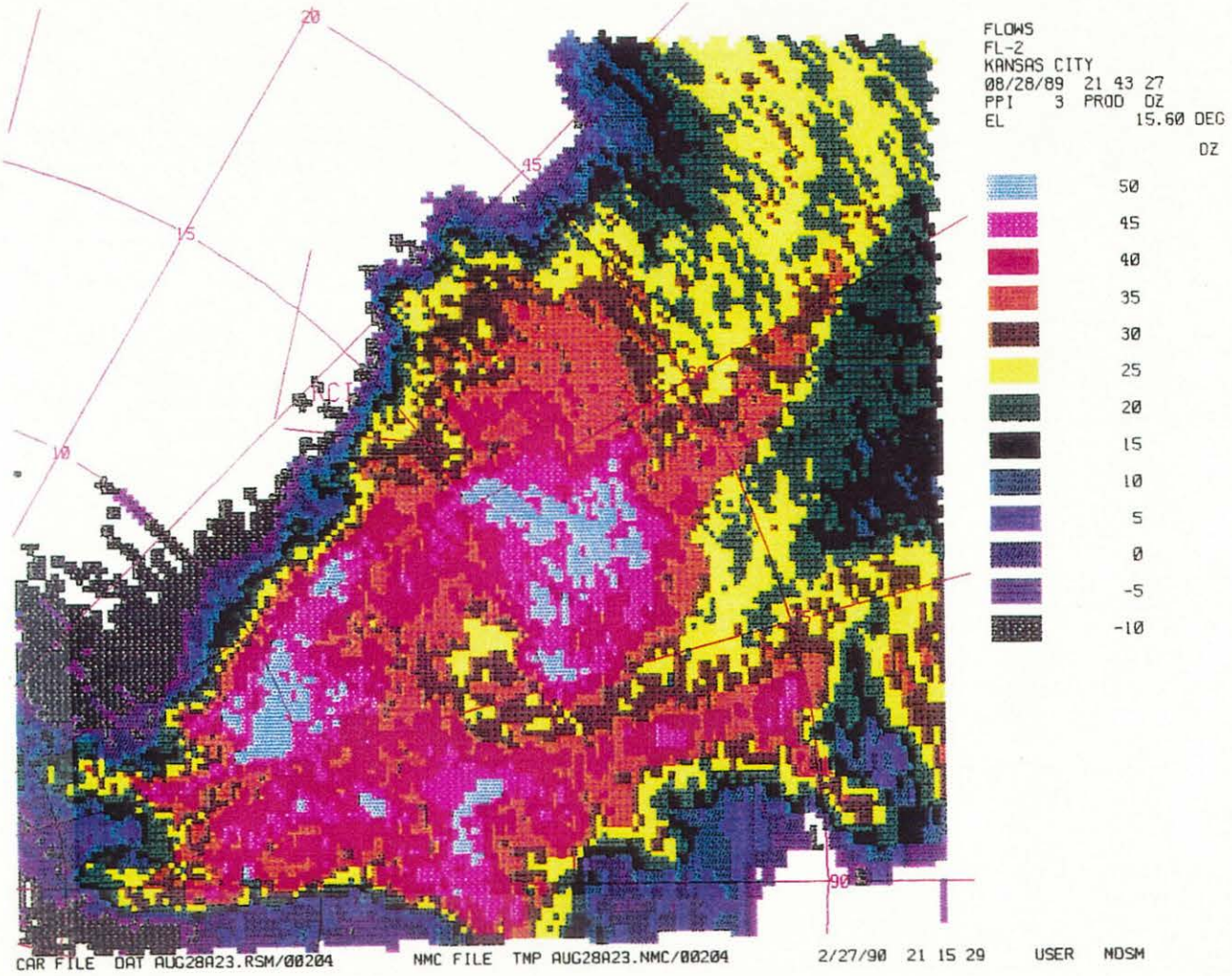

Figure III-28. 21:43:27 PPI Reflectivity Plot - Elevation 15.6.

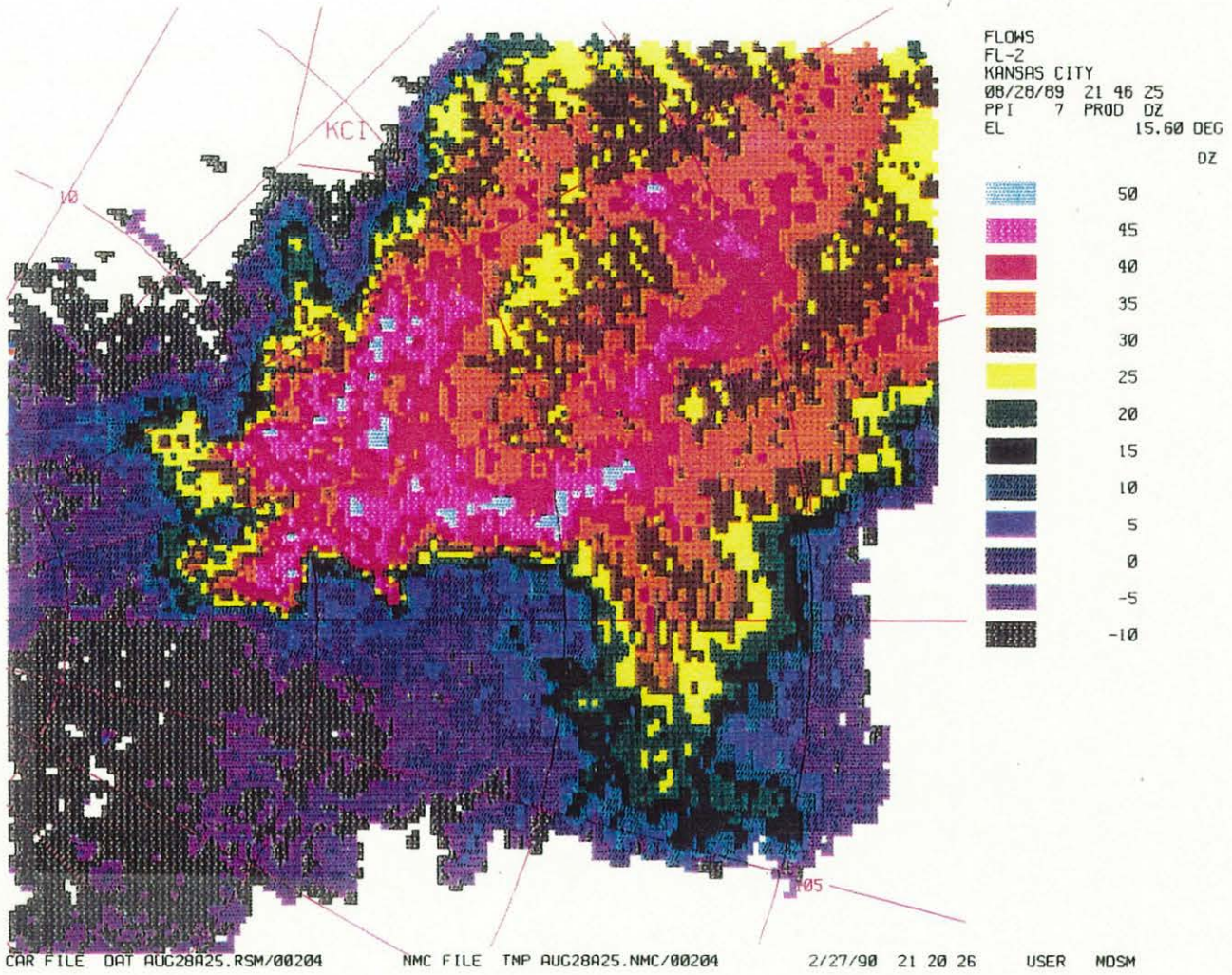

Figure III-29. 21:46:25 PPI Reflectivity Plot - Elevation 15.6.

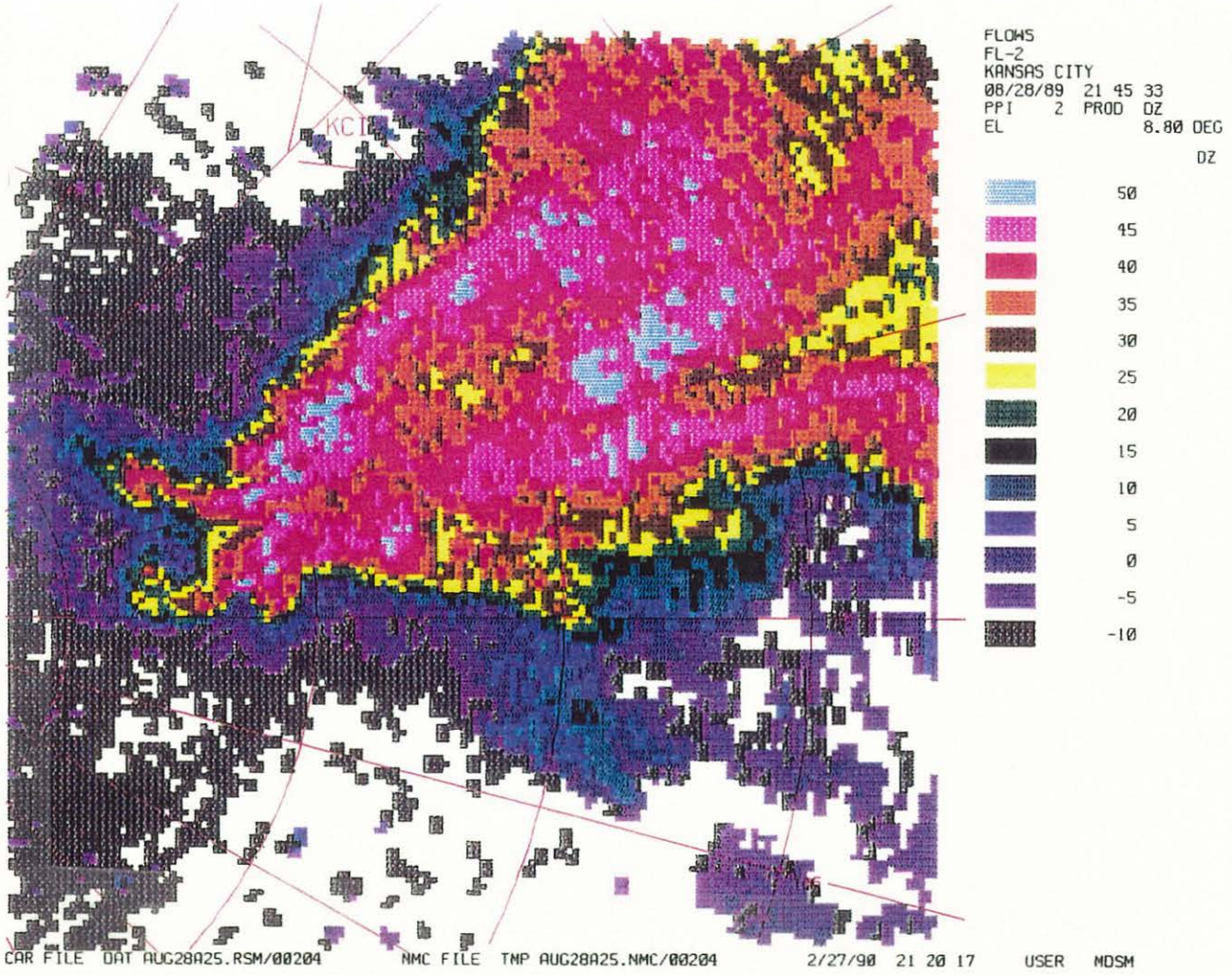

Figure III-30. 21:45:33 PPI Reflectivity Plot - Elevation 8.8.

The reflectivity core reaches the ground at T-1.4 and by the time the microburst reaches 10 m/s intensity, it is initially collocated with the outflow as is apparent in the dual-Doppler plot of 21:46:55 (Figure III-18), as expected in the moderate reflectivity model (Table I-2). In previous research by Roberts and Wilson (1987), it was found that 31 of 31 microbursts initially had reflectivity cores collocated with microburst outflow. In between the plot times of 21:48:56 (Figure III-19) and 21:50:52 (Figure III-20), the reflectivities start to decrease at the center of the outflow, which hints at evaporation processes. By 21:54:09 (Figure III-21), the areal extent of the 40 dBz area has decreased further, where the unlabeled isolines are 30 dBz contours, indicative of evaporation continuing.

2c) Mid-Level Convergence

Convergence into the storm was detected at only two times by the algorithm, both of which are valid. The first was at T-4.4 and the second at T+2.2. The velocity plot of 21:42:29 (Figure III-31) illustrates the convergence into the storm. However, the RHI of 21:41:33 (Figure III-24) indicates weak convergence (< 10 m/s) at a height of 4 km at 15.5 km/68°, and Figure III-32 also indicates fairly strong convergence high in the storm (6.2 km) at 15.5 km/65°. The convergence found on Figure III-32 was missed by the algorithm while the convergence on the RHI is too weak to be considered significant. The significance of convergence so high in the storm is unknown, except for the possibility of flow into the top of the descending core. The convergence into this storm does not follow the timing or duration of the moderate reflectivity event (Table I-2), suggesting that convergence did not play a major role in the formation of this microburst, compared to the typical microburst event. Due to the limited amount of data points, no plot was made comparing the convergence to the outflow velocity.

2d) Upper-Level Divergence

The algorithm detected upper-level divergence at T-2.7 and at T+3.4. The algorithm missed detection of upper-level divergence between these two time periods because it was occurring between the scans of the radar. Additional data can be added to the study of this microburst by using the two RHI plots, which indicate upper-level divergence occurring at heights that were also between the scans of the radar. The additional data changes the starting time period during which the upper-level divergence first existed to T-5.4 and lasting until T+3.4 and is visible in Figure III-33. The period of the microburst to the peak winds is marked by a dramatic increase in the upper-level divergence which dissipates soon after the peak winds are attained. Isaminger (1988) noted that the strengthening of divergent tops is a precursor to the maximum outflow intensity, and this is certainly true in this case.

Table III-1. Upper-Level Divergence based upon RHI Analysis.

Time	RAC	Height (km)	Radial Velocity Difference
21:41:33	16.0/68°	6.5	15 m/s
21:47:30	18.5/66°	8.5	15 m/s

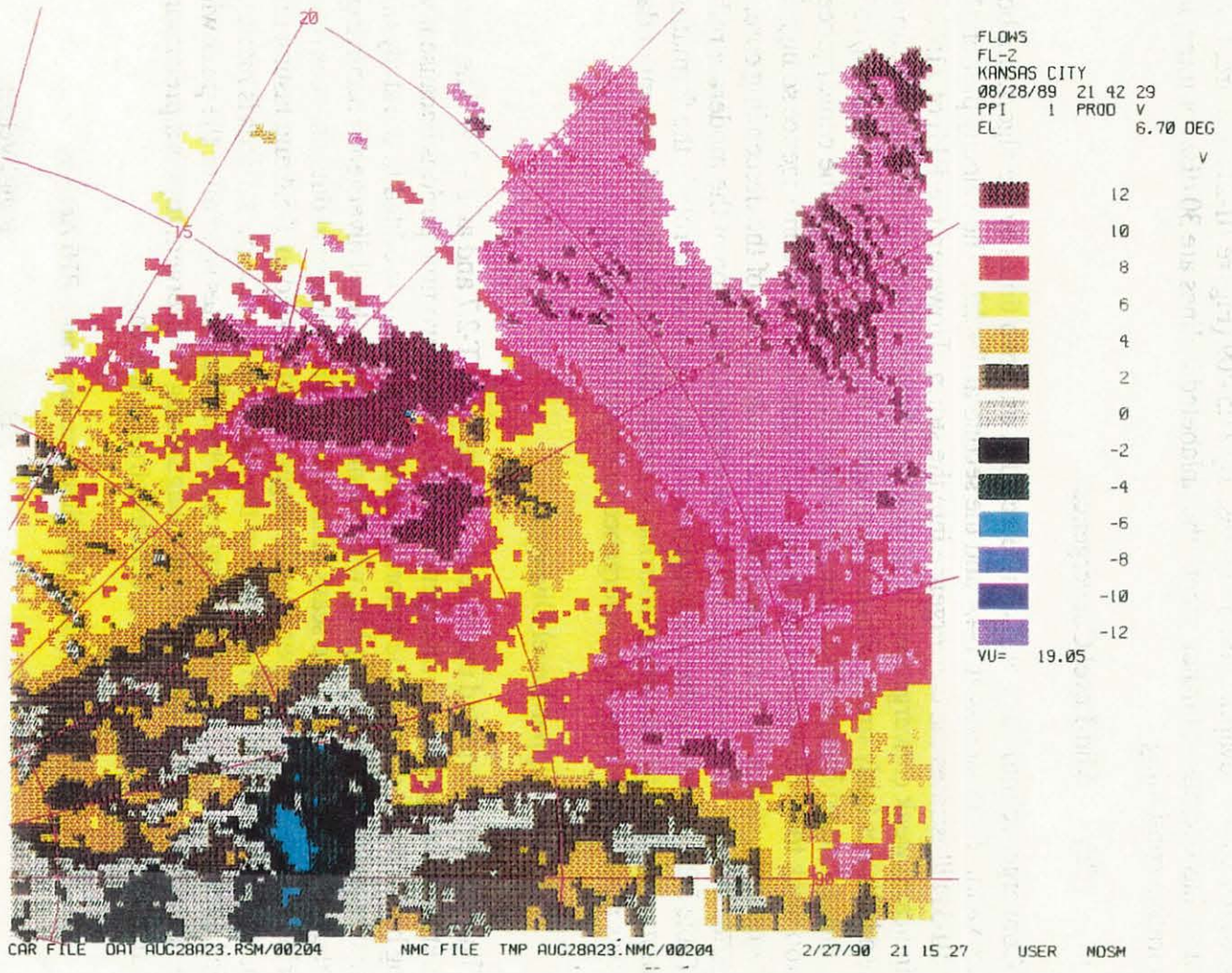

Figure III-31. 21:42:29 PPI Doppler Velocity Plot - Elevation 6.7.

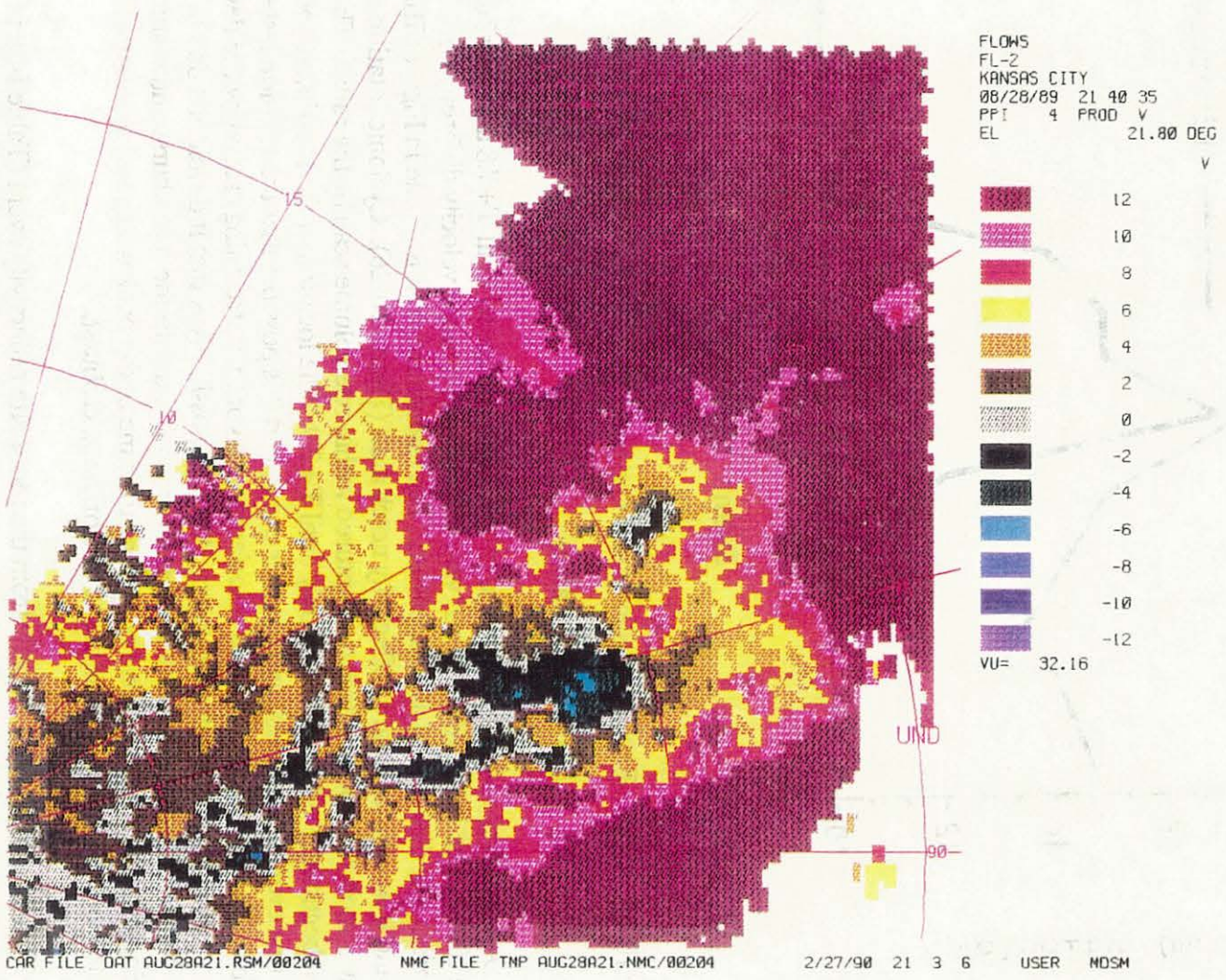

Figure III-32. 21:40:35 PPI Doppler Velocity Plot - Elevation 21.8.

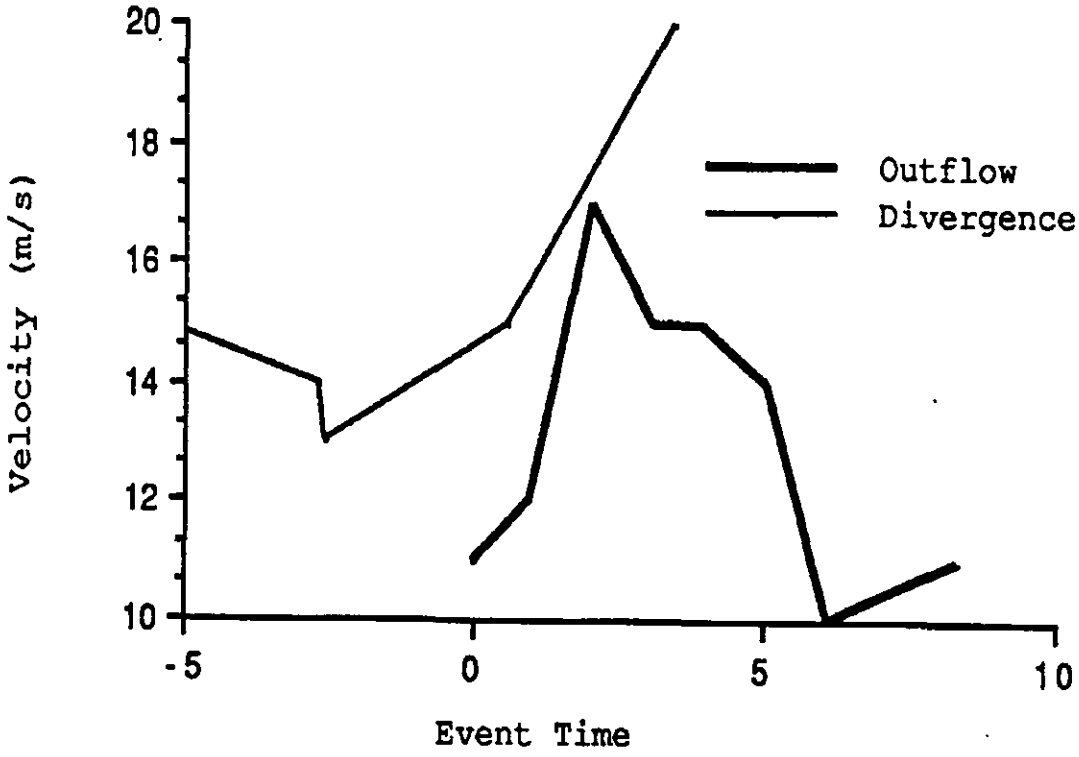

Figure III-33. Upper-Level Divergence and Outflow Velocities for August 28, 1989.

2e) Mid-Level Rotation

Anticyclonic rotation developed at T-7.2 and continued until T+7.8 and is visible in Figure III-34. The initial rotation was very intense with a radial velocity difference of 30 m/s which gradually diminished as time passed. The intense rotation is visible in Figures III-35 and III-36 and is associated with a reflectivity notch aloft (Figure III-26). Cyclonic rotation developed for only a short time period and was captured within one volume scan by the radar. The cyclonic rotation began at T+1.6 and lasted only until T+2.9. The location of the rotation is between the microburst event under study and another event, and it is possible that the rotation lasted for only a brief moment because it was associated with vorticity stretching caused by the descending core associated with another microburst. Another possibility is that it developed due to the shear created by the column of anticyclonic rotation associated with the microburst under study. The anticyclonic rotation has a second peak near the time of the peak winds and another subtle peak when the winds picked up a little at the end of the microburst.

This case differs significantly from the moderate reflectivity event (Table I-2), in that the rotation is not more obvious by T+5. However, Roberts and Wilson stated that rotation may exist at or above 3 km and be associated with a reflectivity notch above 4 km at T-5, and this is exactly what is occurring in this storm. Biron et al (1990) discussed a microburst in which the antirotation peaked slightly after the peak outflow velocity, and this is also occurring in this microburst where a peak in the rotation is observed soon after the maximum outflow velocity.

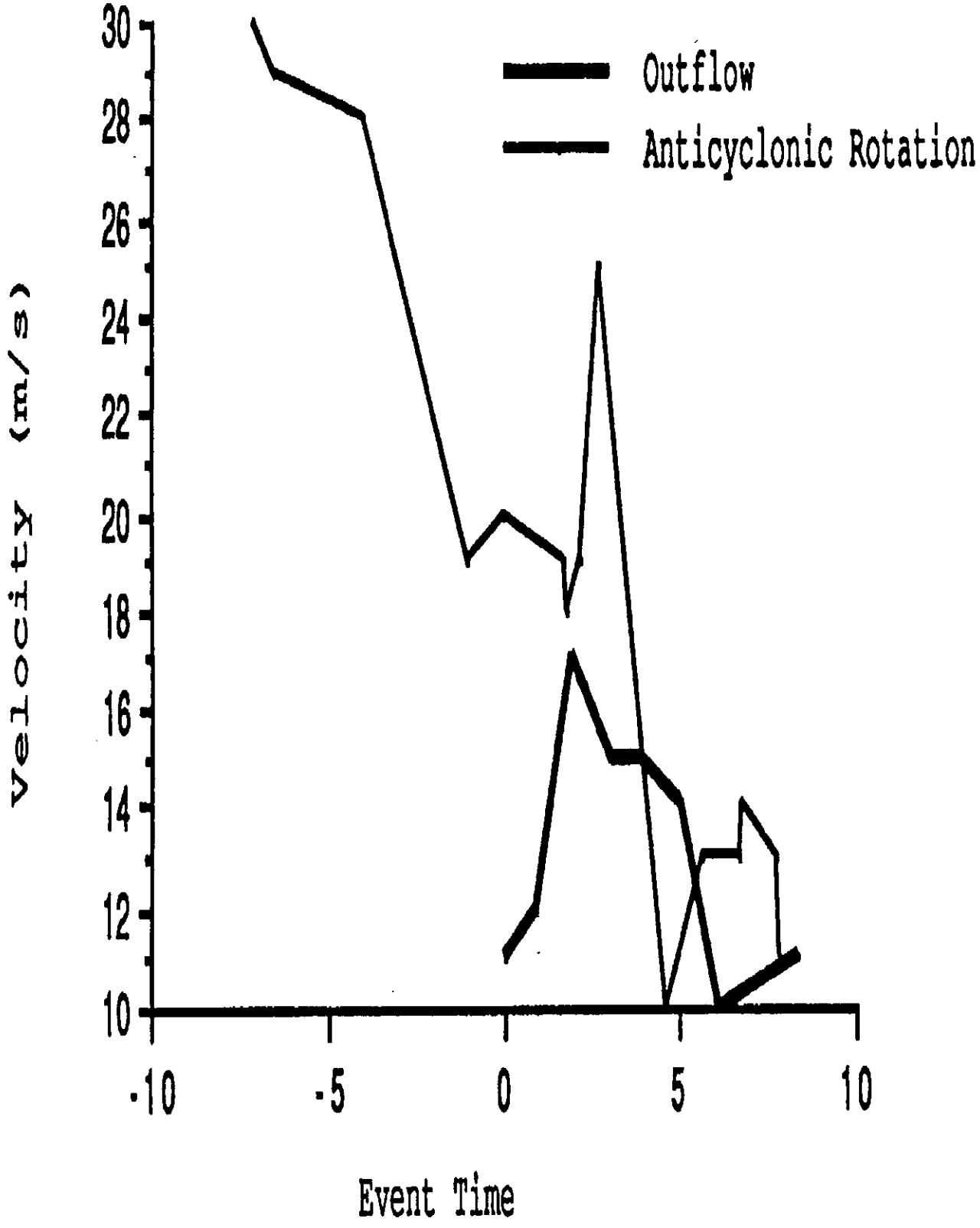

Figure III-34. Anticyclonic Rotation and Outflow Velocities for August 28, 1989.

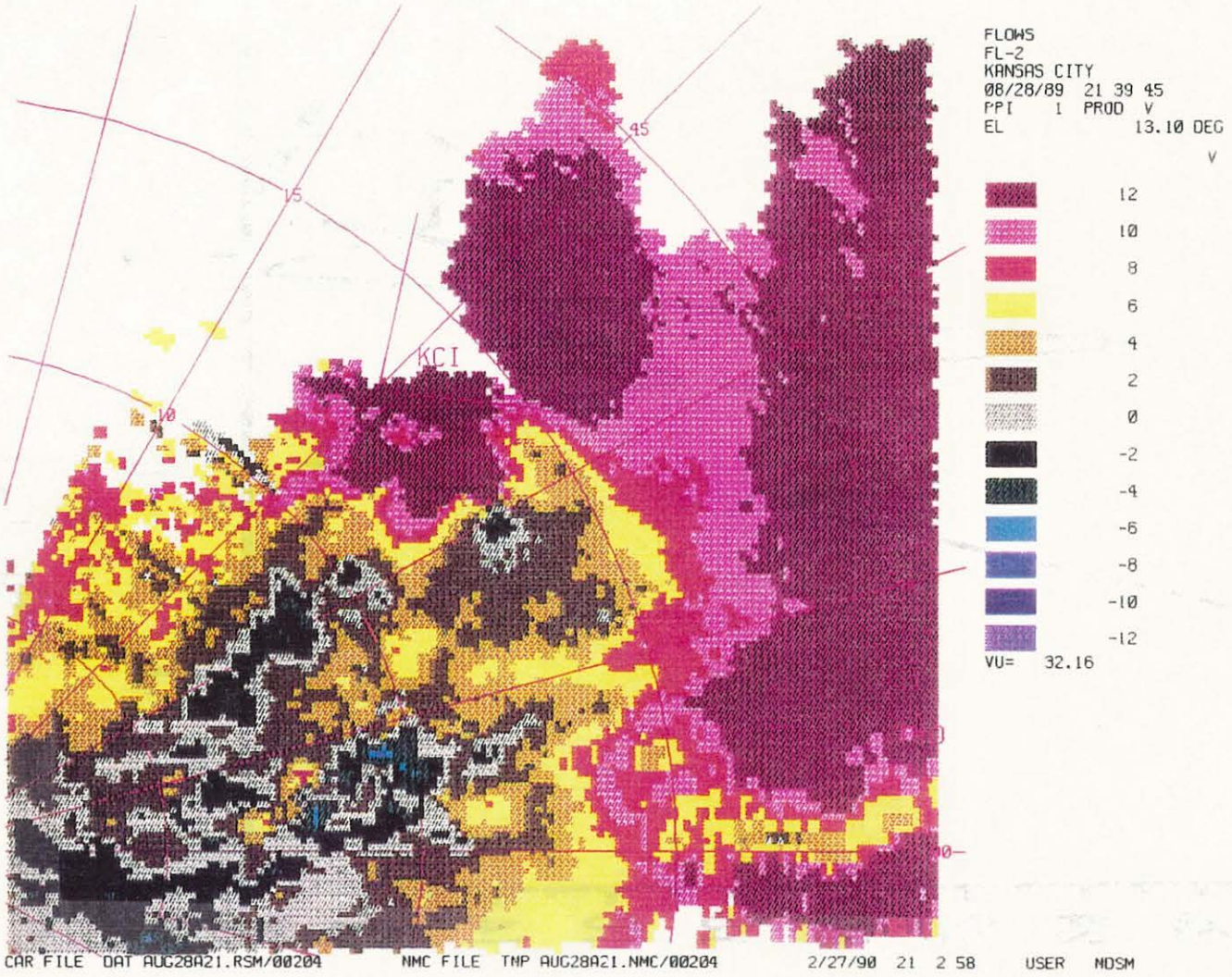

Figure III-35. 21:39:45 PPI Doppler Velocity Plot - Elevation 13.1.

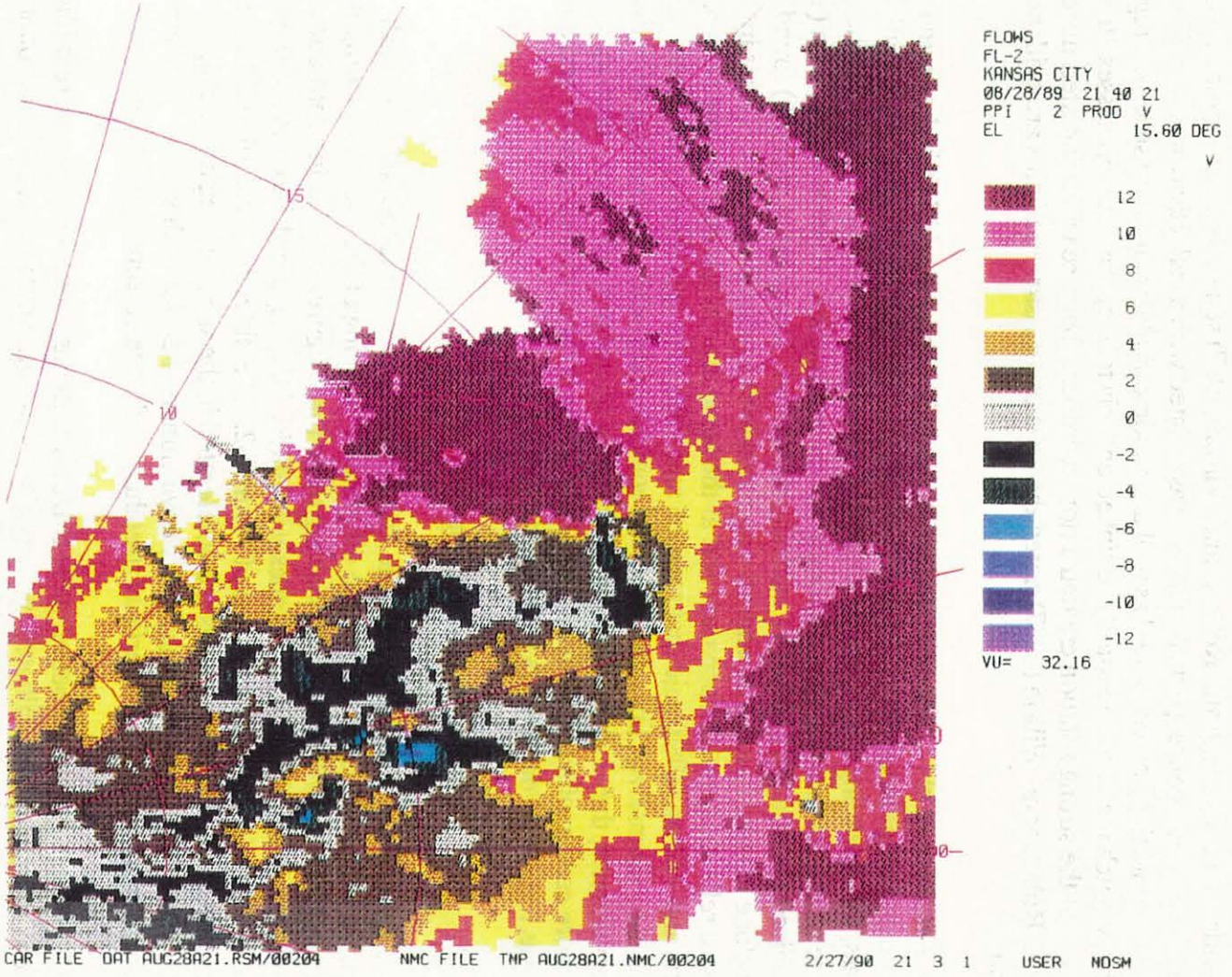

Figure III-36. 21:40:21 PPI Doppler Velocity Plot - Elevation 15.6.

2f) Hypothetical Forcing Mechanisms

The forcing mechanisms for this microburst are subcloud and incloud evaporation, and vertical pressure gradients. The evaporation is evidenced by the loss of reflectivity at the surface as well as within the cloud as a result of the subcloud lapse rate. Since the core started descending between the times given above and convergence started when it did, these two features are good evidence of a downdraft. Roberts and Wilson (1987) stated that evaporational cooling is evidenced by convergence, particularly when associated with a reflectivity notch and/ or a dry layer. The reflectivity notch existed as well as the somewhat dry air in the subcloud region. The reflectivity notch may not necessarily be linked entirely to evaporational processes, though. I propose that the strong rotation created a non-hydrostatic balance which initiated the descent of the core. Roberts and Wilson (1987) noted that vertical pressure gradients are evidenced by rotation.

Kessinger et al (1988), discussed a multi-cellular storm in which it is shown that a misocyclone causes a downward directed vertical pressure gradient because the rotation slings out mass, thus lowering the pressure. This results in high pressure aloft relative to the low pressure within the rotation thus creating a forcing mechanism. Roberts and Wilson (1987) noted misoscale rotation in 24 of 31 microbursts studied. Kessinger et al (1986) found a misocyclone located inside a downdraft associated with a reflectivity notch. This is interesting because a reflectivity notch appeared aloft at the same time as the misocyclone (Figure III-26). Roberts and Wilson (1989) said that rotation and reflectivity notches do not appear to be reliable predictors by themselves, but when observed coincidentally with a descending reflectivity core and convergence, they increase the likelihood that a microburst will occur. Isaminger (1989) was much more certain of a connection and stated that the combination of rotation and a reflectivity notch was a good predictor for a microburst event.

3) Comparison of Model and Events

Figures III-37 and III-38 illustrate the different processes associated with each microburst. Figure III-39 illustrates the differences in timing of the two events compared with the moderate reflectivity model. By viewing these three figures, a quick interpretation of the differences between the events can quickly be made. Both Figures III-37 and III-38 are very similar to the typical microburst event of Figure I-2. The differences are all in the timing of the precursors themselves. Both events are accelerated in the subcloud region by evaporation. Convergence plays a role in supplying dry environmental air for both events. Both events develop rotation associated with vorticity stretching and have descending reflectivity cores.

The main difference between the two events themselves is how they were initiated. The August 28 microburst was initiated by vertical pressure gradients created by a misoanticyclone, while the May 14 microburst was initiated by precipitation loading. Divergent tops peak at the time of the maximum winds for the August 28 microburst but peak at the time of the initial winds in the May 14 microburst. The August 28 storm develops a reflectivity notch (most likely a result of the misocyclone) while the May 14 storm does not.

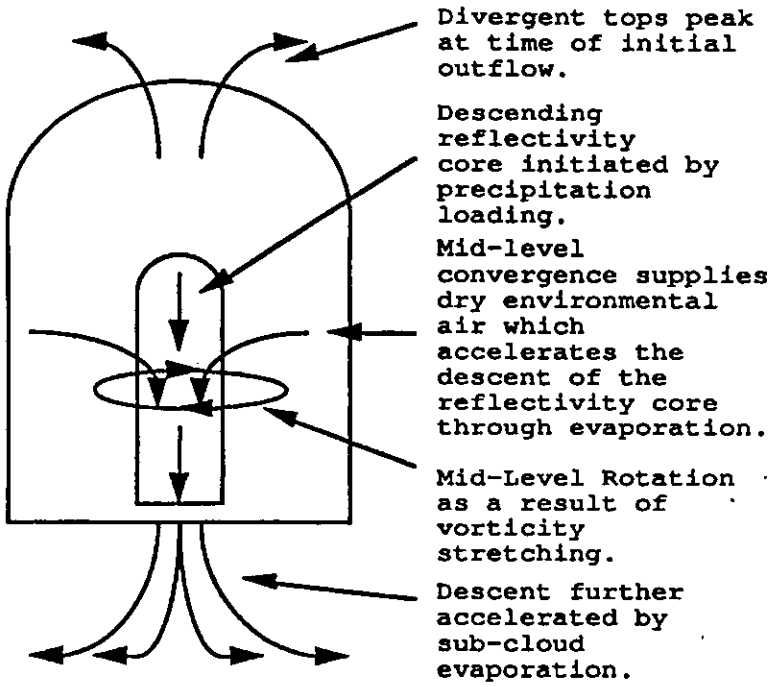

Figure III-37. May 14, 1989 Microburst Event.

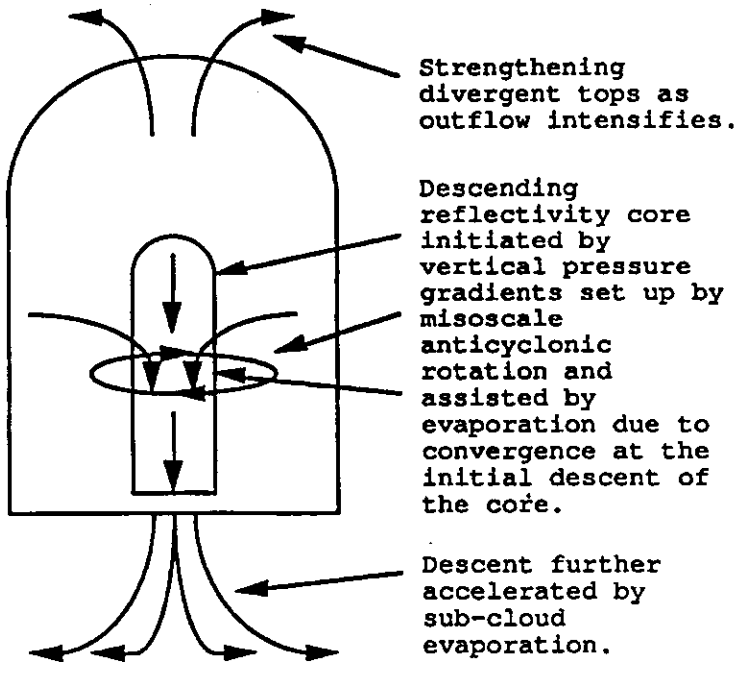

Figure III-38. August 28, 1989 Microburst Event.

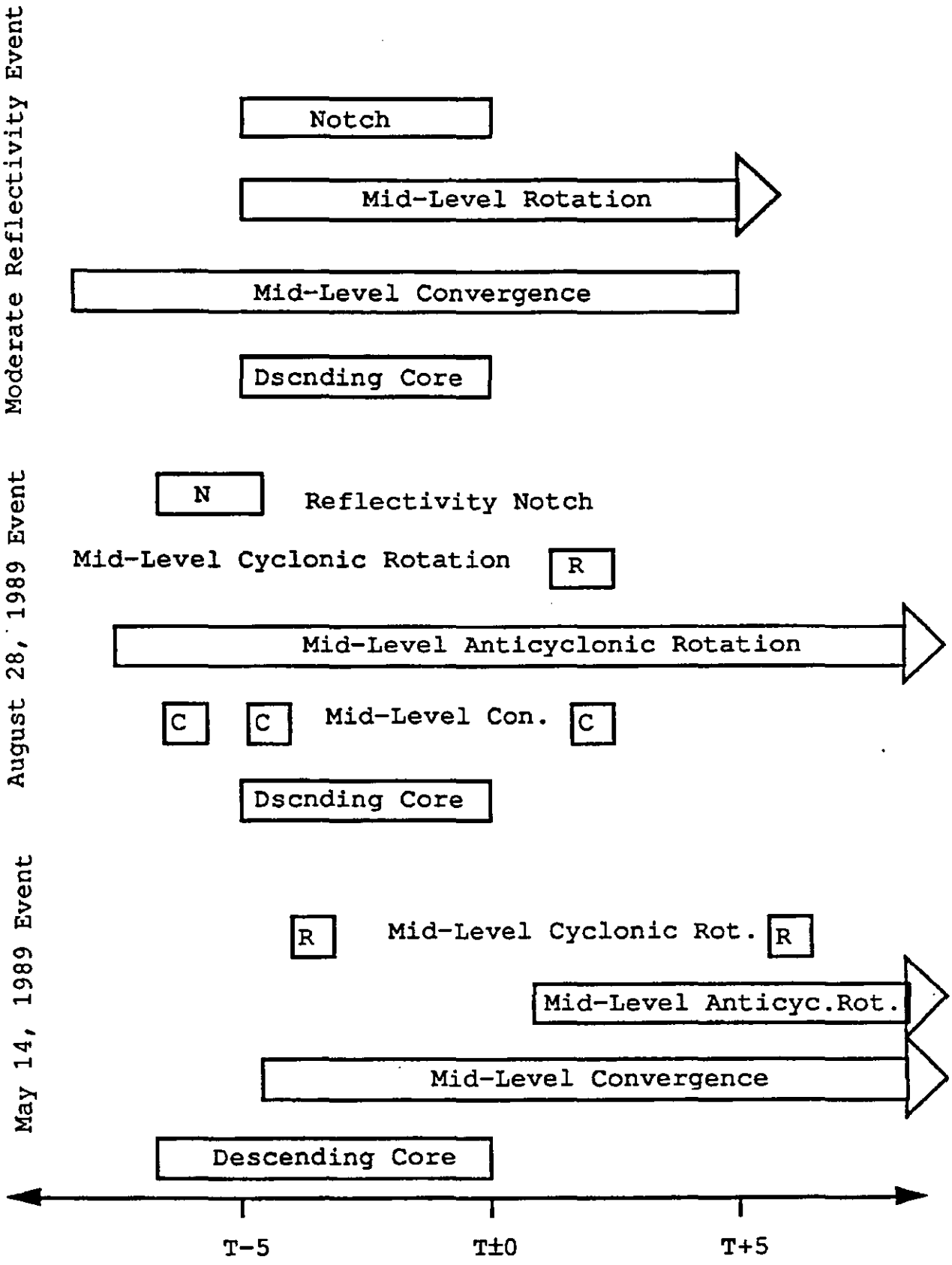

Figure III-39. Comparison Between Events and Model.

Despite the fact that the August 28 storm was multi-cellular while the May 14 storm was not, both displayed the classic microburst precursors of a descending reflectivity core, convergence, rotation, and surface divergence. Compared with the timing of the moderate reflectivity event (Figure III-39), it is readily apparent that several similarities exist. The timing of the descent of the reflectivity core for both events closely matches that of the model. The timing of the rotation shows some deviation from the model in that the August 28 storm had rotation for a larger block of time while the May 14 storm had rotation for a shorter block of time.

The main differences between the model and the two events are that the May 14 storm did not develop a reflectivity notch and the August 28 storm only had weak, intermittent convergence. The differences in the timing and persistence of the rotation in both storms compared to the model is due to the different forcing mechanisms of the two events. The August 28 microburst developed rotation earlier due to the misocyclone which developed the vertical pressure gradients which initiated the descent of the reflectivity core. The rotation associated with the May 14 event developed mostly after the microburst started, most likely in response to the continuing descent of the reflectivity core (illustrated earlier) which resulted in stretching of vorticity.

4) SUMMARY AND ALGORITHM PERFORMANCE

Campbell and Isaminger (1990) found that 94.4% of Kansas City microbursts were associated with a descending reflectivity core, 77.8% with convergence, 72.2% with upper-level divergence, and 77.8% with either type of rotation. The two microbursts studied in this thesis both display descending reflectivity cores and rotation. However, one storm had much more persistent convergence while the other had more persistent upper-level divergence. Compared to the percentages given above, the preponderance of the features in both of the storms seem to conform to a pattern of the typical Kansas City microburst, except for the fact that both storms have lower reflectivities than the typical Kansas City microburst.

Based upon the reflectivity values, these microburst events were classified as moderate reflectivity events. The differences in the timing of the various precursors is most likely due to the different forcing mechanisms. The moderate reflectivity model presents an ideal case based upon empirical observations, and deviations from this should be expected to occur as a result of the variety of different ways that a microburst can develop. Based upon this, I conclude that these two microbursts belong to the set of average events.

The major distinction is that these events are of a lower reflectivity class, which created havoc with the microburst recognition algorithm since it is tuned to high reflectivity storms. Consequently, in order to accurately detect events such as these, the algorithm must have more versatile reflectivity criteria. Biron and Isaminger (1989) noted that the algorithm had difficulties detecting Kansas City microbursts with lesser reflectivities (< 55 dBz) and noted that the threshold for the maximum reflectivity could be lowered to 51 dBz without damaging 112the detection rate. However, this would be insufficient for both storms, especially the May 14 storm which had difficulties maintaining even the minimum reflectivity core requirement of 45 dBz. The best

solution would be to include the moderate reflectivity model in the algorithm and develop a method that allowed the algorithm to decide which reflectivity class the current microburst belonged. The algorithm should also incorporate the use of RHI data, since it was shown that precursors occasionally slip in between the scans of the radar. The RHI data could also be used to verify precursors detected on PPI scans. An additional improvement that can be made on the algorithm concerns the methodology associated with assigning precursors to individual microbursts. It was shown that the algorithm had great difficulty with the multi-cellular storm mainly as a result of insufficient resolution of the reflectivity field. This can be corrected by improving the methodology for selection and vertical integration of the features.

D) CONCLUSION

Microbursts have been affecting aviation for quite some time and strong outflows have been noted by scientists as far back as the 1950s. Microbursts have been implicated in many airplane crashes, and were defined to be a strong outflow with a radial velocity difference of at least 10 m/s over 4 km. A major effort to recognize and predict the microburst event was underway by the 1980s and significant achievements have been made. Through the use of Doppler radar, algorithms have been developed which are capable of recognizing the microburst event and, very recently, even predicting them (Campbell and Isaminger, 1990).

One of the leading microburst recognition algorithms is used in this thesis to study two microbursts which occurred on two summer days in 1989. It was found that the algorithm performed very well on simple, single-cellular storms such as that of May 14, but struggled with the more complex, multi-cellular storms such as August 28. Previous studies have noted these weaknesses, and improvements are currently underway. The algorithms chief difficulty was its inability to recognize reflectivity cores of a lower reflectivity class. Several improvements for the algorithm were suggested. These were: 1) to use RHI data in addition to PPI data to verify precursors and also to detect precursors which have slipped in between the scans of the radar, 2) add the moderate reflectivity model to the algorithm and incorporate a method of determining which reflectivity class a microburst is a member of, and 3) improve the methodology of precursor selection with regards to improper precursor to microburst assignment.

Of the two microbursts studied, it was found that subcloud evaporation played a significant role in the acceleration of the downdraft. Srivastava (1985) pointed out that as long as a near dry adiabatic lapse rate exists in the subcloud region, acceleration due to evaporation will occur for any rainwater mixing ratio. He further points out that the more stable the subcloud region, the more water is required to drive the downdraft. Both storms had near dry adiabatic lapse rates, while the August 28 storm was somewhat more stable, thus requiring more water to drive the downdraft. A reflectivity notch was associated with the August 28 storm and appears to be a direct result of vertical pressure gradients generated by misoscale rotation. This rotation appears to be the instigating factor for this microburst while the May 14 microburst appears to have been initiated by precipitation loading.

Both storms exhibited descending reflectivity cores, which began their descent near T-5, as expected in the moderate reflectivity model. Convergence appeared much longer in the

May 14 storm than in the other, and appeared to play a major role in the evaporation process by supplying dry environmental air to the reflectivity core area. Neither storm followed the timing of the convergence feature in the moderate reflectivity model very closely, but convergence did appear by T-5 in both storms, in accordance with the model. Rotation appeared in both storms, and for the most part the timing of this precursor was generally followed by both microbursts. Once the microburst outflow began, both storms had the reflectivity core collocated with the outflow, as predicted by the model.

Upper-level divergence was found to be a good predictor of the timing of the peak winds in the August 28 microburst. Isaminger (1988) noted that the strengthening of upper-level divergence occurs near the time of the peak winds, which was nearly duplicated by the August 28 microburst. However, in the case of the May 14 microburst, upper-level divergence seemed to dissipate after the microburst formed and was nearly gone by the time of the peak winds, but an interesting point is that the upper-level divergence did reach a maximum near the time of the initial outflow. Rotation was found to reach a relative maximum near the time of the peak winds in the August 28 and the May 14 microburst, a fact which has been noted previously in Alabama microbursts (Isaminger, 1988).

Asymmetry of the outflow was noted in the May 14 microburst with a ratio of the winds observed by the FL-2 radar to the UND radar being 3:1. Asymmetry such as this can cause microbursts to go undetected in a single-Doppler microburst detection system, and is one of the chief arguments for a multiple radar system. Asymmetry of microburst outflows has been noted at every location that the event has been studied. In the May 14 case, it was shown that the asymmetrical outflow may have been a result of the internal core structure, which matched the asymmetrical pattern on the surface. Asymmetry cannot be accurately determined for multi-cellular storms with multiple outflows since combinations of the outflow create the appearance of asymmetry despite the fact that each individual outflow may have been perfectly symmetrical.

Despite a few departures from the standard process of microburst formation as outlined in the moderate reflectivity model, the two microbursts appear to be within the set of average microburst events, just of a lesser reflectivity class. Despite these lesser reflectivities and the fact that the microburst recognition algorithm is geared to the high reflectivity model, these microbursts were successfully detected by the algorithm throughout the lifetime of the event, excepting the fact that the algorithm had difficultly recognizing the reflectivity cores. Once improvements are made to the algorithm to include the moderate reflectivity event and improve the detection and proper placement of precursors, moderate reflectivity microburst events in the Kansas City region will be more successfully detected.

E) ACKNOWLEDGEMENTS

I wish to thank Mark Isaminger of the Massachusetts Institute of Technology for helping me choose the original topic and assisting with the analysis of the Doppler data. And at the University of Kansas, thanks to Curtis Hall for the many hours of listening to my ideas and encouragement and to Dr. Joe Eagleman and Dr. David Braaten for their guidance and support.

F) REFERENCES

Biron, P. J., and M. A. Isaminger, 1989: An analysis of microburst characteristics related to automatic detection from Huntsville, Alabama and Denver, Colorado, *24th Conference on Radar Meteorology*, American Meteorological Society, Boston, MA, 269-273.

_____, _____, K. J. Flemming, and A. A. Borho, 1990: A case study of the Claycomo, Missouri microburst on July 30, 1989. Project Report ATC-173, M.I.T. Lincoln Laboratory, 1-5.

Campbell, S. D., 1988: Microburst precursor recognition using an expert system approach. *4th International Conference on Interactive Information and Processing for Meteorology, Oceanography, and Hydrology*, American Meteorological Society, Boston, MA, 300-307.

_____, 1989: Use of Features Aloft in the TDWR microburst recognition algorithm. *Preprints, 24th Conference on Radar Meteorology*, American Meteorological Society, Boston, MA, 167-170.

_____, and S. H. Olson, 1986: Recognizing low-altitude wind shear hazards from Doppler weather radar: An artificial intelligence approach. *J. Atmos. Oceanic Tech.*, 4, 5-18.

_____, and M. A. Isaminger, 1990: A prototype microburst prediction product for the Terminal Doppler Weather Radar. Project Report ATC-173, M.I.T. Lincoln Laboratory, 7-10.

Caplan, S. J., and A. J. Bedard, Jr., 1990: The 700-500 mb lapse rate as an index of microburst probability: An application for thermodynamic profilers. *J. Appl. Meteor.*, **29**, 680-687.

Eilts, M. D., 1987: Nowcasting low-altitude wind shear with a Doppler radar. *AIAA 25th Aerospace Sciences Meeting*, Reno, Nevada, 1-5.

Evans, J. E., and D. Johnson, 1984: The FAA transportable Doppler weather radar. *22nd Conference on Radar Meteorology*, Zurich, Switzerland. 246-250.

Fujita, T. T., 1981: Tornadoes and downbursts in the context of generalized planetary scales. *J. Atmos. Sci.*, **38**, 1511-1534.

_____, and H. R. Byers, 1977: Spearhead echo and downburst in the crash of an airliner. *Mon. Wea. Rev.*, **105**, 129-146.

_____, and F. Caracena, 1977: An analysis of three weather-related aircraft accidents. *Bull. Amer. Meteor. Soc.*, **58**, 1164-1181.

Hjelmfelt, M. R., 1987: The microbursts of 22 June 1982 in JAWS. *J. Atmos. Sci.*, **44**, 1646-1665.

_____, 1988: Structure and life cycle of microburst outflows observed in Colorado. *J. Appl. Meteor.* **27**, 900-927.

_____, and C.J. Kessinger, 1988: Physical processes and observed features in microburst-producing storms. *Preprints, 10th International Cloud Physics Conference*, 15-20 Aug. 1988, Bad Homburg, FRG.

_____, H. D. Orville, R. D. Roberts, J. P. Chen, and F. J. Kopp, 1989: Observational and numerical study of a microburst line-producing storm. *J. Atmos. Sci.*, **46**, 2731-2743.

Isaminger, M. A., 1988: A preliminary analysis of Huntsville microburst precursors. Project Report ATC-153, M. I. T. Lincoln Laboratory.

_____, P. J. Biron, and R. G. Hallowell, 1989: A case study of the 24 August 1986 FLOWS microburst. Project Report ATC-162, M.I.T. Lincoln Laboratory.

Kessinger, C. J., D. B. Parsons, and J. W. Wilson, 1988: Observations of a storm containing misocyclones, downbursts, and horizontal vortex circulations. Mon. Wea. Rev., **116**, 1959-1982.

_____, R. D. Roberts, and K. L. Elmore, 1986: A summary of microburst characteristics from low-reflectivity storms. Preprints, 23rd Conf. on Radar Meteorology, 22-26 Sept. 1986, Snowmass, CO, American Meteorological Society, Boston, MA.

Krumm, W. R., 1954: On the cause of downdrafts from dry thunderstorms over the Plateau Area of the United States. Bull. Amer. Meteor. Soc. **35**, 122-125.

McCarthy, J., J. W. Wilson and T. T. Fujita, 1982: The joint airport weather studies project. Bull. Amer. Meteor. Soc. **63**, 15-22.

Merritt, M. W., 1987: Automated detection of microburst windshear for Terminal Doppler Weather Radar. SPIE Vol. 846, Digital Image Processing and Visual Communication Technologies in Meteorology. Cambridge, Massachusetts.

Roberts, R. D., and J. W. Wilson, 1984: Precipitation and kinematic structure of microburst show figure III-39 here producing storms. Preprints, 22nd Conference on Radar Meteorology, Zurich, American Meteorological Society, 71-76.

_____, and _____, 1986: Nowcasting microburst events using single Doppler radar data. 23rd Conference on Radar Meteorology, Snowmass, CO, 62-65.

_____, and _____, 1987: Nowcasting microbursts using Doppler radar in a forecasting-computer environment. Proceedings, Symposium on Mesoscale Analysis and Forecasting Incorporating Nowcasting, Vancouver, European Space Agency, ESA SP-282, 43-48.

_____, and _____, 1989: A proposed microburst nowcasting procedure using single-Doppler radar. J. Appl. Meteor., **28**, 285-303.

Srivastava, R. C., 1985: A simple model of evaporatively driven downdraft: Application to microburst downdraft. J. Atmos. Sci., **42**, 1004-1023.

Turnbull, D., J. McCarthy, J. Evans and D. Zrnic, 1989: The FAA Terminal Doppler Weather Radar (TDWR) program. Preprints, Third International Conference on the Aviation Weather System, Anaheim, American Meteorological Society, 414-419.

Wakimoto, R. M., 1985: Forecasting dry microburst activity over the High Plains. *Mon. Wea. Rev.*, **113**, 1131-1143.

Wilson, J. W., and D. Reum, 1988: The flare echo: reflectivity and velocity signature. *J. Atmos. Oceanic Tech.*, **5**, 197-205.

_____, R. D. Roberts, C. Kessinger and J. McCarthy, 1984: Microburst wind structure and evaluation of Doppler radar for airport wind shear detection. *J. Climate Appl. Meteor.*, **23**, 898-915.

Wolfson, M. M., 1988: Characteristics of microbursts in the continental United States. *Lincoln Laboratory Journal*, **1**. 49-73.

NWS CR 47 Practical Application of a Graphical Method of Geostrophic Wind Determination. C.B. Johnson, November 1971 (COM 71-01084).

NWS CR 48 Manual of Great Lakes Ice Forecasting. C. Robert Snider, December 1971 (COM 72-10143).

NWS CR 49 A Preliminary Transport Wind and Mixing Height Climatology, St. Louis, Missouri. Donald E. Wuerch, Albert J. Courtois, Carl Ewald, Gary Ernst, June 1972 (COM 72-10859).

NWS CR 50 An Objective Forecast Technique for Colorado Downslope Winds. Wayne E. Sangster, December 1972 (COM 73-10280).

NWS CR 51 Effect on Temperature and Precipitation of Observation Site Change at Columbia, Missouri. Warren M. Wisner,March 1973 (COM 73-10734).

NWS CR 52 Cold Air Funnel Clouds. Jack R. Cooley and Marshall E. Soderberg, September 1973, (COM 73-11753/AS).

NWS CR 53 The Frequency of Potentially Unfavorable Temperature Conditions in St. Louis, Missouri. Warren M. Wisner,October 1973.

NWS CR 54 Objective Probabilities of Severe Thunderstorms Using Predictors from FOUS and Observed Surface Data. Clarence A. David, May 1974 (COM 74-11258/AS).

NWS CR 55 Detecting and Predicting Severe Thunderstorms Using Radar and Sferics. John V. Graff and Duane C. O'MalleyJune 1974 (COM 74-11335/AS).

NWS CR 56 The Prediction of Daily Drying Rates. Jerry D. Hill, November 1974 (COM 74-11806/AS).

NWS CR 57 Summer Radar Echo Distribution Around Limon, Colorado. Thomas D. Karr and Ronald L. Wooten, November 1974 (COM 75-10076/AS).

NWS CR 58 Guidelines for Flash Flood and Small Tributary Flood Prediction. Lawrence A. Hughes and Lawrence L. Longsdorf, October 1975 (PB247569/AS)

NWS CR 58 (Revised) March 1978 (PB281461/AS)

NWS CR 59 Hourly Cumulative Totals of Rainfall - Black Hills Flash Flood June 9-10, 1972. Don K. Halligan and Lawrence L. Longsdorf, April 1976 (PB256087).

NWS CR 60 Meteorological Effects on the Drift of Chemical Sprays. Jerry D. Hill, July 1976 (PB259593).

NWS CR 61 An Updated Objective Forecast Technique for Colorado Downslope Winds. Wayne E. Sangster, March 1977 (PB266966/AS).

NWS CR 62 Design Weather Conditions for Prescribed Burning. Ronald E. Haug, April 1977 (PB268034).

NWS CR 63 A Program of Chart Analysis (With Some Diagnostic and Forecast Implications). Lawrence A. Hughes, December 1977 (PB279866/AS).

NWS CR 64 Warm Season Nocturnal Quantitative Precipitation Forecasting for Eastern Kansas Using the Surface Geostrophic Wind Chart. Wayne E. Sangster, April 1979 (PB295982/AS).

NWS CR 65 The Utilization of Long Term Temperature Data in the Description of Forecast Temperatures. Arno Perlow,November 1981 (PB82 163064).

NWS CR 66 The Effect of Diurnal Heating on the Movement of Cold Fronts Through Eastern Colorado. James L. Wiesmueller, August 1982 (PB83 118463).

NWS CR 67 An Explanation of the Standard Hydrologic Exchange Format (SHEF) and Its Implementation in the Central Region. Geoffrey M. Bonnin and Robert S. Cox, April 1983 (PB83 193623).

NWS CR 68 The Posting of SHEF Data to the RFC Gateway Database. Geoffrey M. Bonnin, April 1983 (PB83 222554).

NWS CR 69 Some Basic Elements of Thunderstorm Forecasting. Richard P. McNulty, May 1983 (PB83 222604).

NWS CR 70 Automatic Distribution of AFOS Products Created at the NOAA Central Computer Facility via Hamlet (RJE) PunchStream. Billy G. Olsen and Dale G. Lillie, November 1983 (PB84 122605).

NWS CR 71 An Investigation of Summertime Convection Over the Upper Current River Valley of Southeast Missouri. Bartlett C. Hagemeyer, July 1984 (PB84 222389).

NWS CR 72 The Standard SHEF Decoder Version 1.1. Geoffrey M. Bonnin, August 1984 (PB85 106508).

NWS CR 73 The Blizzard of February 4-5, 1984 Over the Eastern Dakotas and Western Minnesota. Michael Weiland, October 1984 (PB85 120087).

NWS CR 74 On the Observation and Modeling of the Slope Winds of the Upper Current River Valley of Southeast Missouri and Their Relationship to Air-Mass Thunderstorm Formation. Bartlett C. Hagemeyer, June 1985 (PB85 226926/AS).

NWS CR 75 Complete Guide to Canadian Products in AFOS. Craig Sanders, July 1985 (PB85 228153/AS).

NWS CR 76 The Reliability of the Bow Echo as an Important Severe Weather Signature. Ron W. Przybylinski and William J. Gery, September 1985 (PB86 102340).

NWS CR 77 Observation of Bow Echoes with the Marseilles Radar System. John E. Wright, Jr., September 1985 (PB86 102340).

NWS CR 78 Statistical Analysis of SHEF Coding Errors. Robert S. Cox, Jr., January 1986 (PB86 145141).

NWS CR 79 On the Midwestern Diurnal Convergence Zone on the West Side of the Warm Season Bermuda High. Bartlett C. Hagemeyer, March 1986 (PB86 171378).

NWS CR 80 Some Characteristics of Northeast Kansas Severe Weather 1963-1984. Larry W. Schultz, March 1986 (PB86 173952/AS).

NWS CR 81 The Severe Thunderstorm Outbreak of July 6, 1983 in Southeast Idaho, Western Wyoming and Southwest Montana. Gary L. Cox, April 1986 (PB86 184322/AS).

NWS CR 82 Some Proposals for Modifying the Probability of Precipitation Program of the National Weather Service. Wayne E. Sangster and Michael D. Manker, July 1986 (PB86 226636/AS).

NWS CR 83 Deformation Zones and Heavy Precipitation. Henry Steigerwaldt, August 1986 (PB86 229085/AS).

NWS CR 84 An Overview of the June 7, 1984 Iowa Tornado Outbreak. Charles H. Myers, August 1987.

NWS CR 85 Operational Detection of Hail by Radar Using Heights of VIP-5 Reflectivity Echoes. Richard B. Wagenmaker,September 1987

NWS CR 86 Fire Weather Verification: The Forecaster Does Make a Difference. Therese Z. Pierce and Scott A. Mentzer, December 1987 (PB88 140744).

NWS CR 87 Operational Use of Water Vapor Imagery. Samuel K. Beckman, December 1987 (PB88 140751).

NWS CR 88 Central Region Applied Research Papers 88-1 Through 88-7. NWS Central Region, Scientific Services Division, May 1988 (PB88-210836).

NWS CR 89 Compendiums of Information for the Missouri Basin River Forecast Center and the North Central River ForecastCenter. NW Central Region, Scientific Services Division, June 1988 (PB88-226204).

NWS CR 90 Synoptic-Scale Regimes Most Conducive to Tornadoes in Eastern Wyoming -- A Link Between the Northern Hemispheric Scale Circulation and Convective-Scale Dynamics. William T. Parker and Edward K. Berry, July 1988 (PB88-231337).

Continued on Back Cover.